New Trapping States and Enhanced Nonlinear Optical Effects in Coherently Driven Systems

A thesis submitted for the degree of

Doctor of Philosophy

by

Harshwardhan Wanare

School of Physics
University of Hyderabad
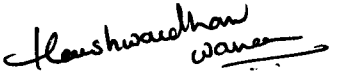Hyderabad - 500 046
INDIA

February 1998

To my parents.....

for their unconditional love and support

DECLARATION

I hereby declare that the matter embodied in this thesis entitled "**New Trapping States and Enhanced Nonlinear Optical Effects in Coherently Driven Systems**", is a result of investigations carried out by me under the supervision of Prof. G.S. Agarwal of the School of Physics, University of Hyderabad, Hyderabad - 500 046 (currently at the Physical Research Laboratory, Ahmedabad - 380 009).
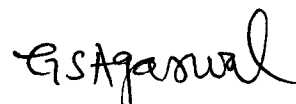
Place: Hyderabad
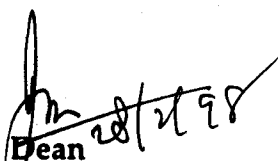
Date: 23/2/98

Harshwardhan Wanare

CERTIFICATE

This is to certify that the work contained in this thesis entitled, "**New Trapping States and Enhanced Nonlinear Optical Effects in Coherently Driven Systems** ", has been carried out by **Harshwardhan Wanare**, under my supervision for the full period prescribed under Ph.D. ordinances of the University of Hyderabad, and the same has not been submitted for the award of research degree of any University.

Place: Hyderabad / Ahmedabad

Date: 23 2 98

GSAgarwal

Thesis supervisor

Dean

School of Physics,

University of Hyderabad,

Hyderabad - 500 046, INDIA.

ACKNOWLEDGMENTS

Contents

Synopsis

This thesis deals with a number of topics falling under the general subject of optical manipulation of atoms. We present new results on population *trapping phenomenon* on one hand and on the other the myriad manifestations of *quantum interference* . We discuss the central role played by quantum interference in phenomena like trapping in two-level and multilevel systems, optical bistability, nonlinear generation of signal and its control. Different chapters are devoted to the following:

New Trapping Phenomenon in Atomic Systems: The trapping phenomenon in atomic systems occupies a very special place in Quantum Optics. The coherent population trapping (CPT) phenomenon in three-level Λ system driven by two monochromatic fields is well known. The trapping phenomenon we describe is quite different from the well known CPT phenomenon. We demonstrate new trapping states in a two-level system, using classical frequency modulated electromagnetic fields.

We further generalize this phenomenon to multi-level systems and discuss its application in creating inversion across multiple levels. We also propose an *optical atom* scheme for the three-level ladder system, where this effect can be realized.

Trapping in Two-Level System - Control of Quantum Tunneling: The two-level systems so far are not known to exhibit trapping except in presence of quantized field. We have demonstrated *new* trapping phenomenon in two-level systems in presence of a *classical frequency modulated (FM) electromagnetic field* . We work in the semiclassical regime, where classical fields are applied to atoms with discrete atomic levels. A proper choice of parameters of the applied field, like the amplitude (M) and the frequency (Ω) of modulation, leads to trapping of the population on the appropriate time scales. These time scales, for observation of trapping, are governed by the frequency of modulation, and are limited by the lifetime of the excited state (γ^{-1}).

This phenomenon has very important applications in tunneling phenomenon. The trapping of population in a two-level system is akin to localization in a double-well

potential. We describe here a method for coherent control of *quantum tunneling* .

The FM field has an $\exp(iM \sin \Omega t)$ kind of time dependence, whose spectrum contains frequency components at $\omega + n\Omega$ for $n = 0, \pm 1, \pm 2, ...$, with $J_n(M)$ as the corresponding weight factors (ω is the central frequency about which the modulation is done). To observe the trapping of population we choose the frequency of modulation such that $\Omega \gg \gamma$, and the index of modulation such that its a *zero of the zeroth order Bessel function* i.e., $J_o(M) = 0$. In terms of tunneling, the suppression of quantum tunneling in double-well potential is analogous to our modulating away the resonant component of the applied FM field and hence suppressing any excitation in the atom.

The population in presence of a monochromatic field undergoes the usual Rabi oscillations between the ground state ($|g\rangle$) and the excited state ($|e\rangle$) of the atom i.e., the population moves back and forth from $|g\rangle \rightarrow |e\rangle \rightarrow |g\rangle \rightarrow |e\rangle$ and so on. The amplitude and frequency of this oscillation depends on the intensity and the detuning of the applied monochromatic field. On the other hand, application of a FM field makes the population undergo a complicated motion in between the states $|g\rangle$ and $|e\rangle$. This is due to the presence of multiple frequency components in the FM field. The effective Hamiltonian governing this complex motion is given as $H_{eff} = H_{dc} + H_{osc}$. The dynamics on a time scale slower than Ω^{-1} is governed mainly by the dc component. Hence, by choosing the index of modulation to be such that $J_o(M) = 0$, we make the term H_{dc} negligible. Moreover, by choosing M to be large we minimize the contribution of H_{osc} since for large M, $|J_n(M)| \ll 1$, for all n. Under these conditions one can observe the trapping of population on the appropriate time scales (i.e. $\tau < \Omega^{-1}$).

In an alternate picture one can understand this in terms of *level crossing* phenomenon. By going into the instantaneous frame of this interaction we observe co-sinusoidal time dependence of the energies of the bare levels. The tunneling of population occurs at times where the energy levels cross i.e., at times $\tau \sim n\pi/2\Omega$, where n is an integer. To observe this phenomenon of crossing of energy levels leading to jumps, we again require that $\gamma \ll \Omega$. The transition probabilities at these crossings have been calculated using the Landau-Zener theory for crossing of two adiabatic levels and was found to match well with the exact numerical calculation. We also propose a possible experimental realization using a transition of Yb atom, whose excited state life time is

$\sim 1~\mu sec$ and a FM field with modulation frequency $\Omega > 1MHz$ would lead to an observation time in the range of nanoseconds.

Multiple Level Crossings - Built up Coherent Effects: We have generalized this trapping phenomenon to multi-level systems and studied the effects of phase accumulation due to coherent evolution. Involvement of multiple atomic levels in this process results in having richer dynamics than the two-level system, due to many more crossings of the energy levels that take place. The application of FM fields ensures coherent evolution in between crossings, and hence inclusion of phase effects, for population redistribution after multiple crossings, becomes essential. We investigate the effect of phase being accumulated along various pathways in between crossings. *Due to coherent evolution of the system in between crossings, population after multiple crossings is not a mere product of Landau - Zener transition probabilities at each crossing* . The population accumulates different phase as it evolves in time, along different states (or paths). This relative phase was tailored to show the existence of *quantum interference* effects. These are similar to the phase effects experimentally observed using *sech* pulses, where interference was observed in the resonant microwave multiphoton *probability* between two states ($21s$ and $19,3$ Stark) of K, as a function of intensity and duration of the microwave pulse. In our system, the phase accumulated along these paths was tailored by changing the detunings ($\Delta_{1,2}$), of central frequency ($\omega_{1,2}$) of the FM fields along both the transitions, from the bare atomic levels. This provides another control over the amount of population transferred at the crossing, apart from the strength of the field-atom coupling (Rabi frequency). Besides, population trapping is observed in all the levels, when the coupling fields along both the transitions of the three-level ladder system are chosen to satisfy the conditions for trapping.

Creating Inversion Across Multiple Levels: As an application of this trapping phenomenon, we have presented a method of *inverting the population across multiple levels* . In our scheme the *population in the intermediate state remains unaffected* . The conventional method used for such inversion, the Rapid Adiabatic Passage method, is very sensitive to the timings of the various sequence of pulses, and cannot be used if the in-

termediate level is populated. The method we propose is better on both these counts, as we use continuous wave fields and the population of the intermediate state remains unaffected. The only requirement other than the trapping condition is that all the three levels cross simultaneously. This occurs whenever we choose $|\Delta_1| = |\Delta_2|$, and the levels cross at times $\tau = \cos^{-1} \Delta / M\Omega$. Hence, this scheme would be experimentally more attractive than the conventional methods adopted for creating population inversion across multiple levels.

Realization of Coherently Driven Atomic Systems by Coupled Cavities: The phenomenon of classical light interacting with an atom can be *simulated* by a purely classical system called *Optical Atom* . The various effects of light - matter interaction discussed earlier can be observed in regimes not accessible in experiments with real atoms. In an Optical Atom, the *atomic levels* of the atom are simulated by various *classical modes* of the field in an optical cavity. The interaction of the atom with an electromagnetic field is equivalently provided by appropriate coupling of these classical modes. In a real atom one does not have any control on its characteristic parameters like lifetime, energies of various levels and the transition probabilities between them. But these parameters can be controlled in its Optical Atom simulation. As of now there has been no scheme to simulate the three-level system in optical atoms. We have proposed a scheme which would *simulate the three-level system* , using two identical coupled optical cavities (say coupled fibre ring cavities).

In the coupled cavity we have four degenerate modes, two counter propagating modes in each of them. We lift the degeneracy of a set of counter propagating modes, using the Sagnac effect, in one cavity. We couple these non-degenerate modes to the (degenerate) modes in the second cavity, using a lossless 2×2 fibre coupler. This conservative coupling results in an anti-crossing in the mode structure of the cavity. Moreover, the degenerate modes of the second cavity are coupled using a dissipative coupler, could be a localized absorber. The Faraday isolator used to obtain the Sagnac effect, provides the appropriate time dependence which simulates the coupling field between the various levels. Thus, effectively we have three non-degenerate modes appropriately coupled to simulate a three-level cascade system with two coupling fields.

We make one to one correspondence of the coupled ring cavity optical atom to the atomic parameters.

Control of Optical Bistability: We have demonstrated application of the effects of Quantum Interferences and Electromagnetic Field Induced Transparency in the cooperative phenomenon of *Optical Bistability* . We have shown that by using a control field which couples the excited state of the usual two-state atomic system to another level, one can obtain *substantial decrease* ($\sim 50\%$) in the threshold intensity required to switch from the *off state* to the *on state* . We use a control field to create another channel along which the system can evolve, and these channels interfere to modify the absorptive and dispersive properties of the atom. We have proposed two schemes (*i*) ladder system, where the control field couples the excited state to a level above it; and (*ii*) Λ configuration with the excited state coupled to another ground state. We consider a collection of such atoms in an uni-directional ring cavity which provides the necessary feedback for obtaining bistable behavior. The control field does not circulate in the cavity but is used to control the polarization at the bistable transition.

The control field creates an *Autler-Townes* kind of splitting of the absorption profile, which decreases absorption at the line center, leading to lower saturation threshold. Furthermore, the control field creates another channel along which the system can evolve. The absorption and dispersion characteristics of the transition involved in the bistable operation, are now dependent on the decay of the coupling level which is not dipole connected. This leads to an interference effect, which is used to lower the threshold of switching. We have achieved this lowering of threshold in both the *absorptive and dispersive* kind of bistability. We have also studied the switching times in presence of the control field. We found that the exponent for critical slowing down is dependent on the control field strength. We have thus utilized these control field induced *Quantum Interference effects* and *Electromagnetically Induced transparency* to achieve lowering of the bistability threshold in an all-optical bistable system.

Multistability Induced by Control Field: We also demonstrate the possibility of control field induced *multistable behavior* . This multistability is achieved at much lower

intensity levels than conventionally possible. By merely changing the control field parameters like intensity and detuning, one can *alter the region of multistability* . This would provide greater operational control on the multistable system and moreover provide a way of using the same device for both bistable and multistable operation, by merely changing the control field parameters.

For experiments in cells, there are various effects that hamper the efficacy of these processes. One major contribution in gases is due to Doppler broadening. We look into this aspect and undertake velocity averaging in the Doppler free geometry for both the Λ and the ladder system for the control of bistability. This would provide the actual extent of lowering of threshold in an experiment.

Enhancement of Nonlinear Optical Effects: In nonlinear optics one of the goals has been - how to improve the efficiency of signal generation. The ideas of atomic coherence and quantum interference have been used in wide variety of applications such as to achieve, electromagnetically induced transparency, lasing without inversion, enhancement refractive index, generation of ultra violet radiation, control two-photon transitions, spontaneous emission noise quenching and host of other phenomenon. Its also well known that the atomic coherence is maximized in a coherent population trapping (CPT) state, between the ground states in a three-level Λ system. We study in detail the enhancement of nonlinear signal by utilizing the maximal *coherence of the CPT state* . In our scheme we essentially have two fields acting simultaneously on each transition in a Λ-system. By choosing the detunings of the pump fields such that we operate at the coherent population trapping condition, we create the required atomic coherence. We have proposed *enhancement of* $\omega_1 + \Omega$ generated by the nonlinear process $(\omega_1 + \Omega) = \omega_1 - \omega_2 + (\omega_2 + \Omega)$, under CPT conditions created by the pumps ω_1 and ω_2. In this process ω_1 and $\omega_2 + \Omega$ are absorbed and ω_2 is emitted, to generate the field at $\omega_1 + \Omega$. We show that one can achieve *enhancement of the order of* $\sim 10^2$ in the generated signal intensity. We also demonstrate that its advantageous to operate at CPT with a finite detuning from the atomic resonance. As we have two fields simultaneously coupling each transition, we have explicit time dependence of $e^{\pm i\Omega t}$. We expand the system density matrix into its Fourier components and then solve numerically a set of

coupled equations using *matrix continued fraction* . The advantage of this method lies in the fact that one is not restricted to weak fields at $\omega_{1,2} + \Omega$, but *all the fields involved could be strong* and of arbitrary strengths. Our non-perturbative treatment is *exact* .

Pulse Matching at Higher Probe Powers: We have also studied the phenomenon of pulse matching at high probe powers, where we study the propagation of these fields through a thick medium. Pulse matching is a consequence of the CPT state in turn modifying the radiation field. While interacting with the CPT state, only the field components that preserve this state survive and do not experience absorption, whereas all the other non-matched Fourier components are attenuated in propagation through the medium. As a consequence after a characteristic propagation distance the transmitted field contains only components that are *matched in amplitude and phase to the CPT state* . Until now all the studies have been undertaken in the limit of weak probe powers. Our non-perturbative analysis enables us to address this issue - whether for a thick medium pulse matching will occur at high probe powers. We found the remarkable result that *even at higher probe intensities pulse matching takes place* . We also observe substantial lowering of the propagation distance required to obtain phase matching, at higher probe powers.

We would like to draw attention to the fact that the effects we discuss can be realized using atomic vapor in cells. There are many atomic species like Na, K, Rb, Cs, Yb, Ne, which can be used as the active medium, with appropriate coupling lasers, to simulate various two-level and three-level systems.

Introduction

The field of *optics* is presently undergoing a second revolution, almost three decades after the first demonstration of laser action. The arrival of lasers brought in the first revolution, which led to a phenomenal development in non-linear optics. Since then, many significant developments have taken place due to experimental realizations of a wide ranging *counterintuitive* concepts, like lasing without inversion, micromaser, and investigations of basic quantum mechanics such as measurement problem and complementarity. There have been exciting advancements in application of quantum optical ideas - in atom optics, all-optical computation schemes, including laboratory demonstration of resonance fluorescence, lasers, micromaser, single one atom lasers, squeezed states, Bose-Einstein condensation etc. The list of these new advancements is almost inexhaustive.

Historically, it was at the turn of the century, Planck [1] thought of quantizing oscillators inside a cavity to explain the complete spectral distribution of the electromagnetic energy radiated by a blackbody source. He achieved that end successfully. Extensions of these ideas led Einstein [2] in 1905 to introduce the hypothesis of corpuscularity of electromagnetic radiation to explain photoelectric effect. The quantum of radiation was named *photon* much later in 1926 [3]. The interaction of electromagnetic radiation with atoms was discussed by Einstein [4] in 1917 where he introduced phenomenologically the basic idea of *stimulated emission* . It was only in 1960 that stimulated emission was utilized to obtain laser action. It was Dirac [5], in 1927 who explained *interference* phenomenon shown by light, which at the same time shows the excitation of a specific atom located along a wavefront by absorbing *one photon* . This essentially combined the wave-like and particle-like characteristics of light.

The essence of the quantum theory of radiation is that a quantized simple harmonic oscillator is associated with each mode of the quantized field. Among the many achievements of the quantum theory of light, are the explanation of spontaneous emission, Lamb shift, Casimir effect, photon statistics of laser - particularly the non-classical

aspects like sub-Poissonian statistics, squeezed states and photon antibunching.

In many of these processes the basic unit of light-matter interaction is the two-level system interacting with a monochromatic field. It has been in vogue right from the days of old quantum theory when Einstein gave the detailed derivation of the black-body radiation formula. Einstein proposed phenomenologically three coefficients, corresponding to various processes involved in the atom-field interaction, (a) the transition rate for *absorption* $|g\rangle \rightarrow |e\rangle$ is proportional to the energy density of the radiation with the proportionality constant B_{ge}, (b) the rate of *spontaneous emission* $|e\rangle \rightarrow |g\rangle$, is given by A_{eg}, and (c) the transition rate of *stimulated emission* $|e\rangle \rightarrow |g\rangle$, is again proportional to the energy density of the radiation and the proportionality constant is B_{eg}. All these constants are independent of the energy density of the applied radiation field and are interrelated,

$$
\begin{aligned}
B_{eg} &= \left(\frac{D_g}{D_e}\right) B_{ge}, \\
A_{eg} &= \left(\frac{\hbar\omega^3}{\pi^2 c^3}\right) B_{eg},
\end{aligned}
\tag{2.1}
$$

hence, the transition rates corresponding to all the phenomenon due to interaction between the applied field and a given pair of energy levels can be expressed in terms of a single coefficient. In eqn. (2.1), D_g (D_e) are the degeneracies of the ground and the excited states, respectively, and ω is the atomic transition frequency. On undertaking a complete quantum mechanical calculation we obtain these coefficients which are intrinsic properties of the specific two-level medium,

$$
A_{eg} = \frac{4}{3} \frac{|\vec{d}_{eg}|^2 \omega^3}{\hbar c^3},
\tag{2.2}
$$

here, $\vec{d}_{eg}$ is the expectation value of the dipole moment operator of the transition $|g\rangle \leftrightarrow |e\rangle$, it will be dealt in detail in the following section. Hence, the response of a medium to an incident electromagnetic field seems as though it is a *rigid characteristic* property of the medium. We have seen in recent past that one can substantially tailor these properties using the ideas of quantum interference and atomic coherence. These ideas have been extensively used in making absorbing medium transparent, refractive index has been modified in a controlled fashion by orders of magnitude, unprecedented efficiencies have been attained in nonlinear optical processes. In this thesis we discuss in detail our contributions to some of these exciting developments.

In many problems of interest in quantum optics, one is interested in the interaction of the radiation field with a medium which contains a large number of atoms. We will deal with such interactions, like in optical bistability (in chapter 5) and pulse matching phenomenon (in chapter 6). We now demonstrate the mathematical framework to deal with such problems. Typically, the set of equations for the *field* and the *matter* are dealt with in a *self-consistent* manner.

The field is treated classically and the atoms are treated quantum mechanically. This is known as the *semi-classical* approximation. One essentially neglects quantum correlations between the atom and the field, i.e. the operator products $\vec{E}(t)\vec{P}(t)$ can be factored in their expectation values as $\langle \vec{E}(t)\ \vec{P}(t) \rangle = \langle \vec{E}(t) \rangle \langle \vec{P}(t) \rangle$. A consistent application of such factorization leads to the semi-classical radiation theory. In the semi-classical theory $\langle \vec{E}(t) \rangle$ is interpreted to be a purely classical field. Most of the applications we are dealing with here involve large number of photons (typically, cw laser would have $\sim 10^9$ photons/mode, whereas the pulsed laser has $\sim 10^{17}$ photons/mode), hence it is quite safe to neglect these quantum correlations.

The classical field induces dipole moments in the medium and the *macroscopic polarization* $(\vec{P})$ of the medium is obtained in a *self-consistent* manner. The calculation of the polarization involves performing a statistical summation of individual dipoles using the density matrix formalism (section 2.1). The classical electromagnetic field is described by the Maxwell's equations, these equations relate the electric and magnetic field vectors $\vec{E}$ and $\vec{H}$, respectively, together with the displacement and inductive vectors $\vec{D}$ and $\vec{B}$, respectively, (in Gaussian units)

$$\nabla \cdot \vec{D} = 4\pi\rho, \qquad \nabla \times \vec{E} = -\frac{1}{c}\frac{\partial \vec{B}}{\partial t},$$
$$\nabla \cdot \vec{B} = 0, \qquad \nabla \times \vec{H} = \frac{4\pi}{c}\vec{J} + \frac{1}{c}\frac{\partial \vec{D}}{\partial t}, \qquad (2.3)$$

where,

$$\vec{D} = \vec{E} + 4\pi\vec{P}, \quad \vec{H} = \vec{B} - 4\pi\vec{M}, \quad \vec{J} = \sigma\vec{E}. \qquad (2.4)$$

where, c is the speed of light in vacuum. We assume that the medium is *homogeneous, nonmagnetic* $(\vec{M} = 0)$, *and non-conducting* $(\sigma = 0)$, and that there are *no free charges* $(\rho = 0)$.

On combining the curl equations in (2.3), taking appropriate time derivatives, and

using the relations (2.4), we obtain the following wave equation,

$$\nabla^2 \vec{E} - \left(\frac{n_o}{c}\right)^2 \frac{\partial^2 \vec{E}}{\partial t^2} = \frac{4\pi}{c^2} \frac{\partial^2 \vec{P}}{\partial t^2}. \tag{2.5}$$

As we see in eqn. (2.5), the polarization $\vec{P}$, acts as a source term in the equation for the radiation field. The electromagnetic field $\vec{E}(\vec{r}_o, t)$, given as

$$\vec{E}(\vec{r}_o, t) = \vec{E}_o(\vec{r}_o)e^{-i(\omega t - \vec{k}.\vec{r}_o)} + c.c, \tag{2.6}$$

acts uniformly on the atom at the position $\vec{r}_o$. If the field is given as in eqn. (2.6), then the the linear response of the medium is given by its *polarization* ,

$$\vec{P}(\vec{r}_o, t) = \vec{P}_o(\vec{r}_o)e^{-i(\omega t - \vec{k}.\vec{r}_o)} + c.c. \tag{2.7}$$

The direction of propagation of the field is along the wave vector $\vec{k}$, with $|\vec{k}| = \omega n/c$, where n is the linear refractive index of the medium at the frequency ω. The vector character of the field comes from its polarization, hence, the field amplitude can be written as $\vec{E}_o(\vec{r}_o) = \hat{\epsilon}\mathcal{E}$, where $\hat{\epsilon}$ denotes the polarization direction. Similarly, the atomic polarization amplitude is given by $\mathcal{P}$. If we neglect the x- and y- dependence of the field and consider a plane wave traveling the z- direction, the Laplacian in eqn. (2.5) goes as a second order derivative along the z- direction.

The amplitudes of the field, $\mathcal{E}$ and the polarization, $\mathcal{P}$ are generally slowly varying functions of position and time on the scale of the optical wavelength and the optical period, respectively. Hence, on substituting eqn. (2.6) and eqn. (2.7) in eqn. (2.5), and on undertaking the *slowly varying envelope approximation* as given in eqn.(2.9), the wave equation reduces to a first order differential equation,

$$\frac{\partial \mathcal{E}}{\partial z} + \frac{1}{c} \frac{\partial \mathcal{E}}{\partial t} = \frac{2\pi i k}{n_o^2} \mathcal{P} \tag{2.8}$$

The following approximations are made in order to obtain eqn. (2.8)

$$|k\mathcal{E}| \gg \left|\frac{\partial \mathcal{E}}{\partial z}\right| \gg \left|\frac{\partial^2 \mathcal{E}}{\partial z^2}\right|, \quad |\omega \mathcal{E}| \gg \left|\frac{\partial \mathcal{E}}{\partial t}\right| \gg \left|\frac{\partial^2 \mathcal{E}}{\partial t^2}\right|. \tag{2.9}$$

In the next section, we introduce the density matrix formalism and derive the explicit form of the response of the medium to the incident electromagnetic field. We include various decay mechanisms and obtain a set of coupled differential equations that govern the dynamics of this system.

2.1 Semiclassical Treatment of Elementary Light-Matter Interaction

We describe here a general mathematical framework to understand light-matter interaction, where the *field* is considered *classical* and the *atom* has *quantized* energy levels (Semiclassical picture). Such a quantum system (i.e. the atom + field system), can be described in the most general way using the *density matrix formalism* . The usual wave function approach has a limitation of not being tenable to account for spontaneous emission from the excited state to the ground state and the dephasing processes, although decays out of the system can be incorporated. The general formulation of density matrix can account for most relaxation mechanisms like, spontaneous emission, collisions, finite laser line widths and any other damping mechanisms [6].

The physical system is completely characterized by its wavefunction $|\psi\rangle$. To obtain a particular information of the system, we calculate the expectation value (quantum mechanical average) of the corresponding operator O,

$$\langle O \rangle_{qm} = \langle \psi | O | \psi \rangle. \tag{2.10}$$

In most realistic situations we do not know $|\psi\rangle$ completely, we only know that the system is in the state $|\psi\rangle$ with a probability P_ψ. This amounts to taking an ensemble average (statistical average) of large number of similar systems prepared identically,

$$\langle \langle O \rangle_{qm} \rangle_{st} = \text{Tr}(O\rho), \tag{2.11}$$

where, the density operator ρ is defined as

$$\rho = \sum_\psi P_\psi |\psi\rangle \langle \psi|. \tag{2.12}$$

We see from eqns. (2.11) and (2.12), that $\text{Tr}(O\rho) = \text{Tr}(\rho O)$. If for a particular state $|\psi_o\rangle$, $P_{\psi_o} = 1$, and all other $P_\psi = 0$, then $\rho = |\psi_o\rangle\langle\psi_o|$ and the state is called a *pure state* . From conservation of probability $\text{Tr}(\rho) = 1$, and in general $\text{Tr}(\rho^2) \leq 1$ (the equality holds for a pure state). The evolution equation for the density matrix is obtained from the Schrödinger equation,

$$|\dot{\psi}\rangle = -\frac{i}{\hbar} H |\psi\rangle, \tag{2.13}$$

where, the overdot represents first order time derivative. We take the time derivative

of ρ in equation (2.12) and obtain

$$\dot{\rho} = \sum_{\psi} P_{\psi}(|\dot{\psi}\rangle\langle\psi| + |\psi\rangle\langle\dot{\psi}|), \tag{2.14}$$

where, the probability P_{ψ} is time independent, and on using eqn. (2.13) for $|\dot{\psi}\rangle$ and $\langle\dot{\psi}|$ in eqn. (2.14), we get

$$\dot{\rho} = -\frac{i}{\hbar}[H, \rho]. \tag{2.15}$$

The decay terms are added phenomenologically to the above equation in the semiclassical treatment. They can be derived from first principles using the complete quantum picture, where the atom interacts with infinitely many radiation modes of the vacuum [7].

If the incident field is nearly monochromatic and if the frequency of the field coincides with one of the transition frequencies of the atom, then the atom can be approximated to a *two-level system* . In reality no such two-level atom exists but under a coherent near-resonant interaction, the approximation is quite valid. We now derive explicitly the equations of motion of the density matrix for such a two-level system. The typical wavefunction of the atom is

$$|\psi\rangle = C_g(t)|g\rangle + C_e(t)|e\rangle, \tag{2.16}$$

where, $|g\rangle$ and $|e\rangle$ represent the ground and the excited states involved in the near resonant interaction. The unperturbed Hamiltonian is

$$H_o = \hbar\omega_g|g\rangle + \hbar\omega_e|e\rangle. \tag{2.17}$$

where $\hbar\omega_g$ and $\hbar\omega_e$ are the absolute energies of the two levels. The interaction of the radiation field and the atom can be reduced to a simple form in the *dipole - approximation* ($\vec{k} \cdot \vec{r} \ll 1$), here $\vec{k}$ is the wave vector of the incident plane wave at $\vec{r}_o + \vec{r}$, the position of the electron, bound to the force center (nucleus) of the atom located at $\vec{r}_o$. Hence, in the dipole - approximation, i.e. when the field wavelength is much larger than the atomic size, the interaction term is given as

$$H_{int} = -e\vec{r} \cdot \vec{E}(\vec{r}_o, t). \tag{2.18}$$

The explicit form of the plane wave electromagnetic field is given in eqn. (2.6). The *dipole operator* is written as

$$\vec{d} = \sum_{ij} d_{ij}|i\rangle\langle j|, \ i \neq j \tag{2.19}$$

6

where, $i, j = g, e$ for the two-level atom. In eqn. (2.19) d_{ij} is the average of the dipole moment between the states $|i\rangle$ and $|j\rangle$ i.e. $d_{ij} = e\langle i|\vec{r}|j\rangle$. As can be seen, $\vec{d}$ is a vector operator with odd parity, hence there are no diagonal elements in eqn. (2.19). For the two-level atom described by the wavefunction in eqn. (2.16), the density matrix elements are

$$
\begin{aligned}
\rho_{gg} &= \langle g|\rho|g\rangle = |C_g(t)|^2, \\
\rho_{ge} &= \langle g|\rho|e\rangle = C_g(t)C_e^*(t), \\
\rho_{eg} &= \langle e|\rho|g\rangle = \rho_{ge}^*, \\
\rho_{ee} &= \langle e|\rho|e\rangle = |C_e(t)|^2,
\end{aligned}
\tag{2.20}
$$

where, as defined in eqn. (2.12), $\rho = |\psi\rangle\langle\psi|$, with the wavefunction $|\psi\rangle$ of eqn. (2.16). In eqn. (2.20) the *diagonal* terms ρ_{gg} and ρ_{ee} are the probabilities of being in the ground and the excited states, respectively; also termed as *populations* of the corresponding states. For the meaning of the off-diagonal terms, we need to consider the atomic polarization. The atomic polarization $P(\vec{r}_o, t)$, for an atom (at $\vec{r}_o$) can be got by taking the average of the dipole moment operator of eqn. (2.19), as was indicated in eqn. (2.11) for any operator O,

$$
P(\vec{r}_o, t) = \text{Tr}(d\rho) = d_{ge}\,\rho_{eg}(\vec{r}_o, t) + c.c.
\tag{2.21}
$$

Hence, the *off-diagonal* elements determine the *atomic polarization* . We emphasize here that the off-diagonal element ρ_{ge} is the measure of *atomic coherence* . As one can see from its very definition, $\rho_{ge} = |C_g(t)||C_e(t)|e^{i(\phi_g - \phi_e)}$, hence we see that a *definite* phase relationship $(\phi_g - \phi_e)$, between the levels $|g\rangle$ and $|e\rangle$ implies finite atomic coherence, otherwise a random phase term would average out, making the atomic coherence negligible. This terminology comes about, because it is conceptually quite similar to *coherence* in electromagnetic fields, where the longitudinal coherence between two wavetrains can be visualized as a definite phase relationship between them as they propagate, in contrast to the incoherent light, wherein wavetrains tend get *out of step* very often, hence the relative phase between such incoherent wavetrains gets averaged out.

We now derive the equations of motion for the density matrix elements under the evolution of the total Hamiltonian $H = H_o + H_{int}$, given by eqns. (2.17) and (2.18).

The field in the interaction Hamiltonian, $\vec{E}(\vec{r}_o, t)$ acts uniformly on the atom, and in the *dipole approximation* is given as in eqn. (2.6). On using eqn. (2.15) and adding phenomenologically appropriate decay rates, we get the following equations of motion for the density matrix,

$$
\begin{aligned}
\dot{\tilde{\rho}}_{ee} &= -2\gamma\tilde{\rho}_{ee} + i[G\,\tilde{\rho}_{ge} - c.c.], \\
\dot{\tilde{\rho}}_{eg} &= -(\gamma_{eg} + i\Delta)\tilde{\rho}_{eg} + iG\,(\tilde{\rho}_{gg} - \tilde{\rho}_{ee}) \\
\dot{\tilde{\rho}}_{gg} &= 2\gamma\tilde{\rho}_{ee} - i[G\,\tilde{\rho}_{ge} - c.c.],
\end{aligned}
\tag{2.22}
$$

where, $G = \vec{d}\cdot\vec{E}_o e^{i\vec{k}.\vec{r}_o}/\hbar$, and the detuning given by $\Delta = \omega_e - \omega_g - \omega$, is the measure of the mismatch of the applied field frequency from the atomic resonance. The decay term 2γ is the *spontaneous emission rate* or the relaxation rate of the excited state through radiative decay to the ground state. The coherence term $\tilde{\rho}_{eg}$, decays *radiatively* as $\gamma_{eg} = \gamma$, for low density atomic (vapor) systems where only the radiative decay contributes, its also called the natural linewidth of the system. There could be other sources of decay of this coherence term, like the collisional dephasing (Γ^{ph}). Hence, in general $\gamma_{eg} = \gamma + \Gamma^{(ph)}$. The radiative decay (or spontaneous emission) arises due to the interaction of the atom with the *reservoir* with a large number of degrees of freedom. Even in the absence of any photons there are quantum fluctuations associated with the vacuum which can be visualized as a collection of a large number of harmonic oscillators, one for each mode of the infinite set of modes of the vacuum state, coupled to the atom. This coupling leads to the decay, that is energy initially in the atom redistributes itself among these oscillators, leading to damping and thus causing the relaxation of the excited atom to the ground state.

In getting the equations of motion for the density matrix eqns. (2.22), we have undertaken the *rotating-wave approximation*. It involves going into the frame of the field, which is varying at the frequency ω, and neglecting the contributions of the counter-rotating terms which oscillate rapidly as $e^{\pm i2\omega t}$. This is a very good approximation at optical frequencies, where the frequencies involved are $\sim 10^{14}\,Hz$, as the oscillations at 2ω would average out. The rotating-wave approximation in the fully quantized picture is equivalent to neglecting the *energy nonconserving* terms of the kind that involve the atom going from the ground state to the excited state and simultaneously emitting a photon, and the term which involves emission of a photon accompanied by a transi-

tion from the excited state to the ground state. The density matrix elements $\tilde{\rho}$ in eqn. (2.22) are the *slowly varying* quantities, which are related to the original ρ as follows:

$$\tilde{\rho}_{ii} = \rho_{ii}, \text{ for } i = e, g$$

$$\tilde{\rho}_{eg} = \rho_{eg}e^{i\omega t},$$

$$\tilde{\rho}_{ge} = \rho_{ge}e^{-i\omega t}. \tag{2.23}$$

The solution of eqn. (2.22) in the steady state and in the limit of no decay (i.e. $\gamma \longrightarrow 0$) leads to the well known *Rabi oscillation* of the atomic inversion. The atomic inversion is given as

$$\tilde{\rho}_{ee} - \tilde{\rho}_{gg} = \left(\frac{\Delta^2 - 4|G|^2}{\Omega^2}\right)\sin^2\frac{\Omega t}{2} + \cos^2\frac{\Omega t}{2}, \tag{2.24}$$

where, the generalized Rabi frequency Ω is

$$\Omega = \sqrt{\Delta^2 + 4|G|^2}. \tag{2.25}$$

In the special case when the atom is on resonance with the incident field ($\Delta = 0$), eqn. (2.24) reduces to $\cos(2|G|t)$, hence, the inversion oscillates cosinusoidally between -1 and 1 at a frequency Ω. This two-level atom interacting with an electromagnetic field has been discussed in detail in the classic book of Allen and Eberly [8].

In the semiclassical regime, we have seen that without inclusion of the decays, a monochromatic field acting on a two-level atom leads to *Rabi oscillations* of the atomic inversion. In contrast, a complete *quantum* treatment of the two-level atom interacting with a *single mode* of the quantized radiation field leads to certain *collapse* and *revival* phenomenon due to the quantum aspects of the field [9]. There are a host of phenomenon which occur due to the quantum nature of the field, like quantum statistics of fields in micromaser; field trapping states, which occur due to the granular structure of the photon distribution. In this thesis we restrict our discussion to the semi-classical regime.

2.2   Coherent Population Trapping

The arrival of monochromatic and tunable laser sources has seen a revolution in a variety of nonlinear processes. These processes no longer involve merely a two-level

atom with a single monochromatic field. Among the various nonlinear processes, application of two continuous monochromatic fields on a three-level system leads the atom into a *coherent superposition of states* . Under certain conditions, the population is *trapped* in these states, and is stable against absorption from the applied radiation field. This phenomenon is known as *Coherent Population Trapping* (CPT) [10, 11]. This coherent superposition is a *non-absorbing* state, where the atoms' evolution is exactly out of phase with the incoming radiation field, and hence no absorption takes place.

This phenomenon was first observed by Alzetta et al. [12] as the disappearance of fluorescent emission in an optical pumping experiment on sodium atoms. They had used a multimode laser irradiating sodium atoms in a cell, in the presence of an inhomogeneous magnetic field, which led to the creation of an non-absorbing state in only a small region in the cell. It appeared as a dark line inside a bright fluorescent cell and hence is also known as *dark resonance* or *non-absorbing resonance* . At the same time, and independently, the pumping and trapping phenomenon originated by two resonant laser fields in the Λ - system was experimentally demonstrated by Gray et al. [13] in the Sodium atom. They pointed out that the Sodium atoms were pumped into the non-absorbing state due to the presence of interfering processes. Early theoretical analysis also showed the presence of such interfering processes [14] that led to pumping of the atoms into the CPT state. The work of Dalton and Knight [15] contained the main characteristics of the phenomenon, and the complete term *Coherent Population Trapping* was used.

Since then many related phenomenon have been discovered, like lasing without inversion, field induced transparency, pulse matching and the corresponding matched photon statistics. The population trapping state of a Λ-system driven by *quantized* fields was discovered by Agarwal [16] where the manifestation of matched photon statistics was observed. Pulse matching also leads to correlation of high frequency phase fluctuations of the two fields [17] and therefore can be used to *reduce noise* in the short time measurement of phase difference.

The coherent population trapping state involves two fields interacting with a Λ-system. The atom is prepared in a coherent superposition of the two ground states, and this leads to cancellation of absorption, even in the presence of resonant fields.
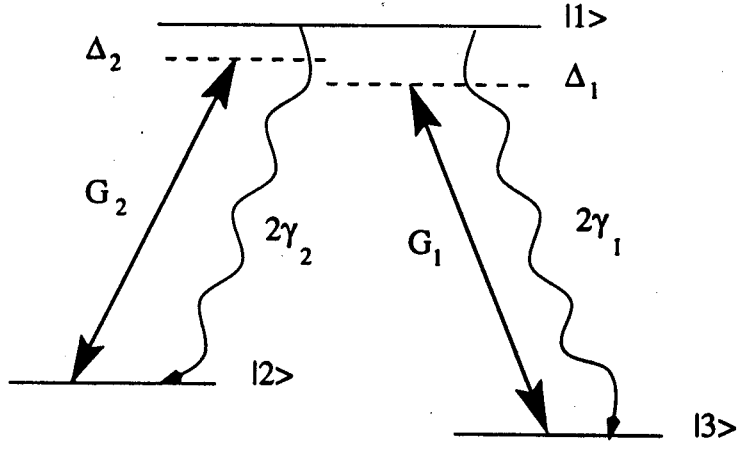
Figure 2.1: A three-level Λ system, interacting with two coherent monochromatic fields G_1 (G_2) which are operating at frequency ω_1 (ω_2), the spontaneous emission rate from the excited state $|1\rangle$ to the two ground states $|3\rangle$ and $|2\rangle$ is $2\gamma_1$ and $2\gamma_2$, respectively.

The total Hamiltonian of the three-level Λ-system, shown in Fig. 2.1, interacting with two monochromatic fields is

$$H = \hbar\omega_{13}A_{11} + \hbar\omega_{23}A_{22} - (\vec{d}_{13} \cdot \vec{E}_1 e^{-i\omega_1 t})A_{13} - (\vec{d}_{12} \cdot \vec{E}_2 e^{-i\omega_2 t})A_{12} + h.c, \qquad (2.26)$$

where A_{ij} is the atomic transition operator $|i\rangle\langle j|$. The energy is measured from the ground state $|3\rangle$ and $\hbar\omega_{13}$ ($\hbar\omega_{23}$) is the energy difference between level $|1\rangle$ ($|2\rangle$) from the ground level $|3\rangle$. Here, $\vec{d}_{ij}$ is the dipole interaction term for the transition $|i\rangle \leftrightarrow |j\rangle$. The transition $|2\rangle \leftrightarrow |3\rangle$ is dipole forbidden. The Rabi frequencies along the two transitions $|1\rangle \leftrightarrow |3\rangle$ ($|1\rangle \leftrightarrow |2\rangle$) is given as $2G_1 = 2(\vec{d}_{13} \cdot \vec{E}_1)/\hbar$ ($2G_1 = 2(\vec{d}_{12} \cdot \vec{E}_2)/\hbar$). We now transform the Hamiltonian in eqn. (2.26) into the time independent form H_I, where $H_I = U^\dagger H U$, where the unitary operator U provides this canonical transformation. This is equivalent to undertaking the rotating wave approximation at the operator level, where the transformed time-independent Hamiltonian is

$$H_I = \hbar\Delta_1 A_{11} + \hbar(\Delta_1 - \Delta_2)A_{22} - \hbar(G_1 A_{13} + G_2 A_{12}) + h.c. \qquad (2.27)$$

We can write the equations of motion of the density matrix using the Hamiltonian eqn. (2.27) on similar lines as indicated in section 2.1, by undertaking the rotating-wave approximation and adding radiative decay due to spontaneous emission from the excited state $|1\rangle$ to levels $|2\rangle$ and $|3\rangle$. We see that at the two-photon Raman condition, i.e.

$\Delta_1 - \Delta_2 = 0$, the Hamiltonian in eqn. (2.27) can be diagonalized such that one of its *eigenvalues* is *zero* and the associated eigenstate is the non-interacting dark resonance. The eigenvector corresponding to it is a specific linear combination of the ground states $|2\rangle$ and $|3\rangle$. The trapping state is given as

$$|\psi_-\rangle = \frac{G_1|2\rangle - G_2|3\rangle}{\sqrt{|G_1|^2 + |G_2|^2}}. \tag{2.28}$$

This state is radiatively stable (there is no spontaneous emission from this state, as its a linear combination of ground states) and is non-interacting with the applied field i.e.,

$$\langle 1|H|\psi_-\rangle = 0. \tag{2.29}$$

Hence, its also called a *non-coupled state* .

This state corresponds to maximum coherence between the ground states, hence the off-diagonal term corresponding to atomic coherence between the two ground states $|\rho_{23}| = 0.5$, and in the steady state the population is completely trapped in these states i.e. $\rho_{22} = \rho_{33} = 0.5$, whereas the excited state is empty, $\rho_{11} = 0$. Moreover, all the other off-diagonal elements, $\rho_{12} = \rho_{13} = 0$, leading to zero absorption even in the presence of near-resonant fields. These aspects of the coherent population trapped state i.e. the zero absorption accompanied with maximal coherence has been exploited in a range of applications like high resolution spectroscopy, nonlinear optics, laser cooling, adiabatic transfer, etc. We briefly discuss only a few of these effects.

2.3 Adiabatic Transfer

There has been a lot of interest in finding ways of inverting population across multiple levels. The CPT phenomenon can be utilized to this end, on observing eqn. (2.28), we see that by adiabatically turning *on* and *off* the fields G_1, G_2 we can achieve the desired effect. If we consider the case, in which we start with the atom in the ground state $|3\rangle$ and $G_2 = 0$, with G_1 finite and then proceed to turn G_1 *off* while turning G_2 *on* , we will end up with the atom in state $|2\rangle$. Initially, the atom need not be in the CPT state, but by the continuous action of the fields accompanied with spontaneous decay, it could be forced into that state. Then the atom would stay in the state $|\psi_-\rangle$, if the fields are varied slowly enough (adiabatically) [18]. In the above method, the

timing and overlap of the two pulses is crucial. The intermediate state experiences substantial population when both the pulses overlap, which can reduce the efficiency of the transfer drastically if the intermediate level has finite decay. This problem is overcome by applying counterintuitive pulse sequences, where the pulse G_2 is applied ahead of G_1. This results in $\sim 100\%$ population transfer, without the intermediate level experiencing any transient population.

In both these kinds of mechanisms, its critical that the intermediate state is empty. We propose another method, using the new trapping states discussed in chapter 3. In our proposal the population of the intermediate state remains *unaffected*, this alleviates a severe restriction of the usual adiabatic method of creating inversion across multiple levels. We use cw excitation, this further simplifies the requirement of careful timing of the pulses. We discuss the details of our proposal in chapter 4.

2.4   Electromagnetically Induced Transparency

Electromagnetically Induced Transparency (EIT) [19] is the modification of the absorption profile of an atomic transition, when the upper level is coherently coupled to a third state by a strong laser field. Under the right circumstances, the absorption of the weak, resonant probe beam will be substantially reduced, see for example Fig. 2.3 (a). In effect, EIT is a technique of *eliminating* the effect of medium on a propagating beam of light. Its been used in a wide variety of applications like eliminating self - focusing or defocusing, to improve transmission through inhomogeneous refracting gases and metal vapor [20] creating large populations of coherently driven uniformly phased atoms. Many of the experiments on EIT by the group of Harris, have been performed on Lead vapor, we show in Fig. 2.2 the relevant levels of Pb and the transitions involved. These coherently prepared atoms have also been utilized in other applications, like modifying the index of refraction, isotope discrimination, nonlinear optics, spontaneous emission noise quenching, pulse matching etc.

In the classical picture, the contribution to the dielectric constant of the medium at the applied frequencies is due to the electronic motion at those frequencies. One can reduce this contribution by driving the electron by two identical sinusoidal forces acting exactly out of phase, which would result in non-movement of the electron. In

$6s^2 6p\, 7s\, {}^3P_1$

$|1\rangle$ ———————

$\lambda_2 = 406\,nm$

$\lambda_1 = 283\,nm$

$6s^2 6p^2\, {}^3P_2$

$|2\rangle$ ———————

$6s^2 6p^2\, {}^3P_0$

$|3\rangle$ ———————
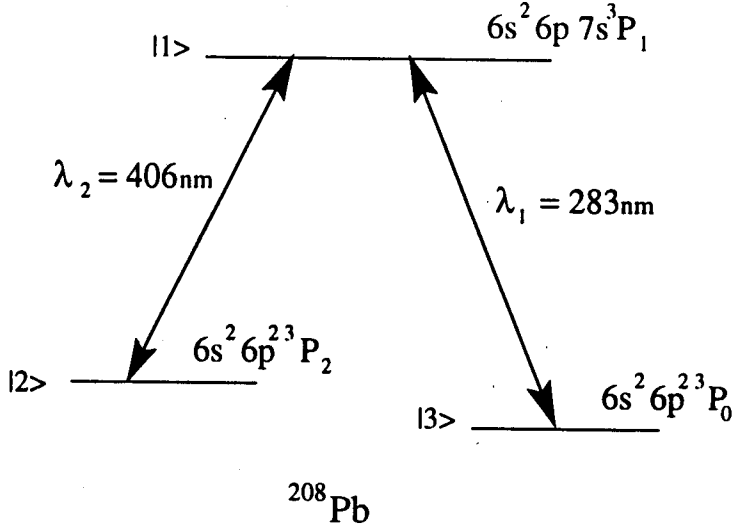
${}^{208}Pb$

Figure 2.2: Schematic of the relevant levels of ${}^{208}Pb$, on the $|1\rangle \leftrightarrow |2\rangle$ transition the pump field is applied, whereas the probe is applied on the $|1\rangle \leftrightarrow |3\rangle$ transition.

quantum mechanical terms, for a typical Λ-system (Fig. 2.1) the probability amplitude of the electron being in excited state is driven by two terms of equal magnitude and opposite phase (sign). One driving term is proportional to the probability amplitude of one ground state (say, $|3\rangle$) and the other term is oppositely phased and is proportional to probability amplitude of the other ground state ($|2\rangle$). These driving terms lead to *complete cancellation* of the probability amplitude of the electron being in the excited state and the expectation value of the sinusoidal motion at each applied frequency is zero.

The first experimental demonstration of EIT was by the group of Harris [21, 22] in optically opaque Strontium vapor. The correspondence between the Λ system of Fig. 2.1 and the three-levels of Strontium vapor was $|1\rangle \rightarrow (4d5d\,{}^1D_2)$, $|2\rangle \rightarrow (4d5p\,{}^1D_2)$ and $|3\rangle \rightarrow (5s5p\,{}^1D_2)$, the field coupling the $|1\rangle \leftrightarrow |2\rangle$ was at 570.3 nm, whereas the probe field at $|1\rangle \leftrightarrow |3\rangle$ transition was at 337.1 nm. The absorption linewidth was broad, as the excited state $(4d5d\,{}^1D_2)$, was chosen so as to lie ($\sim 45926\ cm^{-1}$) above the first ionization threshold of Strontium, so that the decay is much faster through autoionization, than through the radiative channel. On applying a strong monochromatic laser coupling this excited state to another ground state resulted in enhanced transmission ($\sim 40\%$), in contrast to the earlier e^{-20} kind of extinction due to absorption in the medium. The

14
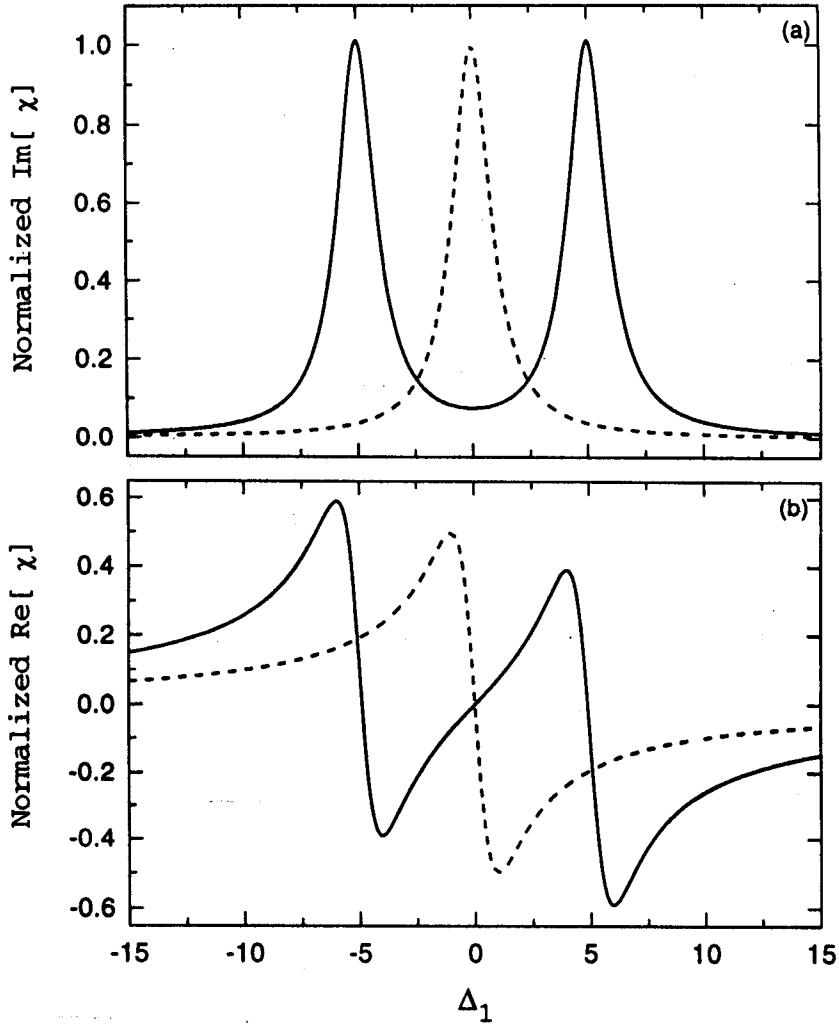
Figure 2.3: (a) Imaginary and (b) real parts of the susceptibility of the probe ω_1 in presence of a strong coupling field ($G_2 = 5\gamma$) at ω_2. The dotted curves are in the absence of the coupling field. Normalization is to the peak value of the imaginary part of susceptibility.

physical effect that is of essence in EIT is the CPT phenomenon. The most essential feature being that unlike the two-level atom, in the multi-level scheme one can create coherence to tailor the atomic response, in other words, absorption and emission line shapes of an atom need not be the same.

Observation of this *quantum interference* effect between dressed states in EIT was done on a three-level Λ-system in *Rb* vapor. Even on reduction of the Rabi frequency of the coupling laser below the spontaneous decay rate of the common excited state (so that there is no Autler-Townes splitting), a narrow dip with sub-natural linewidth in the absorption curve of the probe was observed [23]. This clearly demonstrated that

15

the absorption reduction at low pump intensity was due to *interference effect* between the dressed state, not due to ac-stark shift of the atomic levels.

The *dispersive properties*, of the transition that was made transparent exhibits a *rapidly varying refractive index* and also *zero group velocity dispersion* at the line center, see Fig. 2.3 (b). The slope of the $Re\ [\chi]$ determines the group velocity, not the magnitude of $Re\ [\chi]$ (which is zero at the line center). The group velocity is proportional to real part of $(\partial \chi / \partial \omega)^{-1}$, whereas the group velocity dispersion is given by the higher order derivative, namely the real part of $(\partial^2 \chi / \partial \omega^2)$. This was reported by Harris et al. [24] where they observed slow group velocity of $c/250$ at EIT. The dispersion line shape distortion was confirmed by Xiao et al. [25] for a ladder system in Rb vapor. They reported the first experiment with *inhomogeneous broadening* with cw diode lasers continuously tunable over a wide range of frequencies. They modeled the experiment with the inclusion of Doppler broadening and the finite line widths of the diode lasers. They observed 66.4 % reduction in absorption at EIT, limited only by the laser line width and the finite lifetime of the uppermost level, which was coupled with a strong laser to the excited state of the probe transition.

The temporal and spatial dynamics of propagating EIT pulses in an optically thick medium was done by Kasapi et al. [26] where they got pulse velocities of $c/165$ with 55% transmission in Pb vapor. They also observed strong-probe-field effect, where they observed reshaping of the coupling pulse with the probe pulse, and the subsequent propagation of this pulse pair. The EIT transmission was found to be near diffraction-limited in an otherwise, highly distorting medium. They also developed an interesting method of measuring the Lorentzian line shapes, by merely measuring the energy of the input and the transmitted pulse and its propagation delay [27] without requiring the exact knowledge of the laser frequencies, atomic density or the matrix elements governing the transition.

There have been numerous other demonstrations of EIT in various systems. EIT in laser cooled Rb atom in Λ-system with detailed experimental results was done by Hopkins et al. [28]. Comparison of V, Λ and the Ξ system was done in the presence of Doppler broadening by Fulton et al. [29]. In a Doppler broadened medium the EIT

position shifts across the velocity groups v, such that for the Λ system

$$\Delta_1 = (k_1 \mp k_2)v + \Delta_2, \qquad (2.30)$$

where $\Delta_1(\Delta_2)$ is the detuning of the probe (coupling) laser frequency from the atomic transition frequency, and $k_1(k_2) = 1/\lambda_1(1/\lambda_2)$. The $-$ sign in eqn. (2.30), is for copropagating beams, whereas, the $+$ sign for the counterpropagating beams. Hence, in the *perturbative limit* , if $|k_p| = |k_c|$, then for the copropagating geometry the position of resonance is same for all the velocity groups and the medium can be considered *nearly* Doppler free. Whereas, in EIT one generally has a strong coupling laser which leads to residual Doppler broadening. One assumes a Maxwell-Boltzman distribution for the atomic velocities such that the probability distribution function is given as

$$p(\Delta_1) = \frac{1}{\sqrt{2\pi D^2}} e^{-\Delta_1^2/2D^2}, \qquad (2.31)$$

where, D is the width of the Gaussian.

The peaks due to the strong coupling field G_2, in Λ system of Fig. 2.1, are located at $\Delta_1 = \Delta_2/2 \pm \sqrt{(\Delta_2/2)^2 + |G_2|^2}$ (see Fig. 2.3 (a)). The net widths due to Doppler broadening in presence a strong coupling field have been calculated analytically in [30] in the copropagating geometry and are given as

$$\beta = \frac{\gamma_1 + \gamma_2 + D}{2} \left(1 \mp \frac{\Delta_2}{\sqrt{\Delta_2^2 + 4|G_2|^2}} \right), \qquad (2.32)$$

at the two ac-Stark shifted peaks. Its is clear from eqn. (2.32), that for nonzero Δ_2, one of the peaks is much narrower than D, where as the other peak is correspondingly broader, hence, by controlling the parameters of the coupling field like Rabi frequency G_2 and its detuning Δ_2, one can manipulate the linewidth of the $|1\rangle \leftrightarrow |3\rangle$ transition to obtain *sub - Doppler* resolution.

The wavelength matched enhancement in EIT was discussed by Shepherd et al. [31]. It involves proper choice of relative wavelengths of the coupling and the probe field such that, it would result in reduced residual Doppler line width. The wavelength dependence between the probe and the coupling laser wavelength was studied in Doppler broadened cascade system, where it was found that the best overall transparency for Rabi splitting less than the Doppler width was for coupling laser wavelengths *less* than that of the probe. Another interesting effect is that, for a probe with

finite linewidth only the frequency components that satisfy the two-photon condition with the given linewidth of the coupling laser, experience transparency. It was experimentally demonstrated that the filtered probe field is *locked* in frequency relative to the coupling field [32].

Recently, EIT in an *ideal* Λ-system was for the first time demonstrated in *Rb* by Li and Xiao [33] where they observed 85% reduction in the absorption, at room temperature in the Doppler free geometry. The EIT ideas have been extended to the case where the excited state is a continuum [34], and even to detuned multistate systems [35].

Among the many application of EIT, recently Kasapi [36] demonstrated enhanced isotope discrimination of 0.03 % of ^{207}Pb, seen clearly in the back ground of ^{208}Pb. The dominant species (^{208}Pb) is rendered transparent using EIT (at the two-photon condition). The other species (^{207}Pb) has slightly shifted energy levels hence does not show EIT. This discrimination is further increased in the other species (^{207}Pb). The Rabi frequency of the coupling laser is so adjusted such that the ac-Stark shifted level *matches* with the probe field, thus rendering it *opaque* leading to a significant discrimination of the two species.

There a few limitations / conditions in obtaining EIT, firstly, the number of photons in the coupling transition should exceed the product of the number of atoms or molecules in the laser path times the ratio of the oscillator strengths of the probe and the coupling transitions [37], secondly the peak powers of the lasers should be large so that the EIT width exceeds the linewidth of the Raman transition. Lastly, in order to maintain EIT while using pulses its important to operate within the dephasing time of the Raman transition. Most of the schemes discussed above deal with ideal three level systems (like in Fig. 2.1), if the excited state is in the continuum transparency does not work quite as well [34, 38]. Schemes of obtaining EIT with many lower states being populated as in molecules is still a challenge (till date).

As we have observed earlier, the peak power of the lasers must be sufficient such that the transmission width of EIT should exceed the linewidth of the Raman transitions. Such a requirement on the power of the lasers in solid state systems leads to breakdown of the material, due to exceedingly broad transitions in solids. The first demonstration of EIT in solid was by Zhao et al. [39] in Ruby. They used a magnetic

field to create closely spaced lower levels. These levels were coupled by a microwave field at 16.3 GHz frequency and 0.1 μs pulse width. The Ruby sample was cooled to 2.4 K at liquid Helium temperature. They observed 20 % reduction in the absorption. Recently, there has been another experimental demonstration of EIT in solid - rare earth doped crystal [40]. They observed 100% transmission of the probe field due to EIT in an optically dense Pr^{3+} doped Y_2SiO_5 at 5.5 K. They used three beams derived from the same dye laser at various frequencies through acousto-optic modulator, one was the coupling field, the probe field and the repump field which recharges the holes burnt by the coupling and the probe laser. The ground state linewidth was 30 KHz and power levels of $\sim$ 1000 W/cm^2 were sufficient for achieving EIT with the corresponding powers of the probe and repump fields as 14 and 11 W/cm^2, respectively. Efficient EIT in rare-earth doped crystals would open up exciting potential applications such as high-resolution non-linear optical image processing, high efficiency signal processing, optical data storage and LWI at ultra-violet frequencies in solids.

2.5   Enhancement of Nonlinear Optical Effects

Nonlinear optics on coherently prepared atoms has ushered in a new era of highly efficient nonlinear processes. There have been many experiments where nonlinear processes like sum frequency generation, optical phase conjugation through four wave mixing, vacuum ultra-violet (VUV) and extreme ultra violet (XUV) radiation generation under *coherent preparation* of the active medium, typically gas (atomic vapor) have shown dramatic enhancement in their efficiencies. The important advantage of using gas over a solid medium, as the nonlinear medium, is the *sharp resonance enhancement* of the nonlinear optical susceptibility which can overcome the disadvantage arising from low number density of gas compared to a solid. However, the generated field at resonance also experiences large linear absorption, which seriously limits the conversion / generation efficiency of the nonlinear process. The main limitations at resonance arise due to strong resonant absorption and phase mismatching.

Many of these problems have been addressed by various groups. Tewari and Agarwal [41] showed that strong fields can *modify* the phase matching conditions using additional fields, and thus control the nonlinear generation process more effectively.

The efficiency of generation depends on the ratio $\chi^{(3)}/\text{Im}(\chi^{(1)})$. The linear response $\chi^{(1)}$ can be drastically modified using the strong control field, which could lead to complete suppression of absorption ($\text{Im}(\chi^{(1)})$) and even a change in the sign of linear dispersion ($\text{Re}(\chi^{(1)})$). Amplification of fundamental together with EIT can be used to enhance VUV generation [42]. Tremendous possibilities exist for enhancing nonlinear signals by judicious choice of control field parameters like strength and frequency. Harris et al. [43] proposed that by coupling the excited state to a metastable state using additional coherent field, the nonlinear susceptibility $\chi^{(3)}$ (third harmonic generation) can be *enhanced* through *constructive interference*, while at the same time the linear susceptibility is made *negligible* by *destructive interference*. The comparison between the efficiencies of both these proposals [41, 43] was done in Ref. [44] where they found that these large efficiencies arise from the same mechanism. The efficiencies were found to be *same*, if the four-photon line width of Ref. [41], and two-photon line width of Ref. [43] was chosen same, along with two-photon resonance condition. The first experimental demonstration of enhancement of VUV using a control laser was done by Jain et al. [45].

Recently, Harris and Jain [46] proposed an optical parametric oscillator pumped by population-trapped atoms. The oscillator is based on enhancing the second order nonlinear susceptibility to the *same order* as the linear susceptibility. They obtained gain in a single coherence length, thus taking care of the limitations posed by phase matching condition. The gain bandwidth exceeded the degenerate frequency of the signal and idler. For *Pb* vapor, the calculated gain maximized at 1.88 μm with bandwidth of $\sim 7500\ cm^{-1}$. Again the main point in all these various processes is to utilize effects of quantum interference and atomic coherence to our needs.

In the recent past, series of experiments by Hakuta et al. [47, 48, 49, 50] in atomic hydrogen have utilized coherent preparation of the active medium. Resonantly enhanced second-harmonic generation accompanied with reduced absorption was achieved by coupling the 2s state and the 2p state of Hydrogen using an electric dc field [47]. Zhang et al. [48, 49] demonstrated nonlinear optical sum-frequency generation using EIT by applying a strong coupling laser on the 2s-3p transition. The coupling laser made the Lyman-β (3p-1s) transition *transparent* (due to destructive interference), which led to

continuous growth of the 103 nm Lyman-β (VUV) radiation, without suffering resonant absorption and phase mismatching. Whereas, the two-photon coupling of 1s-2s state produces the required constructive interference to *resonantly enhance* the sum-frequency generation at the Lyman-β transition. Along the similar lines, Zhang et al. [50] demonstrated generation of XUV by using EIT. They obtained radiation in the range of 97.3 - 92.6 nm from coherently coupling the 1s-np transition (n=4-8) in Hydrogen atom. A strong pulsed radiation was used to couple the 1s-np transitions, the generation efficiency was found to be limited only by the availability of the coupling laser power to create EIT.

Recently, Hemmer et al. [51] observed unusually efficient optical phase conjugation (OPC), by utilizing the CPT phenomenon. They showed that CPT can write large-amplitude nonlinear-optical gratings at much lower intensities than required to saturate the optical transitions. The conventional limitations in OPC were because of slow response and/or low efficiencies of the existing nonlinear optical materials at laser intensities achievable with compact cw lasers. Typically, fast response in sodium vapor was observed but with pump powers of 100 W/cm^2. In this experiment, they demonstrated high-efficiency OPC signal (an order of magnitude higher), for pump intensities of 1 W/cm^2 with a response time of 1 μs. Grove et al. [52] demonstrated *high gain* (~ 30) and *low spatial distortion* simultaneously, for the OPC signal in the same system. They also observed high degree of intensity-noise correlation between the amplified probe and the conjugate signal.

Another experiment by Jain et al. [53] utilizing the maximal atomic coherence of the CPT state for efficient nonlinear frequency conversion to the ultraviolet, obtained an efficiency of $\sim 40\%$. The details of which will be discussed in chapter 6. We describe a nonperturbative treatment for this nonlinear generation. We obtain explicit form of the lineshape (in the perturbative regime) and obtain enhancements of the order of $\sim 10^2$ and more at CPT. We also find that, in a thick medium, even in the presence of *strong probe* , pulse matching occurs. In chapter 6, we describe in detail all these non-perturbative effects in the generation of optical signals.

2.6 Quantum Interference and its Various Manifestations

We have seen that coherent preparation of various atomic states using coherent fields, can under certain conditions, lead to atomic coherence that can *cancel* absorption. These non-absorbing resonances due to atomic coherence and interference has led to some interesting effects like the ones we have discussed in sections 2.2, 2.4, 2.5, there have been other unexpected consequences like, lasing without inversion, enhancement of refractive index accompanied with vanishing absorption and quenching of spontaneous emission. These effects arise primarily due to interplay of coherence created within the atomic system. The coherent fields acting on various atomic transitions create *definite phase relationships* between various *atomic states*, thus preparing the system in a coherent superposition of states.

All these phenomenon are usually accomplished in a three-level atomic system in which there are *two coherent routes* along which the population can be absorbed, these *pathways interfere* either destructively or constructively and lead to these interesting effects. These interference effects are generally attributed to interference between dressed states [54, 22]. In many of these proposals a strong field is applied, which one might say shifts the position of the levels and the absorption will then be proportional to (shift of the dressed states from the original bare levels)$^{-2}$. However, it has been established in the Λ-system, that the absorption minima is due to *interference effect* [23] where the minima persists even when the applied field is not strong enough to create dressed states, which in the weak field case are not significantly shifted from the bare atomic resonances.

We present in this section, an interesting viewpoint to understand these quantum interferences as an interplay of contributions from various *line shapes* , as shown by Agarwal [55]. We describe here in brief the underlying physics. The line shapes of these systems consists of four different contributions, two *Lorentzian* contributions corresponding to the absorptive process, and two *dispersive* contributions arising from dispersion (frequency dependent field velocities inside the medium). The absorptive contributions are generally positive, whereas the dispersive contributions could either be positive or negative. In the region of the dressed states, created due to the strong field, the probe field absorption line shape is dominated by only one contribution, the

Lorentzian located at the dressed state; whereas at the bare atomic resonance *all four* contributions are *significant* . Hence due to this a negative dispersive contribution to the line shape leads to destructive interference, whereas a positive contribution will lead to constructive interference. It is to be noted that the absorptive contributions to the dressed states are not independent of each other, and this inter-dependence is provided by the dispersive terms. One can derive these line shapes in the perturbative limit (i.e. to first order in the weak probe and to all orders in the coupling field), using the density matrix equations for the specific system. We now give explicitly the line-shape for the Λ-system (Fig. 2.1), which has been extensively studied in this thesis. For a strong field resonantly coupling the transition ($\Delta_2 = 0$) that is initially empty, and a weak probe coupling the ground state (i.e. $G_2 \gg G_1$), the absorption can be written as

$$A = Re \frac{(\Gamma_{23} + i\Delta_1)\Gamma_{13}}{G_2^2 + (\Gamma_{13} + i\Delta_1)(\Gamma_{23} + i\Delta_1)}. \tag{2.33}$$

In writing eqn. (2.33) we have ignored the constant factors that are not pertinent to our discussion here. From the point of view of various line shapes contributing to the absorption A, we have the two Lorentzian contributions $\mathcal{L}_\pm$ at $\Delta_1 = \pm G_2$ as,

$$\mathcal{L}_\pm = \frac{1}{\pi} \frac{\frac{\Gamma_{13} + \Gamma_{23}}{2}}{(\Delta_1 \mp G_2)^2 + \left(\frac{\Gamma_{13} + \Gamma_{23}}{2}\right)^2}, \tag{2.34}$$

and the dispersive contributions $\mathcal{D}_\pm$ at $\Delta_1 = \pm G_2$ as,

$$\mathcal{D}_\pm = \frac{1}{\pi} \frac{\Delta_1 \mp G_2}{(\Delta_1 \mp G_2)^2 + \left(\frac{\Gamma_{13} + \Gamma_{23}}{2}\right)^2}. \tag{2.35}$$

The absorption A, can be written using eqns. (2.34) and (2.35), as

$$A = \frac{\Gamma_{13}}{2}(\mathcal{L}_+ + \mathcal{L}_-) + \frac{\beta\Gamma_{13}}{2G_2}(\mathcal{D}_+ - \mathcal{D}_-), \tag{2.36}$$

where, the factor β is the *measure* of interference produced, which in this case $\beta = (\Gamma_{13} - \Gamma_{23})/2$. The decays $\Gamma_{13} = \gamma_1 + \Gamma_{13}^{(ph)}$ and similarly, $\Gamma_{23} = \Gamma_{23}^{(ph)}$, where $\Gamma_{ij}^{(ph)}$ represent the contributions due to collisions which lead to dephasing between the states $|i\rangle$ and $|j\rangle$; and $2\gamma_1$ is the spontaneous decay rate of the excited state $|1\rangle$ to the ground state $|3\rangle$. The transition $|2\rangle \leftrightarrow |3\rangle$ is not dipole allowed, hence there is no radiative decay involved between these states. We see that when there is no dephasing (i.e. $\Gamma_{23} = 0$) then the absorptive and dispersive contributions cancel each other completely at the

23

line center ($\Delta_1 = 0$) leading to an *absolute* zero in the *absorption* profile. We have seen that the interference effect and the associated atomic coherence has tremendous possibilities, which we have exploited in a variety of applications in chapter 5 and 6.

Another novel manifestation of quantum interference was proposed by us in the *control of two-photon transition probabilities* [56]. We presented a scheme for the control of two-photon transition probability by applying a control laser that couples the intermediate state to another level, leading to interference between various pathways. This strong coupling results in a dressed state doublet which gives rise to two pathways for the two-photon transition instead of an unique pathway due to the previously single intermediate level. We gave a simple physical picture using the Fermi-Golden rule for the two-photon transition. We found that one could either *enhance* (due to constructive interference) or *inhibit* (due to destructive interference) the two-photon transition probability by merely changing the strength and detuning of the control field. We found that the interference minima that causes inhibition of the two-photon transition is quite robust against Doppler broadening. We also calculated enhancements of the order of $\sim 10^2$, even in the presence of Doppler broadening, for typical parameter values of *Rb* vapor in the Doppler free geometry (section 2.4).

The quantum interference effect discussed above arise within each atom in a dilute medium. There is no coherence between various atoms and the absorption is directly proportional to the density of atoms. We have studied the effects of quantum interference in the *cooperative phenomenon* of *optical bistability* in chapter 5. In such cooperative phenomenon the atoms tend to act in unison leading to a co-operative behavior. Optical bistability occurs only above a certain critical value of the co-operative parameter. This parameter depends on the atomic sample (absorption coefficient × length of the sample), as well as the positive feedback of the cavity (transmission coefficient of the mirrors) that is essential for optical bistability.

The co-operative behavior is best described in the phenomenon of superradiance [57] where the rate at which each atom radiates is significantly influenced by the presence of all the other atoms. Hence if several atoms are very close to each other then, each one has to work against the radiation reaction produced not only by its own field, but also by the fields of its neighbors. This results in enhanced decay rate, so that it

loses energy more rapidly than it would on its own. It could also under certain conditions lead to inhibition of the decay. These cooperative features manifest themselves in the spectrum of the radiated field in optical bistability, where in the lower branch the spectrum of the transmitted light is narrower than the natural line width (due to the co-operative effect), whereas in the upper branch the atoms radiate more or less independent of each other leading to broad spectrum, and beyond the first threshold the spectrum is three peaked similar to the fluorescence spectrum of an atom driven by a strong coherent field.

We have used the effects of quantum interference to control the threshold of switching in *optical bistability* , we describe this phenomenon in detail in chapter 5. We study both the ladder and the Λ-system, where, by applying a control field, that does not circulate in the cavity, we effectively control the various characteristics of optical bistability. We also obtained multistable behavior by merely changing the parameters of this control field.

We next present a brief discussion of the various other manifestations of quantum interference phenomenon, like spontaneous emission noise quenching, lasing without inversion, modification of refractive index. Though these processes are not directly dealt with in relation to our present work, we mention them for completeness, and, also because the underlying features of these phenomenon run all through in relation to those specific processes discussed in the thesis.

2.7 Quantum Interference induced Quenching of Spontaneous Emission

In this section we deal with another aspect of quantum interference, which is *spontaneous emission reduction or cancellation* (equivalently - population inversion without emission). Way back in 1974, Agarwal [7] first found drastic changes in the spontaneous emission in a V - system with degenerate excited states. It was found that for initial population in one of the excited states, the population in the steady state gets trapped equally in an unsymmetrized combination of the excited states and the ground state. This was primarily due the quantum interference effect. More recently

there has been a renewed interest in this direction, Harris [54] in 1989 pointed out the suppression of autoionization in a three-level system, when the upper two levels were degenerate. Scully et. al. [58] extended this idea to the non-degenerate case. They considered the emission process into a single mode, and predicted cancellation of spontaneous emission from the non-degenerate levels into this mode. The decay process was out of the system. Recently, Zhu and Scully [59] further studied spontaneous emission quenching from two non-degenerate levels, while also including the decay from the excited state to the ground state. This general result takes into account the interaction of the vacuum modes with all the transitions of the three-level atom.

In these two systems of Refs. [54, 58] the essential idea is to create atomic coherence by a driving field such that it leads to cancellation of spontaneous emission. The main conditions for achieving this are, the dipole moments of the two upper levels for spontaneous emission and the corresponding dipole moments of the driving field coupling to the fourth level should be parallel or antiparallel. Spontaneous emission cancellation is observed if the the ratio of the decays of both the levels is equal to the ratio of the Rabi frequencies of the driving field of both the transitions to the fourth level. All these conditions are satisfied in Sodium dimers, where Xia et al [60] *experimentally* observed spontaneous emission cancellation. They observed complete depression of the spontaneous emission peak, and at the *same time* they experimentally showed that considerable amount of population is present in the upper pair levels.

Spontaneous emission noise in Lasers without population inversion was compared for various systems by Agarwal [61] like in the Λ-system, the two-level system driven by strong pump and a weak probe, and systems with externally pumped dressed states and also the autoionizing states. He found substantial reduction of the linewidth of such lasers as compared to the linewidth of conventional lasers. Hence there is not only reduction in spontaneous emission but also narrowing of the linewidth (also called *subnatural linewidth*). Narducci et al. [62] had predicted narrowing of the linewidth in a V system driven by one strong and one weak field. This was experimentally observed by Zhu et al. [63]. Line narrowing in ladder systems was reported by Zhu et al. [64]. Agarwal [65] demonstrated in Λ-system that this quenching is due to dispersive contributions to the lineshape.

Another technique of controlling spontaneous emission noise is to create and utilize coherence induced *correlations* in the atomic system. The origin of the laser linewidth is due to the random diffusion of phase, which arises due to addition of spontaneously emitted photons with random phases to the laser field. Its possible to eliminate the spontaneous emission noise in the relative linewidths, by *correlating* the spontaneous emission events via atomic coherence. Lasers operating via such phase coherent atomic ensemble are known as *correlated spontaneous emission lasers* . It has been realized experimentally [66].

2.8 Lasing Without Inversion

Since the advent of laser in 1962, there was almost an universal acceptance of the fact that *population inversion* was the essential *key* to *lasing* . It was only about 20 years later that the first proposal of lasing without population inversion was made by Harris [54]. He undertook a semiclassical analysis of a three-level system where the upper two levels were lifetime broadened and could decay by autoionization to the same continuum. It was found that the stimulated emission and absorption line shapes were *different* . This was due to the Fano [67] type *interferences* which arise due to the coupling to the continuum. The complete quantized treatment of the same system was undertaken by Imamoglu [68]. Another scheme was suggested by Scully et al. [58] where the three-level atoms pass through a resonant cavity and interact with the same monochromatic field at both the optical transitions, creating the desired coherence. There were other schemes [69] where atoms interact with periodic train of ultrashort pulses (at such a repetition rate R, so that $\omega_{23} = q\,R$, where q is an integer) to create coherence between the two low lying states of a Λ-system (Fig. 2.1). In all these schemes, its the combination of externally created *atomic coherence* (using either coherent fields or coupling to the same continuum) and *interference effects* , which leads to gain without population inversion.

Among these various schemes there has always been a search for determining whether the gain mechanism is due to some kind of *hidden inversion* in an appropriate set of basis states or a *purely coherence effect* . Origin of gain has been discussed by Agarwal [70] where it was found that in the system proposed by the group of Harris

[71] the gain was due to coherence effect, whereas schemes due to Scully et al. [58] the initial coherence led to appropriate inversion between the lasing levels. Hence, generally speaking, LWI could be classified into two categories, firstly, LWI in *any state basis* , and secondly, LWI in *bare state basis* , but inversion in hidden (dressed) state basis. One can usually distinguish these two mechanisms by the spectrum of their gain profile. In the first case, the coupling laser near resonance on another transition creates the desired coherence and the gain on the lasing transition appears on the line center (which without the coupling laser would correspond to absorption maxima) [71, 72]. The schemes involving the inversion in the dressed state generally involve strong coupling laser detuned from resonance and asymmetrical gain feature occurring on one of the Autler-Townes doublet transitions [73, 74, 75]. Zhu and Lin in Ref. [75] obtained steady state sub-Doppler amplification in coherently pumped *Rb* atoms, due to LWI in the bare state basis but with inversion in the dressed states. This scheme was same as proposed by Imamoglu et al. in Ref. [71].

The very first experimental report of *lasing without inversion* was by Zibrov et al. [76]. They used inversionless gain of the *V* system to demonstrate LWI. They observed inversionless amplification of weak probe in *Rb* vapor using low power cw diode lasers, they verified the absence of inversion and finally obtained noninversion laser oscillation in a cavity. Two sublevels of the ground state were coupled to a pair of excited states via three fields, one strong driving, one weak probe, and the third incoherent pump to partially undo the effect of optical pumping to one of the ground sublevels. They observed a gain of 8 - 16 % per pass. They *confirmed* the interference / coherence effect by increasing the linewidth of the probe laser, which led to disappearance of the amplification peak. They finally observed self-generated laser oscillation in a ring cavity, when the inversionless gain medium was placed in it. Unlike the previous experiments, where the CPT state was used - which meant inversion in the dressed state basis, in the *V* system the cancellation of absorption is purely due to *quantum interference* . Alternatively, it could be viewed as a result of Fano-type interferences between the dressed states [73, 77, 78].

Continuous wave (cw) amplification and laser oscillation without population inversion was observed for the first time, in the Λ system within the D_1 manifold of

the Sodium atom, by Padmabandu et al. [79]. They used atomic beam as the lasing medium and the essential idea was the use of EIT in combination with optical pumping. The scheme was close to what was suggested by Imamoglu et al. [71]. For detailed reviews on LWI see Refs. [80, 81, 82].

Recently, there have also been other experiments where gain has been observed without the associated conventional population inversion. In the time dependent transient regime, Fry et al. [83] observed amplification without inversion (AWI) at CPT in Sodium. Other transient regime experiments in AWI are discussed in Refs. [84, 85, 86]. These experiments not only observed amplification, but established unequivocally the *absence of population inversion* at the same time [83, 86].

2.9   Modification of Refractive Index

Quantum coherence and interference have led to many new techniques in nonlinear optics. The index of refraction of a gaseous medium can reach large values at optical frequencies (at $\Delta \approx \gamma$), but the price one pays for such high dispersion is the accompanying high absorption which is of the same order. But utilizing principles of atomic coherence and quantum interference one can *cancel absorption* at certain frequencies near the atomic resonance and *simultaneously increase the index of refraction* .

Scully [87] first proposed that if atoms are initially prepared in a coherent superposition of ground (or excited) state doublet, then under appropriate conditions it can lead to large resonant enhancement of the refractive index accompanied with vanishing absorption. In this system without any population in the excited state, the absorption cancellation coincided with vanishing refraction (though with a large slope [88]), but by providing a small fraction of atoms in the excited state, absorption vanishes away from resonance where the corresponding index of refraction is quite large.

Since then there have been a host of other proposals that exploit the idea of quantum coherence dramatically modifying the susceptibility of the medium. In real experiments coherence degrading processes like Doppler broadening and collisions need to be taken into account. Fleischhauer et al. [78] demonstrated cancellation of absorption and high refractive index in a variety of schemes, and particularly the Raman system (a coherently driven scheme) which is less sensitive to Doppler broadening.

29

These coherences could also be created by incoherent processes as shown in Ref. [54, 68]. Where, two closely spaced levels decay radiatively to common ground state, leading to coherence between them. The requirement being that they have the same J and m_J quantum numbers, so that they couple to the *same vacuum modes* with the same strength. In analogy to the coupling of spontaneous emission, incoherent pump processes can lead to atomic coherence as well [89]. Along similar lines Shnitman et al. [90] recently demonstrated the control of electronic branching ratio in photodissociation of Na_2 using *incoherent* control. First a laser was used to dress the continuum with an initially empty bound state, this created a laser induced continuum structure, which was made to interfere with a two-photon excitation from the ground state. They observed that the yields along the two product channels could be altered by more than 25% by merely changing the frequency of these fields. These fields are independently applied leading to incoherent control.

Recently, there has been an experimental demonstration of the enhanced index of refraction via quantum coherence in Rb [91]. Earlier experiments [25, 92] have demonstrated large dispersion of the index of refraction (steep slope of the dispersion profile) accompanying EIT, but in this experiment the index enhancement not only allows for *large dispersion* but also for a *large refractive index* in itself, while maintaining a transparent medium. They had two fields, one the coupling laser and the probe laser along the two arms of the Λ-system in the D_1 manifold of ^{87}Rb, and another incoherent pump field that populates one of the ground states via one way pumping to the other ground state. They obtained zero absorption accompanied with a phase shift $\approx 7\pi$, which corresponds to a change in refractive index $\Delta n \sim 10^{-4}$. They performed the experiment in an optically thick medium. They also found that the index of refraction and its slope at the point of zero absorption can be increased with appropriate incoherent pumping.

This enhanced refraction suggests application to optical interferometry, it could be used for high precision magnetometry [93] where if a material showing EIT is placed in one arm of the interferometer, then a small change in the magnetic field would cause a Zeeman shift of the Raman levels (ground states of the Λ-system) causing an unusually large change in the path in that arm and hence highly improved measurement sensitivity.

Among other methods of creating maximal coherence to obtain vanishing absorption and ultralarge index of refraction, recently Kocharovskaya et al. [94] suggested that spontaneous emission can be drastically modified with strong coherent field, if one of the dynamic Stark levels crosses a neighboring atomic state. Now this unperturbed atomic *ground state can decay into the dressed excited states* and surprising enough, this leads to maximum coherence between the excited states and large refractive index.

New Trapping Phenomenon in a Two-Level System with Phase Modulated Fields[1]

In quantum optics the trapping states of a system occupy a very special place, there has always been a search for trapping phenomenon in various systems. We have seen in chapter 2 the importance of the coherent population trapping states in three-level systems and the seminal role it plays in various applications. Here we are looking for trapping phenomenon in the *two-level system* which is the fundamental unit of matter - field interaction. Its well known that when a two-level system interacts with a *monochromatic* field the population undergoes Rabi oscillations in absence of decays, as was shown in section 2.1. At a first glance it seems as though the two-level system does not show any trapping phenomenon. We analyze the two-level system interacting with a *polychromatic field* . We find that for a specific kind of multi-colored excitation one indeed has trapping of population in the two-level system.

The motivation for using a multi-colored field comes from the well known coherent population trapping phenomenon, which occurs in a Λ-system that is driven by two fields of *distinct* frequencies, so adjusted so as to satisfy the two-photon Raman condition. In the steady state through an interplay of quantum interference and incoherent decay processes the coherent population trapped state is formed. Once the trapped state is formed it does not any longer interact with the fields that generated it. We have discussed in detail the coherent population trapping phenomenon in section 2.2. Most of the existing investigations discuss the trapping states in the three-level systems.

The two-level systems so far are *not* known to exhibit trapping states except when the two-level atom is interacting with a *quantized field* [96]. These trapping states due to the quantized field were predicted for the micromaser, where the intra-cavity field shows trapping behavior. These field states are number states that remain trapped because successive atoms undergo $2\pi q$ pulses where q is an integer, leaving the field

---

[1]This work was published as a Rapid communication in Physical Review A, titled **Realization of Trapping in Two-Level System with Frequency Modulated Fields**, Ref. [95].

in the micromaser cavity unaffected. These effects can be seen only at extremely low temperatures and tend to get washed out even if the temperature corresponds to only $0.1 \rightarrow 1$ thermal photons.

In this chapter we demonstrate the existence of *new population trapping* states in a two-level system driven by a classical poly-chromatic field. The two-level system is excited by a *classical* phase-modulated field and under appropriate conditions of the applied field one observes trapping of population. We present both analytical and numerical results on trapping and also on jumps in the system which occur when the *bare energy* levels cross. This point of view comes about *naturally* by observing the dynamics from a frame that is oscillating with the instantaneous field frequency. We also give explicitly the conditions under which this phenomenon can be observed in real atomic systems.

We would like to emphasize here that the trapping states we describe here are quite *different and unrelated* to the coherent population trapping states described in section 2.2. Unlike the steady state CPT states these trapping states are observed in the transient regime. Moreover the underlying mechanism involved in the formation of these trapped states is quite different from that of the coherent population trapping case. The *trapping* in these systems is more akin to *localization* and the *jumps* correspond to the *tunneling* phenomenon in the context of the double-well potential. We will bring out the relation between them in section 3.6.

There has been another closely related work by Lam and Savage [97] where they achieved complete inversion in a two-level atom by modulating away the resonant component and retaining only the *correlated sidebands* of the applied field. They observed suppression of excitation which is similar to the trapping phenomenon we discovered. Many studies have been undertaken with a poly-chromatic field, wherein specifically the response of the two-level atom subject to a bichromatic field has been very extensively studied [98, 99, 100, 101]. However most of the literature concerns the steady state though some papers deal explicitly with the transient response [102, 103].

In chapter 4 we study the consequences of this trapping phenomenon in a *three-level* system. From the point of view of level crossing it leads to richer multiple crossings. We calculate the Landau-Zener like probability at the crossing of these bare energy
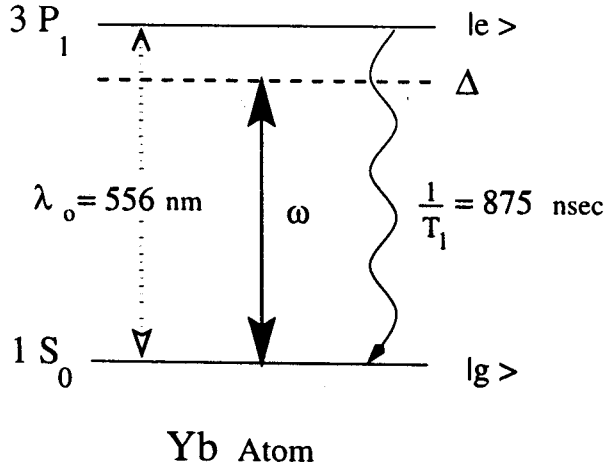
Figure 3.1: Schematic of a two-level system, and the relevant levels of the Yb atom, which has an excited state lifetime of 875 $nsec$. The atomic resonance frequency is ω_o, and the applied field frequency is at ω.

levels. We find that *quantum interference* effect due to coherent accumulation of phase *between* crossings, plays a crucial role in determining the population after multiple crossings. We further use the trapping states, and propose a new scheme of *inverting population across multiple levels* even if initially there is *finite population in the intermediate state* . This scheme would be experimentally more attractive as it lifts certain stringent conditions required in the usual rapid adiabatic passage method. These issues will be discussed in detail in chapter 4.

3.1 Two-Level Dynamics : A Spin - 1/2 System

A two-level atom is conceptually the same kind of object as a spin-1/2 particle in magnetic field. The basic dynamical equations i.e. the Schrödinger equation that governs the evolution of the two-level atom variables are practically same as those appropriate to the spin-1/2 system. Feynman et al. [104] developed a simple but rigorous and complete geometrical picture of the Schrödinger equation describing a two-level system interacting with a near resonant field. This analogy between the two-level system and the spin-1/2 system is quite convenient and one can apply the Pauli spin operators instead of the Fermi operators for the atomic levels. We give below the correspondence

between the Fermi operators $A_{ij} \equiv |i\rangle\langle j|$ and the pseudo-spin operators

$$
\begin{aligned}
S^+ &\leftrightarrow |e\rangle\langle g|, \\
S^- &\leftrightarrow |g\rangle\langle e|, \\
S^z &\leftrightarrow \frac{1}{2}(|e\rangle\langle e| - |g\rangle\langle g|).
\end{aligned}
\tag{3.1}
$$

A two-level system with the excited state $|e\rangle$ and the ground state $|g\rangle$ interacting with a monochromatic field is shown in Fig. 3.1. The field at frequency ω could in general be detuned from the atomic resonance frequency ω_o by an amount $\Delta \,(= \omega_o - \omega)$. The initial inversion is given by η, which is $+\frac{1}{2}$ or $-\frac{1}{2}$ when the atom is initially in the excited state or the ground state, respectively. The equations of motion that would govern the dynamics of such a system in the pseudo-spin notation for the Hamiltonian $H = \hbar \Delta S^z + \frac{\hbar}{2}(gS^+ + H.c)$ is

$$
\begin{aligned}
\langle \dot{S^+} \rangle &= -\left(\frac{1}{T_2} - i\Delta\right)\langle S^+\rangle + ig^*\langle S^z\rangle \\
\langle \dot{S^-} \rangle &= -\left(\frac{1}{T_2} + i\Delta\right)\langle S^-\rangle - ig\langle S^z\rangle \\
\langle \dot{S^z} \rangle &= -\frac{1}{T_1}(\langle S^z\rangle - \eta) + i\frac{g}{2}\langle S^+\rangle - i\frac{g^*}{2}\langle S^-\rangle
\end{aligned}
\tag{3.2}
$$

The decay constant $1/T_2$ determines the decay of the polarization and, T_2 is also known as *transverse* relaxation time as it involves transverse directions; similarly, the decay of the inversion is given by $1/T_1$ where T_1 is known as the *longitudinal* relaxation time. For *purely radiative decay* the decay times of polarization and the inversion obey the simple relation $T_2 = 2T_1$. The well known steady state solutions of the eqn. 3.2 are as follows:

$$
\begin{aligned}
\langle S^+\rangle &= \frac{ig^* T_2(1 + i\Delta T_2)\eta}{(1 + (\Delta T_2)^2 + |g|^2 T_1 T_2)}, \\
\langle S^-\rangle &= \frac{-ig T_2(1 - i\Delta T_2)\eta}{(1 + (\Delta T_2)^2 + |g|^2 T_1 T_2)}, \\
\langle S^z\rangle &= \frac{(1 + (\Delta T_2)^2)\eta}{(1 + (\Delta T_2)^2 + |g|^2 T_1 T_2)}.
\end{aligned}
\tag{3.3}
$$

In the two-level system described in section 2.1 we saw that the atom undergoes a Rabi oscillation (flopping) between the upper and the lower states under the action of an electromagnetic field in complete analogy with the spin-1/2 system. In the next section we describe the dynamics of the two-level atom interacting with a frequency

35

modulated field. We discover that for appropriate parameter values of the frequency modulated field we get *trapping of population* .

3.2 Population Trapping in Two-Level Systems

In order to keep the analysis as simple as possible we consider the phase modulated field on *resonance* with the frequency of the atomic transition. The interaction Hamiltonian in the interaction picture can be written as

$$H = \hbar \left(\frac{g}{2} S^+ e^{-i\Phi(t)} + H.c. \right), \tag{3.4}$$

$$\Phi(t) = M sin(\Omega t), \tag{3.5}$$

where M and Ω are the *index of modulation* and the *frequency of modulation* , respectively, and g is the Rabi frequency.

The phase modulated field has a rich spectrum with Fourier components at integral multiples of the frequency of modulation i.e. at $\omega \pm n\Omega$; each of the n components are weighted by the corresponding Bessel functions J_n. The index / depth of modulation M determines how far away from the central frequency (ω) is the variation of phase undertaken to obtain the phase modulated field. The spectral features can be seen on using the generating function for the Bessel functions [105]

$$
\begin{aligned}
exp(iz sin\theta) &= \sum_{k=-\infty}^{+\infty} e^{ik\theta} J_k(z), \\
&= J_o(z) + 2\sum_{k=1}^{\infty} J_{2k}(z) \cos([2k]\,\theta) + 2i\sum_{k=0}^{\infty} J_{2k+1}(z) \sin([2k+1]\,\theta).
\end{aligned}
\tag{3.6}
$$

where on making the following correspondence we get the spectrum of the phase modulated field, i.e. $\theta \rightarrow \Omega t$ and $z \rightarrow M$. Following this expansion of eqn. (3.6), the interaction Hamiltonian (3.4) can be written explicitly as

$$H = \frac{\hbar g}{2} \sum_{k=-\infty}^{+\infty} e^{-ik\Omega t} J_k(M) S^+ + H.c. \tag{3.7}$$

We now provide the motivation for the choice parameter values required to obtain the trapping phenomenon. On assuming that Ω is large we can make a second rotating wave approximation (the first rotating wave approximation was already made in

writing eqn. (3.4) by going into the frame rotating at the field frequency) leading to

$$H \simeq \frac{\hbar g}{2} J_o(M) S^+ + H.c. \tag{3.8}$$

For *weak coupling* g and *large* Ω one expects this rotating wave approximation to be a good one. Note further that if M is chosen such that

$$J_o(M) = 0, \tag{3.9}$$

then the interaction Hamiltonian (3.8) vanishes, and in such a case one is left only with the rapidly oscillating terms in eqn. (3.7), i.e. $e^{\pm in\Omega t}$ for $n = 2, 3, 4....$ Clearly under these conditions one would expect that *no dynamical evolution will take place on a time scale that is slower than the scale of periodic exponentials in eqn. (3.7) and that the populations will thus be trapped on this slow time scale*. At times $t \approx n\pi/2\Omega$ the other exponentials in (3.7) become important and these would lead to a transition between the two states of the system. As seen in eqn. (3.6) at times $t = \pi/2\Omega$, $3\pi/2\Omega$, $5\pi/2\Omega$... only the terms corresponding to odd values of k would contribute (i.e. last term in eqn. (3.6) where $\sin\theta|_{t=\pi/2\Omega} = 1$); whereas the even orders would be negligible at these times. Again one would expect trapping in the time interval $(\pi/2\Omega, \pi/\Omega)$ followed by a jump. We will verify these qualitative results by integrating numerically the time dependent Schrödinger equation. We do *not* make any approximations on the Hamiltonian, in the numerical calculation like large Ω and neglecting higher order terms in eqn. (3.7), but use the *complete form* as in eqn. (3.4). We show in Fig. 3.2 the phenomenon of trapping for some typical parameter values.

Among various control schemes to coherently tailor the end results of a phenomenon the phase modulated field can be used to dramatically change/redistribute the ionization of a single ground state. Recently Radmore et al. [106] showed that our trapping condition can be used to alter ionization spectrum. They showed that by choosing appropriate index of modulation such that certain Fourier components are suppressed, akin to our choice as in eqn. (3.9), the final-state ionization spectrum exhibits a redistribution of population.

The jump at time $\pi/2\Omega$ can also be understood in terms of the *crossing* of the bare-energy levels of the system in an appropriate reference frame. We can transform (3.4)
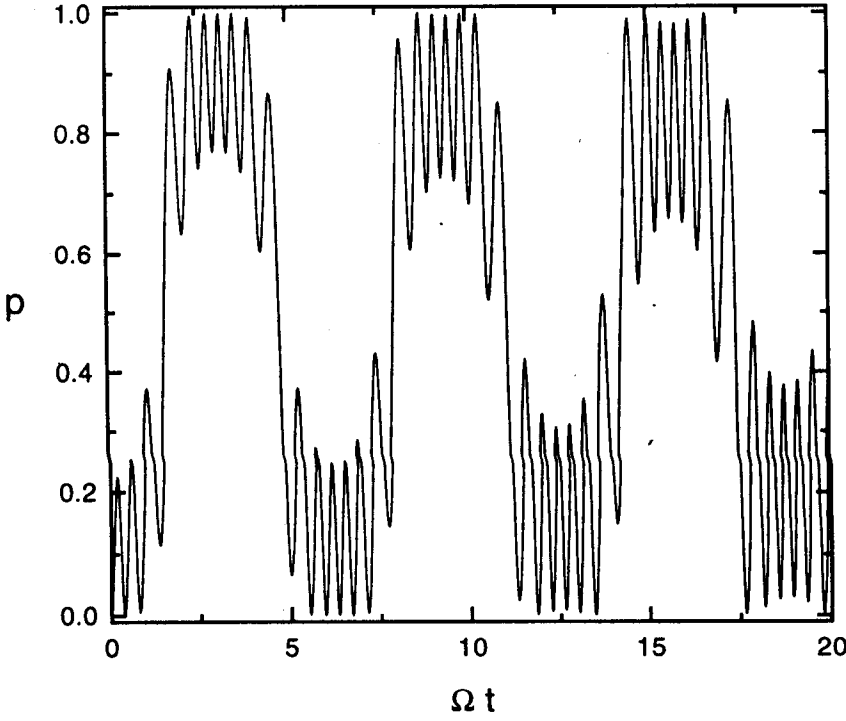
Figure 3.2: Probability p of excitation as a function of Ωt, where we choose $M = 14.9309177086$ the fifth zero of J_o and $g/\Omega = 8.0$; $\gamma/\Omega = 0.0$ (i.e. in the absence spontaneous emission).

into a frame that is rotating with the *instantaneous frequency* of the field, then the effective Hamiltonian becomes

$$H_{eff} = \hbar M \Omega cos(\Omega t)S^z + \left(\frac{\hbar g}{2}S^+ + H.c.\right). \tag{3.10}$$

We see in eqn. (3.10) that the cosinusoidal time dependence periodically lifts the degeneracy between the two levels of Fig. 3.7 whereas the tunneling between these two states is due to the coupling g. In other words one can look at it in terms of real crossing of energy levels and the coupling between the two levels, denoted by g, transforms these into *anti-crossings* . The energies of the two levels cross each other whenever $cos(\Omega t) = 0$, i.e. when $t = n\pi/2\Omega$ (n=1,3,5...). The Landau-Zener theory predicts the transition probability between such crossings under some simplified approximations which is discussed in detail in the next section.

The periodic coefficient of S^z in eqn. (3.10) is reminiscent of the Flouquet analysis. Such an analysis arises from the dressed state approach in the semiclassical limit of large photon number, in this limit they are fully equivalent. The limitation of the Flouquet analysis however is that it cannot take into account quantum effects of the

38

driving field. The evolution of the probabilities in these two levels will be governed by this periodic Hamiltonian and would result in a second-order differential equation with periodic coefficients. The Flouquet's theorem states that if the coefficients along with being uniformly periodic are also devoid of singularities but for poles, then, one can always find solutions of the form $e^{\mu_i t}\Phi_i(t)$ where $\Phi_i(t)$ are periodic with the same periodicity as the coefficient. This analysis is widely used to obtain spectrum of such systems, which would correspond to transitions between various Flouquet states $\Phi_i(t)$. We do not undertake such a treatment as we are interested in the dynamic evolution of the system, in our work we present a simple analysis where the physical motivation becomes immediately transparent.

3.3 Landau-Zener Formula

Landau and Zener calculated in 1932 the the transition probability when energy levels cross [107, 108]. Landau-Zener (LZ) formula deals with non-adiabatic transitions between two adiabatic states as the system traverses a crossing of the energy levels. The LZ formula has been used extensively in calculating probabilities of transitions that occur between adiabatic states when they energetically cross each other, say at crossing of two potential energy curves in problems of slow atomic and ionic collisions. There the motion of the heavy nuclei is treated classically and the various inelastic processes are investigated by solving non-stationary Schrödinger equation, LZ theory is used extensively to calculate various transition probabilities. The states involved should depend weakly on the parameter which when varied causes the crossing leading to transition between them. This means that LZ formula is valid only if the departure from adiabatic behavior is not too large [109]. The LZ model is quite simplistic as was shown in detail by Bates [110] but due to its simple analytical form (in the asymptotic limit) its been in vogue for quite some time. Bates pointed out that the validity of the LZ formula is more restrictive than is commonly supposed. The major objections raised were, the failure of the LZ formula to take in to account the transitions that occur away from the crossings, the atomic orbitals being spherically unsymmetric, and the variation of interaction (coupling) energy with nuclear separation.

In this section we indicate the essential steps and approximations that go into the

derivation of the Landau-Zener (LZ) formula. We consider two states ϕ_1 and ϕ_2 evolving under the following Hamiltonian

$$
H\begin{pmatrix} \phi_1 \\ \phi_2 \end{pmatrix} = \begin{pmatrix} \epsilon_1 & \epsilon_{12} \\ \epsilon_{12} & \epsilon_2 \end{pmatrix}\begin{pmatrix} \phi_1 \\ \phi_2 \end{pmatrix},
\tag{3.11}
$$

where the term ϵ_1 (ϵ_2) are the time dependent energies (eigenvalues in absence of the coupling) of the two states ϕ_1 (ϕ_2), respectively. These states are coupled to each other through a *constant coupling* term ϵ_{12}. We start with a wave equation of the form

$$
\left(H + i\hbar\frac{d}{dt}\right)\left\{ C_1(t)e^{\frac{i}{\hbar}\int \epsilon_1 dt} + C_2(t)e^{\frac{i}{\hbar}\int \epsilon_2 dt} \right\} = 0
\tag{3.12}
$$

Using relation (3.11) we get the following simultaneous first order differential equations

$$
\begin{aligned}
-i\hbar\frac{d}{dt}C_1 &= \epsilon_{12}e^{\frac{i}{\hbar}\int(\epsilon_2-\epsilon_1)dt}\, C_2, \\
-i\hbar\frac{d}{dt}C_2 &= \epsilon_{12}e^{\frac{i}{\hbar}\int(\epsilon_1-\epsilon_2)dt}\, C_1.
\end{aligned}
\tag{3.13}
$$

We need to know the asymptotic values of the solutions of eqns. (3.13). The boundary conditions that are used correspond to our knowledge that the system is initially in state ϕ_2, i.e. $|C_2(-\infty)|^2 = 1$ and $C_1(-\infty) = 0$. We are interested in the probability of the system making a transition to the other state ϕ_1, which is given by the term $|C_1(\infty)|^2$. On eliminating C_2 from eqn. (3.13) and making a suitable transformation $C_1 = e^{\frac{i}{2\hbar}\int(\epsilon_2-\epsilon_1)dt}\, U_1$ we get the standard *Weber equation*

$$
\frac{d^2U_1}{dt} + \left(f^2 - i\frac{\alpha}{2} + \frac{\alpha^2}{4}t^2\right)U_1 = 0,
\tag{3.14}
$$

where the *constant* $f = \epsilon_{12}/\hbar$ and the energy difference is assumed to be a *linear* function of time, i.e. $(\epsilon_1 - \epsilon_2)/\hbar = \alpha t$. This can be thrown into the standard form by redefining the temporal variable to $z = \sqrt{\alpha}e^{-i\pi/4}\, t$, and the constants $n = if^2/\alpha$. Then the Weber function "$D_{-n-1}(iz)$" is a particular solution of the differential equation (3.14). On using the boundary conditions described earlier and undertaking the asymptotic limit i.e. $t \to \infty$, we have

$$
|C_1(\infty)|^2 = \frac{2\pi\kappa e^{-2\pi\kappa}}{\Gamma(i\kappa + 1)\Gamma(-i\kappa + 1)} = 1 - e^{-2\pi\kappa},
\tag{3.15}
$$

where $\kappa = \epsilon_{12}^2/\hbar|\frac{d}{dt}(\epsilon_1 - \epsilon_2)|$. We now make the correspondence of various parameters ϵ to our system. Though our system involves multiple crossings, for large Ω the crossings are well *separated* hence we can approximate each crossing, say at $\Omega t = \pi/2$, as a *single* two-level crossing. The constant coupling term $\epsilon_{12} \to \hbar g/2$, the energy difference $(\epsilon_1 - \epsilon_2) \to M\Omega \cos(\Omega t)$, we note that the cosinusoidal variation is linear at $\Omega t = \pi/2$. Hence for sufficiently large Ω the asymptotic derivation of the LZ formula (3.15) will be closer to the observed and also the effect of multiple crossings will be minimal at the first crossing. We discuss in detail the effects of multiple crossings in chapter 4.

Hence the transition from the ground to the excited state will occur with a probability

$$p = 1 - e^{-2\pi\kappa}, \tag{3.16}$$

where

$$\kappa = \frac{(\hbar g/2)^2}{\hbar|\frac{d}{dt}[\hbar M\Omega \cos(\Omega t)]|} \approx \frac{g^2}{4M\Omega^2}, \quad sin(\Omega t)|_{t=\frac{\pi}{2\Omega}} \approx 1. \tag{3.17}$$

3.4 Results and Discussion

In continuation of our earlier qualitative discussion in section 3.2, we demonstrate in this section the trapping phenomenon *quantitatively* when the various conditions including the one in eqn. (3.9) are satisfied. We assume that the system has a very long excited state life-time and that the atom is initially in the ground state at time $t = 0$. Some typical results are shown in the Fig. 3.2 and 3.3 where the probability of excitation is plotted as it evolves in time (Ωt is the dimensionless quantity denoting time). In the interval $0 < \Omega t < \pi/2$ the atom remains trapped in the ground state except for the small oscillations at the fast time scales. These fast oscillations are due to the other higher order Fourier components as discussed in section 3.2. At time $\Omega t = \pi/2$ the atom makes a transition to the excited state. This transition can also be understood as an effect of crossing of the adiabatic states. The transition probability matches closely to the LZ formula of eqn. (3.16) in the region of the crossing, where our system is approximated by the Landau-Zener model. In Fig. 3.2 we choose the fifth zero of the $J_o(M)$ at $M = 14.9309$, and the tenth zero at $M = 30.6346$ in Fig. 3.3. We see that the trapping of population is more pronounced for larger values of M because $J_n(M) \ll 1, \forall n$ for
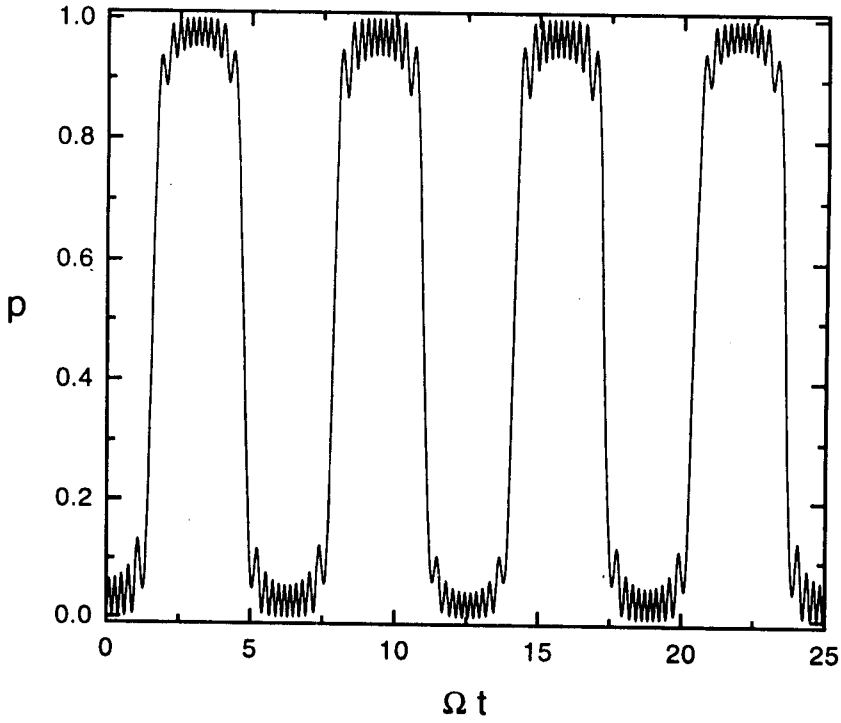
Figure 3.3: Probability p of excitation as a function of Ωt, where we choose the tenth zero of J_o i.e. $M = 30.6346064684$; $g/\Omega = 8.0$; $\gamma/\Omega = 0.0$ (i.e. in the absence spontaneous emission).

$M \gg 1$.

In Fig. 3.4 we plot different contour plots of the evolution of the *polarizations* from $\Omega t = 0 \to 2\pi$. The system starts evolving in the ground state with $S^z \approx -0.5$ and the polarizations S^x, S^y along the perpendicular directions x-, y-, respectively. While the population is trapped the polarizations vary with large magnitude (≈ 0.3) in a circular fashion. Then at times $\Omega t = \pi/2$ the value of inversion is reversed, whereas the polarizations S^x, S^y continue to vary with large magnitude in the interval $\pi/2 < \Omega t < 3\pi/2$. Again at time $\Omega t = 3\pi/2$ the inversion reverts back to its original value. As pointed out by Lam and Savage [97] this excitation scheme could result in obtaining complete inversion in a two-level system even in the absence of resonant excitation (as $J_o(M) = 0$). We also observe that in the region $\pi/2 < \Omega t < 3\pi/2$ the atomic polarization is quite significant. Thus the atomic state in this region is a *coherent state* or a Bloch state [111] which is essentially obtained by a rotation of the ground state $|-1/2\rangle$. Moreover other initial conditions like the atom prepared in a dressed state lead to similar behavior.
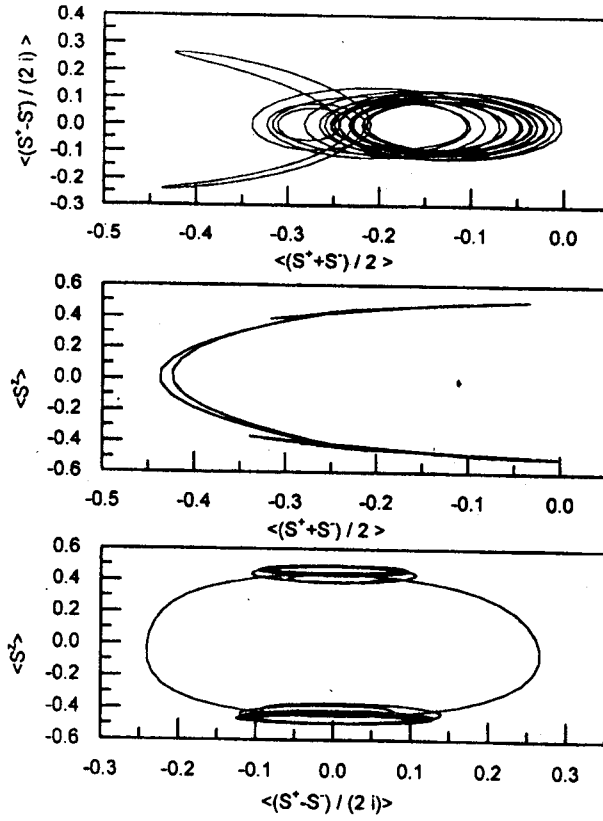
42

Figure 3.4: Contour plots for the atomic polarizations and inversion when $M = 30.6346064684$; $g/\Omega = 8.0$; $\gamma/\Omega = 0.0$ (i.e. in the absence spontaneous emission).

3.5 Effects of Spontaneous Emission

We also study the effect of radiative decay from the excited state to the ground state on the trapping phenomenon. In Fig. 3.5 we show the effect of the atomic spontaneous emission which is expected to change the characteristics of the trapping state particularly if $\gamma \sim \Omega$. The decay destroys the trapping like character of the evolution but leaves a signature of the correlated sideband excitation. In the steady state the population is *larger* than the one with just a single detuned monochromatic field [97]. The correlated sideband excitation results from the phase modulated field, where for every $n\Omega$ component with weight factor $J_n(M)$ there is a $-n\Omega$ component having the same strength ($J_{-n}(M)$) acting together in a *correlated* fashion. In the presence of decay the trapping feature is lost but the jumps still occur, this is due to the presence of the bare state crossings which continue to occur even in presence of decays. We show this feature in Fig. 3.6 where we compare the excitation through a monochromatic field
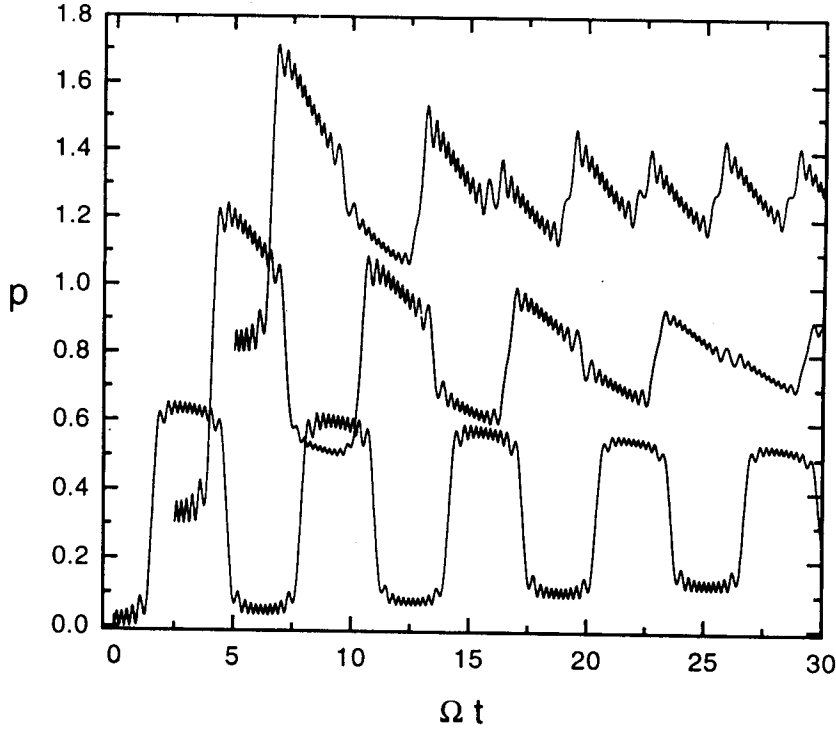
43

Figure 3.5: Effect of weak spontaneous emission on the probability p of excitation for different values of γ (= 1/2 Einstein A coefficient), $\gamma/\Omega = 0.01(x = x + 0.0, y = 2/3y)$, $\gamma/\Omega = 0.05(x = x + 2.5, y = y + 0.3)$, $\gamma/\Omega = 0.1(x = x + 5.0, y = y + 0.8)$; $M = 30.6346064684$; $g/\Omega = 8.0$. For clarity the different curves have been displaced as indicated by the transformations in the bracket. For example, $y = y + 0.8$ means: the value on the y axis equals the actual value plus 0.8.

and the frequency modulated field. We observe the effects of energy crossing in the dynamics of these two cases.

3.6 Trapped States and Control of Tunneling

We bring out in this section the connection between these new trapping states and the traditional tunneling phenomenon. The tunneling phenomenon has continued to attract considerable attention since the early days of quantum mechanics [107, 108, 112, 113] as it is of fundamental importance in many branches of physics. The very first demonstration of the effects of quantum tunneling was by Hund [114] for intra-molecular rearrangement in pyramidal molecules which physically manifested as the *tunnel splitting* of the vibrational spectra. Since then there have been a host of physical
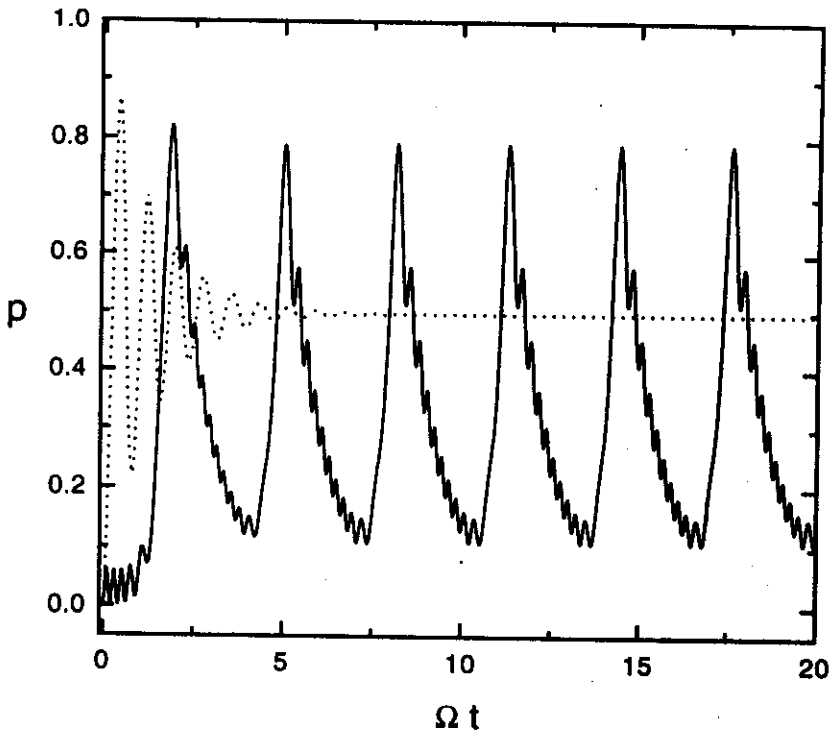
44

Figure 3.6: The effect of large spontaneous emission leads to disappearance of the trapping like character, but the jumps still exist, we have $\gamma/\Omega = 0.5$ with $g/\Omega = 8.0$, and $M = 30.6346064684$ (solid line), the case of the usual monochromatic excitation ($M = 0.0$), is plotted in dotted lines, for comparison.

systems where the phenomenon of tunneling has been observed.

The essential system in these phenomenon is again the two-level system coupled to an external driving field. Such a two-level system typifies many physical systems in diverse fields, it can either exactly represent a spin-1/2 particle or approximately the chiral states of an optically active molecule. A particle in a double well potential can also be approximated as a two-level system in the regime of low excitation. In Fig. 3.7 we show the equivalence between the two-level system we deal with and the double-well potential.

The problem at hand is, say if initially the wavefunction (representing the particle or population etc.) is in one of the wells, equivalently one could say its *trapped* in one of the levels, then one studies its evolution in time under the influence of the external driving field. In our system, the population (depicted by small circles in Fig. 3.7) is trapped in one of the states while the coupling between these states is provided by g.
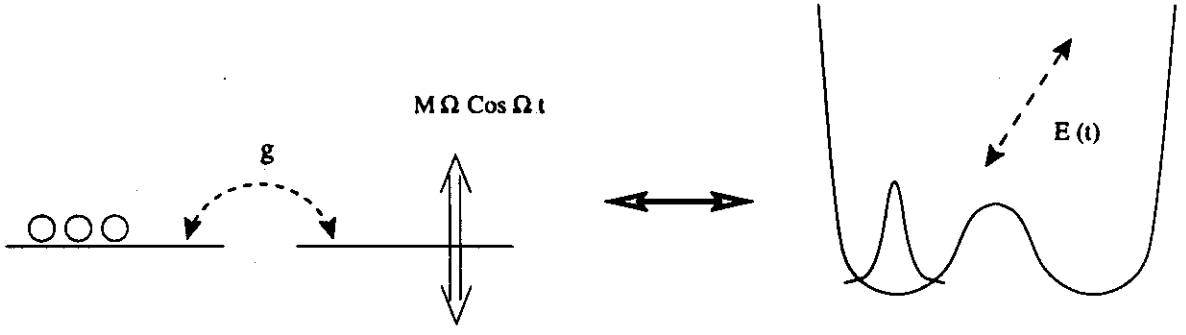
45

Figure 3.7: Equivalence between our two-level system and the double-well potential. In (a) the coupling g leads to tunneling in the two-level system, whereas the term $M\Omega\cos(\Omega t)$ periodically lifts the degeneracy between the levels. In (b), the particle is initially localized in one of the wells of the double-well potential, while the tunneling is controlled through a time dependent external field E(t) represented by the dashed arrow.

The degeneracy between these states is periodically lifted in a cosinusoidal fashion. Its the coupling term g that leads to tunneling between the levels at those times when the levels become degenerate. In the double well potential, the particle (denoted by the Gaussian wave packet in Fig. 3.7) is initially in one of the wells and this system is driven by a time-dependent external field which is responsible for the *tunneling* of the particle between the two wells. Essentially the exchange of population between these states is equivalent to the tunneling phenomenon in the double-well potential.

In the recent times there has been a lot of interest in control of tunneling, we give a brief review of some relevant developments. Lin and Ballentine [115] found that monochromatic (oscillatory) external field acting on a quartic double well oscillator can *increase* the rate of coherent tunneling to several orders of magnitude $\sim 10^4$ higher than the undriven system. They also found a coherent oscillatory property of this tunneling phenomenon, the initial wave packet launched in one stable zone oscillates back and forth and retains the coherence character between the two wells (stable zones). In contrast the phenomenon of *suppression* of tunneling in double well systems was discovered by Grossman et al. [116] for certain parameter values of the driving force. They found that periodic driving can slow down tunneling by any desired degree or

46

even suppress it altogether in a perfectly coherent way.

These effects in driven two-level model were analyzed in the context of *controlling tunneling* [117] and it was found that tunneling could either be enhanced, reduced or totally suppressed. The control of tunneling has many applications, like Bavli and Metiu [118] demonstrated that a semi-infinite Gaussian pulse can take the electron from a delocalized energy eigenstate of the double well, localize it in one of the wells and keep it there. The emission properties of the electron in the double well [119] are quite interesting and leads to low-frequency generation due to *strong* localization in one of the wells [120].

Along similar lines the suppression of this quantum dynamical tunneling using *laser* fields has been proposed for a quantum system (molecule or impurity center), embedded in a host environment, such embedding leads to a symmetric double well potential for the ground electronic state and an asymmetric one for the excited electronic state of this quantum system [121]. The external laser field couples the symmetric ground electronic state to the asymmetric excited electronic state. It was observed that for Rabi frequency of the coherent driving field larger than the ground state double well *potential splitting* there was suppression of the dynamical tunneling. The potential splitting in this system occurs because initial localization in one well implies a superposition of symmetric and antisymmetric states, which are energetically non-degenerate and this energy difference appears as the potential splitting. There are numerous other examples of such quantum dynamical tunneling like it describes the internal rotation in molecules [122], or rotation of a single molecule in a crystalline or amorphous environment [123], or complex conformational changes in glasses [124], biological systems [125] etc.

We have seen that in our system we can not only create the population trapping phenomenon but also control the tunneling to the other level at the crossing. By varying the frequency of modulation one can either increase or decrease the times for which the trapped population remains in a particular state, whereas by changing the coupling g the tunneling from one state to another can be controlled. Thus, in conclusion the conditions under which the trapping states can be observed on the time scale t are

$$\Omega \gg \gamma; \quad J_o(M) = 0, \quad t < \frac{\pi}{\Omega}. \qquad (3.18)$$

47

In earlier transient experiments Mossberg and co-workers [103] used Yb atom transition which has the lifetime $\tau \sim 875$ $nsec$, see relevant levels of Yb in Fig. 3.1. This atom seems suited for observing trapping states discussed here as we can use $\Omega \sim 1$ MHz and observation time in the range of nanoseconds to microseconds to observe jumps. Hence we have demonstrated the possibility of producing new trapping of population in two-level system in presence of classical fields; the existence of which depends on the conditions summarized in the eqn. (3.18). We further show that jumps occur whenever the energy levels in the frame rotating with the instantaneous frequency of the field cross each other. One has complete control over trapping and tunneling dynamics by appropriate choice of frequency of modulation and the amplitude of the applied frequency modulated field. The issues discussed in this chapter would be quite interesting in the context of *higher spins* or *multi-level* systems where several levels can cross at the same time, and we discuss these aspects in the next chapter.

Multiple Landau-Zener Crossings and Quantum Interference Effects using New Trapping Phenomenon [1]

We have seen in the previous chapter demonstration of new trapping phenomenon in two-level system driven by classical phase modulated field. In this chapter we extend these ideas to the multilevel systems, typically the three-level ladder system. Many interesting effects come to fore in this three-level scheme. We find that the excitation amplitude after multiple crossings is not a mere product of Landau - Zener transition probabilities at each crossing due to *coherent evolution* of the system in between crossings. In this system the trapping of population by frequency modulated fields ensures *coherent* evolution, and inclusion of *phase effects* for population redistribution after multiple crossings becomes necessary. The relative phase accumulated by various adiabatic states as they evolve along different paths is tailored to show the existence of *quantum interference* effects.

We have shown in section 3.3 the derivation of the Landau-Zener (LZ) [107, 108] formula. Extension of the LZ formula for multilevel crossing (even infinite set of two-level crossings) when they are *well separated* has been shown to decompose into elementary LZ factors at each crossing [127]. Each crossing mixes only a pair of adjacent states. On the other hand, multilevel crossing in the context of scattering of atoms and ions has been dealt in detail by Nakamura [128] where the dependence of the probability amplitude on stokes phase is noticed. Its inclusion leads to a better matching of the LZ theory with the exact quantum calculation. This provides the motivation for including the effects of coherent evolution between multiple crossings.

Further, in this chapter we also deal with such multiple crossing where for an ap-

propriate choice of parameters *simultaneous* crossing of all the three-levels takes place. We utilize this type of crossing to demonstrate a new mechanism for achieving nearly complete population inversion across multi-level systems, even if the intermediate levels are *occupied* . This inversion of population takes place *without affecting the population in the intermediate state* . We discuss the advantages of this method over the usual rapid adiabatic passage process (RAP) which uses unconventional sequence of pulses [129] to achieve such inversion. This inversion can also be completely undone/ reversed at the next crossing. We also present an *optical atoms* implementation of the three-level ladder system. It is a classical, *all optical* analog of the quantum system - particularly of the three-level ladder system where these and many other effects related to the three-level systems can be realized.

4.1 Model

As we had demonstrated in chapter 3, a two-level system in presence of frequency modulated electromagnetic field shows trapping of population and its redistribution at periodic intervals of time [95]. These times correspond to the times at which the adiabatic levels cross each other. The applied field being coherent ensures coherent evolution between the crossings. As a generalization, we consider here a three-level ladder system (Fig. 4.1) in presence of frequency modulated electromagnetic field. Here, its not a mere generalization of the earlier spin-1/2 system to a spin-1 system but to a more general three-level ladder system, as we also include arbitrary detunings of the fields from the atomic levels. The phase modulated field at the atom is given as

$$\vec{E} = \vec{E}_1 e^{-i(\omega_1 t + \phi_1(t))} + \vec{E}_2 e^{-i(\omega_2 t + \phi_2(t))} + c.c \; ; \quad \phi_i(t) = M_i sin(\Omega_i t), i = 1, 2, \qquad (4.1)$$

where M_i and Ω_i are the index of modulation and the frequency of modulation, respectively. This field interacts with a three-level cascade system, as shown in Fig. 4.1. The field centered at ω_1 couples the transitions $|1\rangle \leftrightarrow |2\rangle$, and ω_2 couples $|2\rangle \leftrightarrow |3\rangle$. The total Hamiltonian of the system is

$$H = \hbar\omega_{12}|1\rangle\langle 1| - \hbar\omega_{23}|3\rangle\langle 3| - \vec{d}\cdot\vec{E}, \qquad (4.2)$$

where $\vec{d} = \vec{d}_{12}|1\rangle\langle 2| + \vec{d}_{23}|2\rangle\langle 3| + c.c.$ The first two terms in H correspond to the unperturbed system where the energies are being measured from the *middle level* $|2\rangle$, and the
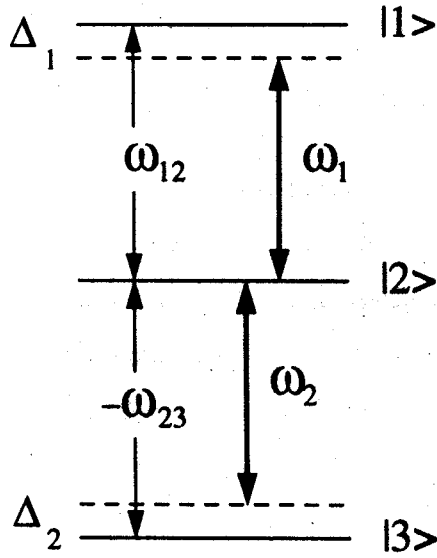
Figure 4.1: Three-level ladder system with the energies being measured from the middle level $|2\rangle$. Transitions $|1\rangle \leftrightarrow |2\rangle$ and $|2\rangle \leftrightarrow |3\rangle$ are coupled by frequency modulated fields centered at ω_1 and ω_2 respectively. Δ_1, Δ_2 and $2G_1$, $2G_2$ are the detunings and Rabi frequencies of the corresponding transitions, respectively.

last term in eqn (4.2) is the interaction term in the *dipole approximation* . We describe the dynamics of the atom plus field system by the Schrödinger equation

$$i\hbar \frac{d|\psi\rangle}{dt} = H|\psi\rangle, \qquad (4.3)$$

where $|\psi\rangle = C_1|1\rangle + C_2|2\rangle + C_3|3\rangle$, and H denotes the *total Hamiltonian* given in eqn. (4.2). We have already discussed in section 3.2 the various conditions for localization of population in a two-level system in presence of a frequency modulated field, we extend those conditions for the multilevel system. The interaction Hamiltonian for this three-level ladder system (Fig. 4.1) is

$$H_{int} = -\vec{d}_{12} \cdot \left(\vec{E}_1 \sum_{k=-\infty}^{+\infty} J_k(M_1)e^{-ik\Omega_1 t} \right) |1\rangle\langle 2| - \vec{d}_{23} \cdot \left(\vec{E}_2 \sum_{k=-\infty}^{+\infty} J_k(M_2)e^{-ik\Omega_2 t} \right) |2\rangle\langle 3| + H.c.$$
$$(4.4)$$

where, as indicated by subscripts 1 and 2 one could in general have two different frequency modulated fields coupling these transitions.

As we have discussed in section 3.2 for large Ω the major contribution on the time scales slower than the periodic exponentials in eqn. (4.4) would be from the $J_0(M_{1,2})$ terms, moreover magnitudes of $J_n(M)$ diminishes with increase in $|n|$ for any finite

index of modulation M. Hence for large frequency of modulation Ω

$$H_{int} \approx -\vec{d}_{12} \cdot \vec{E}_1 J_0(M_1)|1\rangle\langle 2| - \vec{d}_{23} \cdot \vec{E}_2 J_0(M_2)|2\rangle\langle 3|. \qquad (4.5)$$

By choosing M_i to be a zero of the zeroth order Bessel function *simultaneously* along both the transitions, *i.e.* $J_0(M_i) = 0$ for $i = 1$ and 2, the *dominant term* in the interaction Hamiltonian becomes *negligible*, which effectively leads to trapping of the population on the appropriate time scales. At times $t \sim \frac{\pi}{2\Omega}, \frac{3\pi}{2\Omega}, \frac{5\pi}{2\Omega}...$, (for the resonant case) the other exponentials would dominate the interaction term (particularly the terms with odd k, which vary as $sin(\Omega t)|_{t=\pi/2\Omega} = 1$, as was described in the discussion following eqn. (3.6)) causing transitions between different levels.

We now transform equation (4.3) into a frame rotating with the *instantaneous frequency* of the field. We define new complex amplitudes $\tilde{C}_i$'s in the instantaneous frame, using the following transformation,

$$\tilde{C}_1 = C_1 e^{i(\omega_1 t + \phi_1(t))},$$

$$\tilde{C}_2 = C_2,$$

$$\tilde{C}_3 = C_3 e^{-i(\omega_2 t + \phi_2(t))}. \qquad (4.6)$$

We undertake the rotating wave approximation and hence neglect the rapidly rotating terms at twice the optical frequency which vary as $e^{\pm 2i(\omega_i t + \phi_i(t))}$ (for $i = 1, 2$), then the equations of evolution for the slowly varying $\tilde{C}_i$'s are

$$\begin{bmatrix} \dot{\tilde{C}}_1 \\ \dot{\tilde{C}}_2 \\ \dot{\tilde{C}}_3 \end{bmatrix} = \begin{bmatrix} -i(\Delta_1 - M_1\Omega_1\cos{(\Omega_1 t + \theta)}) & iG_1 & 0 \\ iG_1^* & 0 & iG_2 \\ 0 & iG_2^* & i(\Delta_2 - M_2\Omega_2\cos{(\Omega_2 t)}) \end{bmatrix} \begin{bmatrix} \tilde{C}_1 \\ \tilde{C}_2 \\ \tilde{C}_3 \end{bmatrix}, (4.7)$$

where the overdot denotes the first order time derivative, $\Delta_1 = \omega_{12} - \omega_1$ and $\Delta_2 = \omega_{23} - \omega_2$ are the detunings, the parameters $2G_1 = \frac{2\vec{d}_{12} \cdot \vec{E}_1}{\hbar}$ and $2G_2 = \frac{2\vec{d}_{23} \cdot \vec{E}_2}{\hbar}$ are the Rabi frequencies of the corresponding transitions, θ provides the initial phase mismatch between the fields $\vec{E}_1$ and $\vec{E}_2$. In order to solve equation (4.7), if we proceed along the lines of Landau and Zener as in Ref. [107, 108], *i.e.* consider only linear terms in the expansion of $\cos{(\Omega t)}$ at the crossing ($\Omega t \sim \pi/2$), we obtain a *third-order differential equation* which cannot be solved analytically. Hence, we resort to numerically solving the eqns. (4.7).

Thus the conditions for observing trapping of population and and its redistribution due to jumps (at the crossings) are firstly, the choice of the *modulation index* M_i such that $J_0(M_i) = 0$ for *both* $i = 1, 2$ simultaneously, and secondly the choice of *modulation frequency* Ω_i which would set the times at which jumps (crossings of the bare energy levels) would occur. The trapping states are limited by the decay processes in the atom as was discussed in detail in section 3.5; hence we require $\Omega_i \gg \gamma_i$, where $2\gamma_i$ is the spontaneous emission rate between various transitions $|1\rangle \rightarrow |2\rangle$ and $|2\rangle \rightarrow |3\rangle$, for $i = 1$ and 2 simultaneously, to observe the trapping and jumps.

There have been manifestations of similar trapping phenomenon in solid state systems. Kenkre et al. [130] have demonstrated *dynamic localization* in quantum transport theory where they considered the motion of a charged particle in an infinite lattice driven by a harmonic time dependent electric field. The condition for this dynamic localization is very similar to the condition obtained here. The essential difference being that they have finite number of lattice sites in the problem, which would be equivalent to an equispaced multilevel (finite number) system in our case. This leads to competition between *two* length scales, one is the length scale of localization (similar to our Ω) and the other being reflection scale due to finiteness of the lattice size. Some features of this reflection due to finite size of the lattice size (in our case, levels), are utilized in section 4.2.2, where we exploit this to invert population across the multi-level system. Another difference between dynamic localization and our trapping phenomenon is the sensitivity to the $J_o(M) = 0$ condition, the dynamic localization is lost if M is chosen to be slightly away from the zero of the Bessel function. A detailed comparison between our quantum optic trapping phenomenon and the dynamic localization in solid state systems is made by Raghavan et al. in Ref. [131] where they also discuss the interplay of these two length scales and bring out the differences between these two systems.

4.2 Calculations and Discussion

In this section we demonstrate the phenomenon of trapping and jumps and the need to consider phase effects, due to coherent evolution of the population along different interfering pathways. To observe trapping we choose the index of modulation such that its a zero of the Bessel J_0 function. The jumps occur at times when the *bare* energy
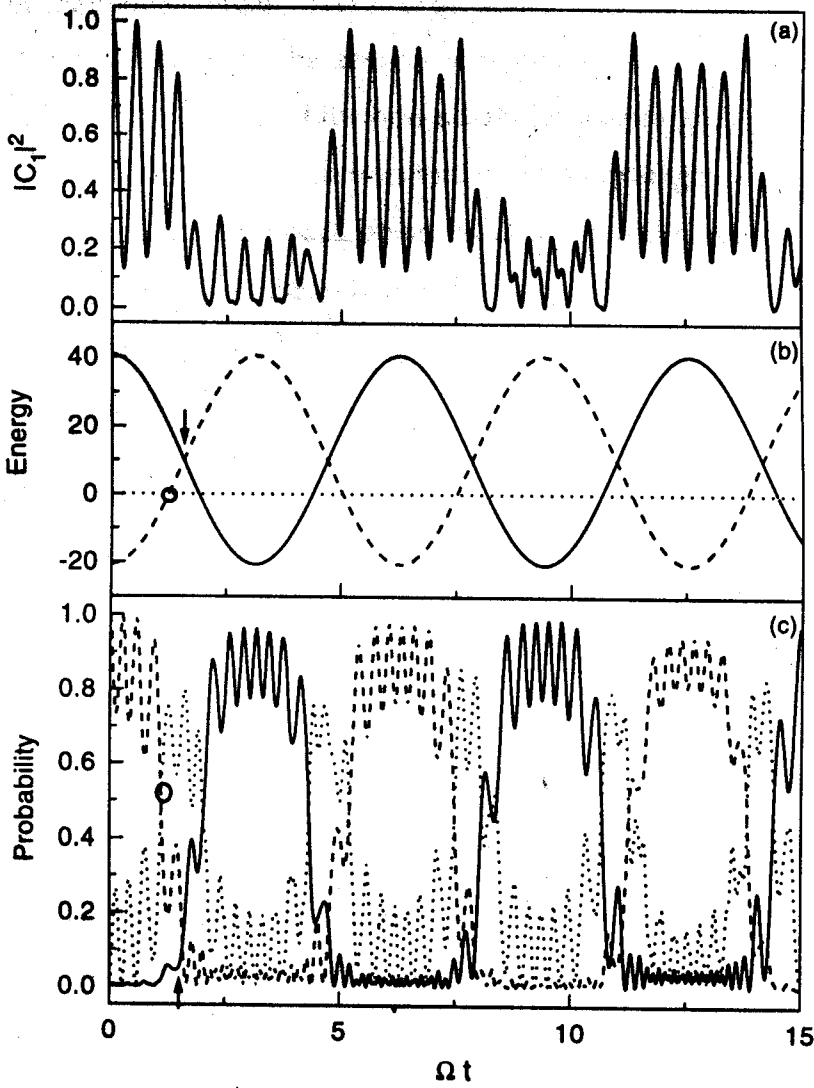
Figure 4.2: (a) There is no trapping of population if the M_i's are chosen such that $J_0(M_i) \neq 0$. For $M_1 = M_2 = 7$, $\Omega_1 = \Omega_2 = 1$, $\Delta_1 = 10$, $\Delta_2 = -10$, $G_1 = G_2 = 6$, with the initial condition $|C_1|^2 = 1$, $|C_2|^2 = |C_3|^2 = 0$. (b) The evolution of the energy levels, given by (4.8) and the crossings of these levels for a choice of M such that $J_0(M) = 0, M = 30.6346$ and the other parameters being same as in (a). The dashed, dotted and solid lines are for energies of levels $|1\rangle, |2\rangle$ and $|3\rangle$ respectively. (c) Dynamic evolution of the trapping of population in various states. At every crossing of the energy levels (first two crossings are denoted by circle and arrow) there is redistribution of population, for $M = 30.6346$ and other parameters being same as in (a). Similar to (b) the dashed, dotted and solid lines denote $|C_1|^2$, $|C_2|^2$ and $|C_3|^2$ respectively. Δ_i and G_i are in the units of Ω.

54

levels cross. Fig. 4.2 shows the trapping of population and its transfer at the times when the energy levels cross. The energy levels and the various crossings depicted in the figures correspond to the *zero-order Hamiltonian* in the rotating frame. As is well known the consideration of the non-adiabatic coupling G_i's between the adiabatic states would transform these crossings into *avoided-crossings* .

We initially put in all the population in state $|1\rangle$ and show the importance of the choice of M for trapping to occur. In Fig. 4.2 (a) we do not have any trapping, as M is not a zero of the Bessel J_0 function (for simplicity we take $M_1 = M_2$ and $\Omega_1 = \Omega_2$, the general case is discussed later). For $M_i = 30.6346$ (tenth zero of the J_0 Bessel function) we have trapping of population, see Fig. 4.2 (c). The zero-order *energies* (*i.e.* without the non-adiabatic coupling term) of the adiabatic levels $|1\rangle$ and $|3\rangle$, as measured from $|2\rangle$, in the frame corotating with the instantaneous field frequency are

$$
\begin{aligned}
E_1(t) &= \Delta_1 - M_1\Omega_1 cos(\Omega_1 t + \theta), \\
E_2(t) &= 0, \\
E_3(t) &= -(\Delta_2 - M_2\Omega_2 cos(\Omega_2 t)).
\end{aligned}
\tag{4.8}
$$

Hence whenever $E_i = E_j$ (for $i \neq j$; $i, j = 1, 2, 3$), the levels $|i\rangle$ and $|j\rangle$ cross at those times causing a population transfer, see Fig. 4.2 (b). The first crossing takes place when $E_1 = E_2$ at $\Omega t \sim 1.23$; the second crossing is at $\Omega t \sim 1.57$ when $E_1 = E_3$; the next crossing takes place when $E_2 = E_3$ at $\Omega t \sim 1.90$ and so on. Most of the population evolves *adiabatically* for the parameters chosen, which results in a *change of character* at the avoided crossing. Only a small fraction of the population suffers no change across the crossing due to the non-adiabatic coupling.

Here its the G_i's that provide the coupling between various adiabatic states $|i\rangle$'s and transform these crossings into *avoided crossings* . As the system evolves quasi-adiabatically (i.e. $G^2 > M\Omega$) across the crossing, it leads to an exchange of character (in our case the population) at the avoided crossing. The purely adiabatic limit would be $G^2 \gg M\Omega$, which would lead to negligible population in the initial state after the avoided crossing. The population transfer probability at the crossing of *two levels* can be approximated by the Landau-Zener formula by taking only the linear terms in the expansion of $cos(\Omega t)$ in eqn. (4.8) about the crossing time (i.e. at $\Omega t = \pi/2$). The probability at the first crossing turns out to be $p = 1 - e^{-2\pi\kappa}$ with $\kappa = G^2/|\frac{d}{dt}(E_1 - E_2)|$
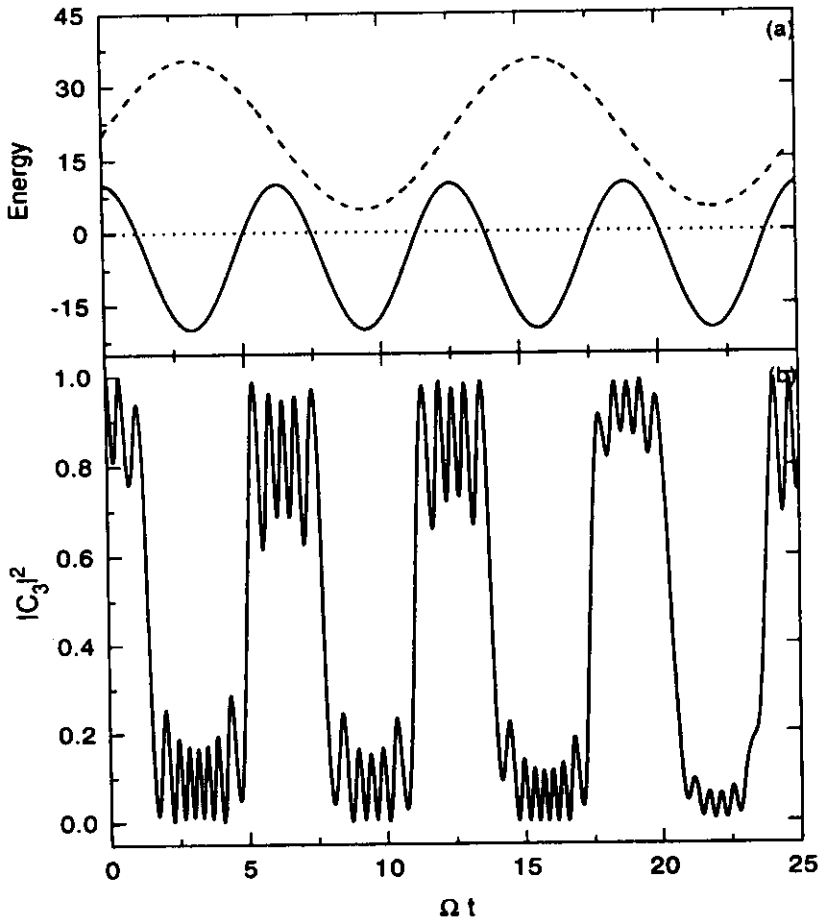
Figure 4.3: (a) The level $|1\rangle$ (dashed) does not cross any other level for a choice of $\theta = \pi/2$ and $M_1 = 30.6346, M_2 = 14.9309, \Omega_1 = 1/2, \Omega_2 = 1, \Delta_1 = 20, \Delta_2 = 5, G_1 = 8, G_2 = 3$ and initially the population is in level $|3\rangle$. The energies of $|2\rangle$ and $|3\rangle$ are denoted by dotted and solid line, respectively. (b) Trapping is clearly seen even when $M_1 \neq M_2, \Omega_1 \neq \Omega_2$ and a finite θ, all parameters being same as in (a). Δ_i and G_i are in the units of Ω_2.

as described in section 3.3. At $\Omega t \sim 1.23 \; p = 0.8$, which is comparable to the observed probability after the first crossing.

The crossing of energy levels is essential for population transfer, otherwise it remains trapped in various levels depending on the initial condition. In general trapping is also observed when $M_1 \neq M_2$, however they have *both* to be chosen as zeros of the J_0 Bessel function. Choice of unequal Ω_1 and Ω_2 does not affect these trapping states. Trapping is also unaffected by the initial phase mismatch between the fields $\vec{E}_1$ and $\vec{E}_2$. If the phase mismatch θ or choice of Ω_i's does not result in *extra* crossings of the energy levels, the characteristic trapping dynamics of the system does not suffer. We show in

56

Fig. 4.3 that trapping persists for a general choice of parameters, i.e. when $M_1 \neq M_2$, $\Omega_1 \neq \Omega_2$ and a finite phase difference θ is present between the two fields.

4.2.1   Quantum Interference Effect due to Coherent Evolution

To illustrate the need to consider *phase* accumulated between two crossings along the various paths of evolution, we choose the values of $\Delta_{1,2}$ such that level $|1\rangle$ does not cross the other levels, see Fig. 4.4 (a). There is a periodic exchange of population, predominantly between levels $|2\rangle$ and $|3\rangle$, whereas the population in $|1\rangle$ remains practically unaffected. We begin initially with the population in $|3\rangle$. The probability of it being transferred to $|2\rangle$ at the first crossing is $p = 0.9$ using the Landau - Zener theory. If one considers each crossing independently, the probability at every crossing is the same because the absolute value of the *slope* of the energy difference $(E_2 - E_3)$ is same at all crossings, see Fig. 4.4 (a). To determine the population after multiple crossings one cannot merely take the individual Landau - Zener probabilities [127] at each crossing, as it would imply *a steady decrease in the probability of population transfer with increasing number of crossings* . While the observed probability is more or less independent of the number of crossings the system has undergone. The population in $|3\rangle$ revives completely after *even* number of crossings, Fig. 4.4 (b). Thus the probability after multiple crossings requires consideration of the *phase accumulated* by the system between such crossings along with the transition probabilities at each crossing.

It was shown by Berry [132] that when a quantum system is forced round a cycle by an adiabatic change, it will return with an extra phase which is purely *geometric* in nature. It is well known that if the evolution is dissipative then this geometric phase could be complex leading to a geometric contribution to the amplitude and hence to the probability of being in the initial state. Berry [133] discovered the possibility of geometric amplitude in non-dissipative (unitary evolution) systems, and proposed a *twisted Landau - Zener model* . In the conventional Landau - Zener model (section 3.3), the coupling between the two states is constant (ϵ_{12}), whereas the energies vary linearly ($\epsilon_1 - \epsilon_2 = \alpha t / \hbar$) along the evolution path (in our case time). In contrast the twisted Landau - Zener model has a coupling of the kind $\epsilon_{12} e^{-i\Phi(t)}$, its this term $\Phi(t)$ that results in the geometric amplitude factor. Berry studied a particular case where $\Phi(t) = \beta t^2$,
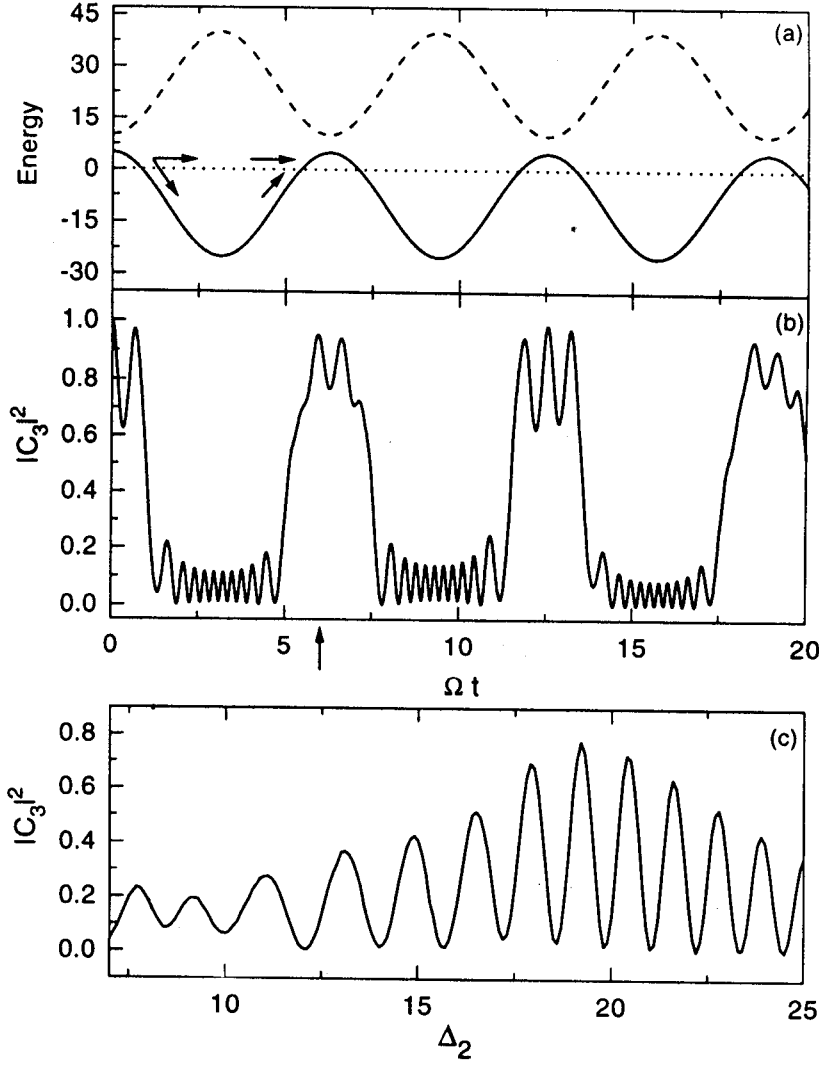
57

Figure 4.4: (a) The energy level $|1\rangle$ (dashed) does not cross with $|2\rangle$ (dotted) and $|3\rangle$ (solid) for $M = 14.9309$, $\Delta_1 = 25$, $\Delta_2 = 10$, $G_1 = 7$, $G_2 = 3$, with the initial condition $|C_3|^2 = 1$, $|C_1|^2 = |C_2|^2 = 0$. The arrows denote the various paths along which the system evolves in between crossings. (b) The population in $|3\rangle$, where after multiple crossings the probability is not a mere product of Landau -Zener probabilities at each crossing. (c) Quantum interference effect observed in the net population in level $|3\rangle$ at $\Omega t = 6.0$, by changing the path (which depends on Δ_2) along which the system evolves (shown by arrows in (b)) and thus, accumulates different phase. Δ_i and G_i are in the units of Ω.

58

whereas in our case we have a sinusoidal dependence for $\Phi(t)$. This geometric amplitude factor arises even for systems for which the corresponding path is *open*. At first sight a geometric contribution due to an open path seems impossible, but if the open path represents an avoided crossing then the transition dynamics depends on relative difference between the two adiabatic eigenstates. In addition a finite *curvature* would induce *opposite* geometric contributions to these adiabatic states in which case a relative phase difference is *locally* defined. If this contribution changes as a function of time then observable effects can arise in the transition probability. Bouwmeester et al. [134] have implemented the Gaussian twisted Landau - Zener model for the two-level system in *optical atoms* and demonstrated the effect of phase due to curvature of the path followed in the parameter space. As a result even for open paths *phase effects* strongly influence transition probability as is *also demonstrated in our system*. This Gaussian twisted Landau - Zener model takes care of the unphysical property of the twisted Landau - Zener model of Berry where $\Phi(t)$ diverges as $t \to \pm\infty$. The Gaussian twisted Landau - Zener model has the form $\Phi(t) = \mu(1 - e^{-(t/a)^2})$, hence near the avoided crossing at ($t = 0$) it behaves like a βt^2, and far away from it it takes the constant value μ.

In an interesting experiment Gatzke et al. [135] observed *quantum interference effects* in microwave multiphoton transitions. The interference resulted due to different phase accumulated along different paths as the system evolved. They applied a microwave pulse that brought into resonance two-photon transition between the 21s state and the 19,3 Stark state of Potassium. When a *sech* pulse is applied the system traverses resonance (akin to crossing in our case) *twice*, once on the rising edge of the pulse, and another on the falling edge. The superposition of the two states involved evolves coherently in between these resonances. The Landau - Zener probabilities are considered at each traversal of the resonance and also the phase accumulated in between these crossings. Due to the coherent evolution between the crossings, this phase plays a pivotal role in determining the population after the second crossing. This leads to interference in the transition probability when the *relative phase* accumulated by each state during the pulse is *varied* by changing either the *width* or the *intensity* of the radiation pulse. In our system this relative phase can be varied by changing the *detuning*

of the field.

As is shown Fig. 4.4 (a), there are *two distinct pathways* (indicated by the arrows) at each crossing along which the system evolves, thereafter the levels cross again and so on. In between these crossings the superposition of the corresponding states evolves *coherently* in time. The net transition probability between the two states depends on the relative phase accumulated along each path. The *path* traversed by the system can be *varied* by varying the *detunings* . We examine, the probability of population being in level $|2\rangle$ and its dependence on the path traversed between the first two crossings. We observe the evolution of the system from $\Omega t = 0$ to 6.0, by which time level $|2\rangle$ has crossed a second time with level $|3\rangle$. By varying Δ_2 the phase accumulated by the system as it evolves along the two paths between the two crossings is varied, and we see quantum interference effect as shown in Fig. 4.4 (c). The probability of population transfer varies substantially from 0.2 to 0.8, by varying the relative phase between the paths of evolution of the system between crossings.

There have been other proposals where due to coherent evolution phase effects play an important role. Vitanov and Knight [136] considered non-perturbative treatment of coherent excitation of two-level system by a train of equally spaced identical pulses. They found that the phase accumulation during the free evolution between the pulses plays as important a role as the phase accumulation during the pulse.

4.2.2 Creating Inversion Across Multiple Levels

We now exploit this combination of the trapping condition and simultaneous crossing of all the levels for creating inversion across the ladder system. We first describe in brief the usual rapid adiabatic passage (RAP) method thats conventionally used and then bring out the advantages of our method. Our method is quite different from the usual population transfer in three-level systems by RAP [129]. As was described in brief in section 2.3 in RAP one requires a sequence of unconventional pulses, so that first the empty set of levels is pumped and only thereafter - with some temporal overlap - the initially populated levels are addressed. In this way the intermediate level remains practically *unpopulated* . Another RAP proposal is to apply temporarily co-incident pulses with frequency sweep in an anti-intuitive manner so that again the

unpopulated levels experience the resonance and thereafter the populated level. Recent calculation have also shown that this unconventional pulse sequence results in negligible population in the intermediate state hence inversion is unaffected even if the intermediate state is in the continuum [137].

Efficient population transfer has been achieved experimentally in a three-level ladder system by *frequency-swept* ultrashort laser pulse in *Rb* by Broers et al. [138]. They demonstrated complete population inversion using *intuitive* sequence of two successive adiabatic passages. They also obtained 100 % inversion by an *counterintuitive* direction of sweep of frequency which resulted in a strong reduction of the intermediate level population. This was due to direct crossing of the bottom and the topmost level. Their proposal of using a *single counterintuitively* chirped pulse is not applicable to a Λ system because of absence of direct crossing between the dressed initial and final states. Whereas our scheme could be applied even to the Λ system by proper choice of detunings. Hence our scheme is more *flexible* in terms of arranging appropriate crossings of levels, which is done by changing the detunings of the coupling fields *independently* along the two transitions rather than careful timing / overlapping of various pulses and / or direction of chirping of the pulse.

We now describe our mechanism for creating inversion. In addition to the trapping condition we require that *all the three levels* cross simultaneously at each crossing. This results whenever $\Delta_1 = \Delta_2$, and at times $\Omega t = cos^{-1}(\Delta/M\Omega)$. We observe a periodic exchange of population between the top and the bottom level at every crossing, whereas the population in the middle level remains *intact* . If the population is initially put in level $|1\rangle$ ($|3\rangle$) after the first crossing the population is transferred to $|3\rangle$ ($|1\rangle$), with the intermediate level experiencing only a little transient population, see Fig. 4.5 (a). Note further that the population transfer to the intermediate state is not complete only $\sim 10 - 20\%$ goes into it. The inversion achieved at the first crossing is completely *undone* at the next crossing. Here we deal with cw fields and as the application of the FM fields lead to simultaneous trapping and crossing of all the levels, it is experimentally more attractive. In contrast the RAP proposals involve dressing of unpopulated levels first and thereafter the populated level cross with the appropriate state using careful timing. Hence RAP schemes are extremely *sensitive to timing* of various pulses. An-
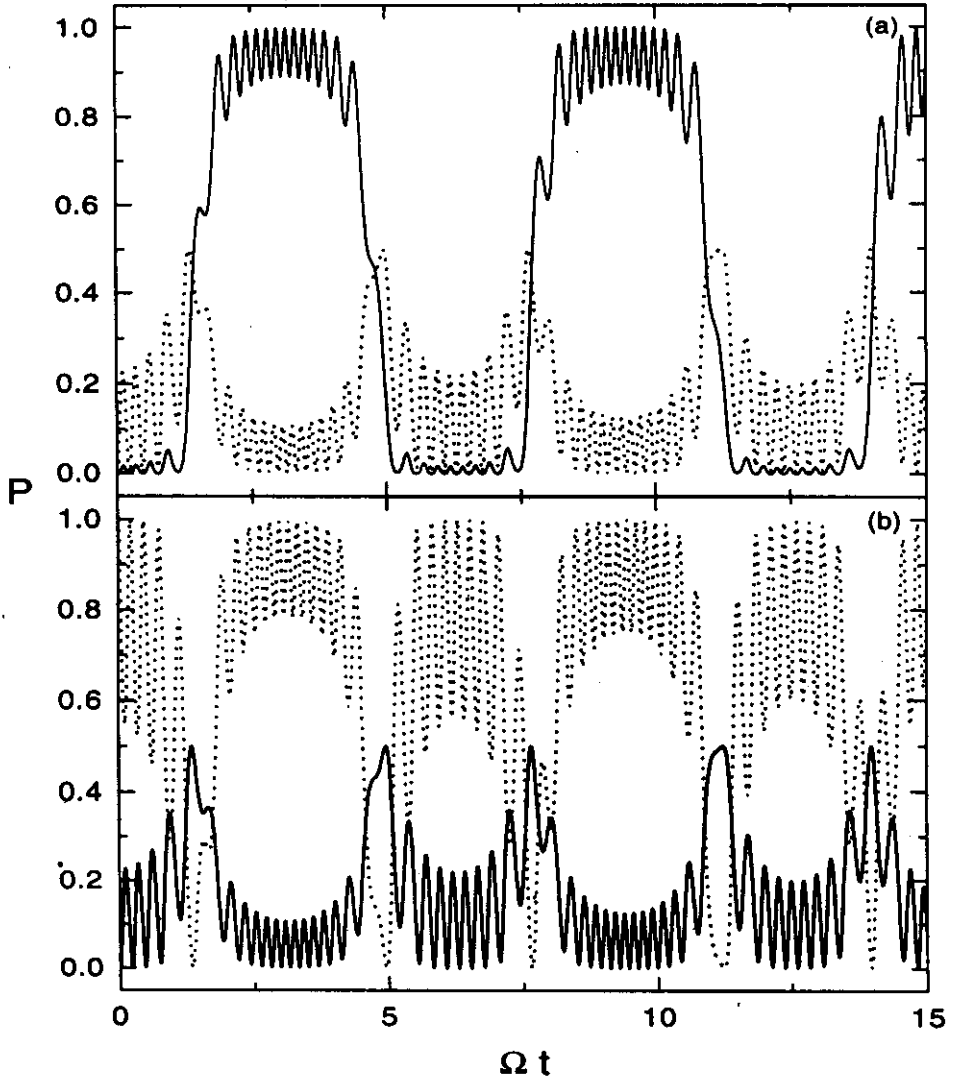
Figure 4.5: (a) When all the three-levels cross at every crossing, there is a periodic exchange of population between $|1\rangle$ and $|3\rangle$, the population of level $|3\rangle$ is plotted in solid line, whereas the level $|2\rangle$ which experiences partial population transfer is plotted in dotted line. For $M = 30.6346$, $\Delta_1 = \Delta_2 = 5$, $G_1 = G_2 = 7$, with the initial condition $|C_1|^2 = 1$, $|C_2|^2 = |C_3|^2 = 0$. (b) Same as in (a) with initial condition $|C_2|^2 = 1$, $|C_1|^2 = |C_3|^2 = 0$, the population in the intermediate state (dotted) remains unaffected even after multiple crossings with other levels. Population in $|1\rangle$ and $|3\rangle$ are denoted by the solid lines (these lines overlap each other exactly). Δ_i and G_i are in the units of Ω.

other major advantage of our scheme over RAP is that the presence of *finite population in the intermediate level* renders the RAP process very *inefficient*. Whereas in our scheme population in the intermediate state remains *untouched*. Only the population in |1⟩ and |3⟩ get exchanged at every crossing. Fig. 4.5 (b) shows this feature, when all the population is initially in |2⟩, it remains *unchanged* even after multiple crossings with levels |1⟩ and |3⟩. Thus we have demonstrated a new method of inverting population across multiple levels even if initially there is *finite population in the intermediate state*.

4.3 Classical Analogue of Coherently Driven Atomic Systems : An Optical Atoms Realization

The basic unit one deals with in the physics of atomic optical resonance is a *two-level* atom interacting with an electromagnetic radiation of a frequency that matches the energy level separation in the atom. Woerdman et al. [139] have shown in detail that a system formed using two distinct coupled classical optical modes show *analogous* characteristics, this system has been termed as an *optical atom*. There are many advantages of carrying out studies with optical atoms; they being *macroscopic* in nature one has precise control on *all* the parameters over ranges that are sometimes not accessible in experiments with real atoms. Moreover, one can make *continuous measurement* on this classical optical field *without* influencing the dynamics of the system, whereas in the quantum case a measurement yields a *collapse* of the wavefunction.

Classical analogue of the two-level quantum system has thrown light into issues like validity of the rotating wave approximation which is taken for granted at optical frequencies used to excite real atom; in optical atoms the manifestations of the inclusion of counter rotating terms has been experimentally observed. Among the phenomenon associated with the breakdown of rotating wave approximation are the Bloch-Seigert shift and multiphoton transitions. The Bloch-Seigert effect results in a change in the transition frequency which can be considered, for the single-photon case, as the consequence of dynamic stark shift produced by the non-resonant terms which are neglected in the rotating wave approximation. Among realizations of the multi-level systems Woerdman et al. [139] have shown that systems with even number of

levels like four, six etc. can be simulated in optical atoms by an appropriate choice of different longitudinal modes of the cavity and coupling them appropriately. The three-level system has so far eluded an optical atom realization.

Here we propose an *optical implementation* of a *three-level ladder system* . Moreover in the trapping phenomenon we describe the trapping is more effective if the contribution of $J_n(M)$ for $n > 0$ to the interaction term of the Hamiltonian is minimal, which can be ensured by choosing high index of modulation M. The experimental difficulty with real atoms lies in achieving high index of modulation at optical frequencies, and hence *optical atoms* would be best suited in this regime.

In an optical atom Spreeuw et al. [139] considered a single longitudinal mode of an optical ring cavity. This mode has twofold *propagation* degeneracy (waves traveling in the clockwise, counterclockwise direction), as well as twofold *polarization* degeneracy (modes with polarization along x,y directions or the σ^+, σ^- polarization states). By lifting either of these degeneracies we obtain two modes with separate frequencies. For brevity we deal with only one type of degeneracy - the propagation degeneracy; the polarization implementation can be carried out on the lines of Ref. [139]. The propagation degeneracy can be lifted using the *Sagnac effect* which produces a frequency difference, quantified by $2S$, for the two counter propagating modes. By increasing the tuning parameter S the modes are pulled apart yielding a *real crossing* for the two modes at $S = 0$ (i.e. when there is no rotation the modes are degenerate). An *avoided crossing* is obtained by coupling these two modes by means of *backscattering* . The rate of backscattering W (for a reflecting element with amplitude reflection coefficient $r \ll 1$ the backscattering rate is rc/L where L/c is the roundtrip time in the cavity of length L) determines the minimum frequency separation at $S = 0$. Similar tuning and coupling can be obtained for the polarization degeneracies, using electro-optic modulators.

In contrast to a single ring cavity used in Ref. [139] for the two-level atom, here we require *two identical coupled ring cavities* as shown in Fig. 4.6. One possibility could be two *identical* fiber-optic ring resonators coupled using a lossless 2×2 fiber optic coupler. We distinguish the various modes by their *direction of propagation* . The eigenmodes, for a particular polarization state of a single longitudinal mode in the
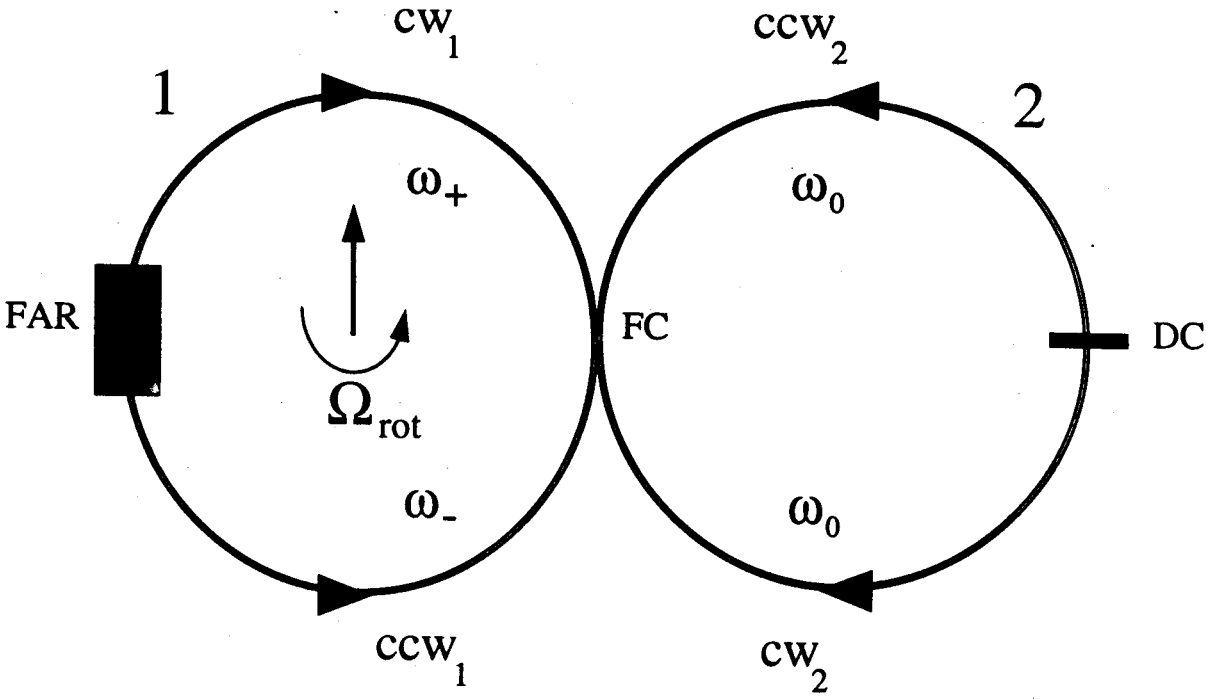
Figure 4.6: Schematic of the Optical implementation of the three-level ladder system. Ω_{rot} depicts the effect of the Faraday rotator (FAR). The *conservative* coupling of both the cavities is got by a lossless 2×2 fiber coupler (FC). The *dissipative* coupler (DC) is a thin localized absorber. The three non-degenerate *propagation* modes simulating the three-level ladder system are the cw_1, ccw_1 and cw_2-ccw_2.

coupled cavity, would be two degenerate set of modes traveling clockwise (*cw*) and counterclockwise (*ccw*) in each cavity. Thus there would be four degenerate modes cw_1, ccw_1, cw_2 and ccw_2 (where 1 and 2 label the two cavities). Now the basic idea is to lift the degeneracies of two modes in *one* of the cavities, and couple all these modes appropriately. The two-mode description in each cavity is valid in the regime where the frequency splitting of the longitudinal mode is much smaller than the free spectral range of the ring cavity.

The Faraday rotator in the ring-resonator 1 would simulate mechanical rotation of only the ring cavity 1 (we assume weak coupling between the two cavities), this would result in a round-trip phase difference between the cw_1 and ccw_1 modes due to the *Sagnac effect* thus lifting the degeneracy between these counter propagating modes. This would create a mode structure for the coupled cavity which would be quite similar to the two-level case, but would also contain the degenerate modes of

cavity 2 (cw_2, ccw_2) which would *not* change as the parameter S ($\propto$ rotation rate of cavity 1) is varied.

We require that the coupling between the modes cw_1 and ccw_2 (as well as, ccw_1 and cw_2) should be *conservative* [140], which would result in *frequency splitting* in the passive mode structure of the coupled cavity. Whereas the coupling (by backscattering) in cavity 2 between cw_2 and ccw_2 should be of the *dissipative* kind, which would cause frequency locking of these two modes.

These various couplings can be realized in the following way. To realize a *conservative coupling* a *lossless* 2×2 fiber optic coupler can be used which would merely redistribute the intensity between the cw_1 and ccw_2 (and correspondingly between ccw_1 and cw_2) modes. This coupling causes a frequency splitting between the modes and would result in an *anticrossing* in the passive coupled cavity mode structure. The width of this frequency splitting would be proportional to the coupling ratio of the 2×2 coupler. On the other hand the *dissipative coupler* (DC) could be a localized *absorber* i.e., a thin (as compared to the wavelength of the input field) absorbing layer placed perpendicular to the mode axis, that would cause frequency locking of the modes in cavity 2. This phenomenon of frequency locking is same as the so called *locking problem* of the counterpropagating modes due to injection signal (caused by scattering etc.) in laser gyroscopes at low rotation rates [141]. As there is no rotation of cavity 2 the cw_2 and ccw_2 modes get frequency locked and become degenerate. Without this dissipative coupler we would have *two* two-level systems shifted in frequencies such that cw_2 and ccw_2 would be uncoupled and near degenerate. Whereas with the dissipative coupling there would be *three* non-degenerate modes in the system cw_1, ccw_1 and $cw_2 - ccw_2$ (as the modes in the cavity 2 are coupled and frequency locked).

These three non-degenerate frequencies would be $\omega_\pm$ and ω_o, where $\omega_\pm$ near a specific crossing point (ω_o^i, Ω_{rot}^j) in the energy band structure, along the lines of Ref. [142] is given as in eqn. (4.9). The index i corresponds to possible different longitudinal modes of the cavity, and the index j denotes different rotation rates.

$$\omega_\pm = \omega_o^i \pm \frac{1}{2} \left[\frac{L^2}{n^2 \pi^2 c^2} (\Omega_{rot} - \Omega_{rot}^j)^2 + \frac{\Delta_\pm}{\omega_o^i} \right]^{\frac{1}{2}}, \tag{4.9}$$

where L is the length of each cavity, Ω_{rot} is the uniform angular frequency with which the cavity 1 rotates, n is the refractive index and $\Delta_\pm = (\frac{\sqrt{7}\pm}{\pi}) \Delta\omega_1$. Here $\Delta\omega_1$ is the

free spectral range of the ring resonator 1, and $\gamma_{\pm}$ is the intensity coupling coefficient per round trip between the modes at frequencies $\omega_{\pm}$ and the mode with frequency ω_o, respectively (which depend on the coupling ratio of the 2×2 fiber coupler).

On similar lines as in Ref. [139] the two parameters S and W in the three-level case correspond to the Faraday isolator strength which is proportional to S and is essentially a measure of the frequency splitting. Whereas W is proportional to intensity coupling of the modes $cw_1 \leftrightarrow ccw_2$ ($\propto W_+$) and $ccw_1 \leftrightarrow cw_2$ ($\propto W_-$), via the 2×2 coupler (see Fig. 4.6). We define the eigenvectors of the Hamiltonian H_S for $W = 0$ as the S-basis, and those for $S = 0$ as the W-basis. In the S-basis we have the following Hamiltonian

$$H_S = \begin{bmatrix} S & W_+ & 0 \\ W_+ & 0 & W_- \\ 0 & W_- & -S \end{bmatrix}. \tag{4.10}$$

For simplicity we assume a symmetrical 2×2 coupler *i.e.* $W = W_+ = W_-$. On diagonalizing eqn. (4.10) we get the eigenfrequencies which are $\omega_o = 0$ and $\omega_{\pm} = \pm\sqrt{2S^2 + W^2}$. On varying the parameter S one obtains an avoided crossing due to the coupling W.

Now let us consider the three-level optical atom in presence of a harmonically time dependent field at the frequency ω_l *i.e.*, $S = S_0 e^{-i\omega_l t} + c.c.$ We transform the Hamiltonian (4.10) into the W-basis which after the rotating wave approximation is

$$H_W = \begin{bmatrix} \Delta_+ & S_0 & 0 \\ S_0 & 0 & S_0 \\ 0 & S_0 & -\Delta_- \end{bmatrix}. \tag{4.11}$$

The detunings are defined as $\Delta_+ = \omega_l - W_+$ and $\Delta_- = \omega_l - W_-$. The generalized Rabi frequency of the optical atom between the various transitions is proportional to $\sqrt{\Delta^2 + 2S_0^2}$ (for $W_+ = W_-$). A comparison of eqn. (4.11) with the three-level ladder system shows that the analogy between the three-level atomic system and its optical

implementation is *complete* if the following connections are made

$$
\begin{aligned}
\omega_{12} &\leftrightarrow \omega_+ \\
\omega_{23} &\leftrightarrow \omega_- \\
\Delta_{12} &\leftrightarrow \Delta_{\pm} \\
\vec{d}_{12}, \vec{d}_{23} &\leftrightarrow \text{magneto-optic coefficient of FAR} \times \text{its length.}
\end{aligned}
\tag{4.12}
$$

To observe the phenomenon of trapping states discussed earlier, one would have to generate an appropriate field S at the Faraday rotator so that $\partial B / \partial t$ simulates frequency modulated field with an modulation index M such that $J_o(M) = 0$; and also the frequency of modulation Ω, the choice of which would determine the times at which various levels cross each other leading to jumps.

Furthermore a three-level Λ-configuration is also possible with an appropriate choice of a set of longitudinal modes in the cavity and the corresponding coupling of these modes. Unlike the fiber optic possibility one could even go in for bulk optic cavities where a variable coupling between the cavities can be obtained using various methods of evanescent coupling [143]. This optical atom implementation would open avenues to observe richer dynamics of the three-level systems in hitherto unexplored parameter regime.

Thus in conclusion, we have discussed the following issues in this chapter: (a) We have shown parameter regimes where various kinds of multi-level crossings occur causing population redistribution, we have shown that trapping of population persists, even if there is an initial phase mismatch between the two applied fields or unequal choice of the modulation index and modulation frequency; (b) The phase accumulated by various states in between these crossings plays a vital role in determining the transition probabilities after multiple crossings leading to quantum interference effect; (c) We have demonstrated a new method for near 100% population inversion in three-level ladder system even in presence of finite intermediate state population without affecting it; (d) We have proposed a classical optical implementation of the three-level ladder system using coupled cavities for optical atoms in which such a phenomenon can be observed.

Control of Optical Bistability [1]

Quantum coherence and interference has led to many new optical phenomenon like possibility of producing laser action without population inversion (section 2.8), generation of large refractive index with zero absorption (section 2.9), enhancement of nonlinear signal generation (section 2.5), quenching of spontaneous emission noise (section 2.7) and Electromagnetic field induced transparency (section 2.4). The three-level schemes are usually the most popular ones in considerations of field induced transparency. The transparency arises from the Autler-Townes splitting of the absorption line as well as due to *interferences* which makes the absorption proportional to the decay of the atomic coherence between two states that are not directly connected by a dipole transition.

All the applications listed above involve either *single atom* situations or those which are equivalent to *non-interacting atoms*, for example even in the context of pulse matching [145] where coherently prepared medium inturn drives the fields that prepare them. In this chapter we investigate the role of atomic coherence and interferences in the context of *collective phenomenon* inside a resonator. An external electromagnetic field is used in tandem with the usual bistable field and is tuned close to resonance along another transition in the atomic system. This external field controls the polarization along the bistable transition. We examine the *modification* of the *bistability characteristics* such as the thresholds, switching times etc. We also find that this control field can lead to *multistability*.

Historically absorptive bistability in *all-optical* systems was first predicted by Szöke et al. [146]; McCall [147] showed that under suitable conditions *differential gain* with *transistor* action is possible for absorptive bistability in a Fabry-Perot cavity. This led to the very first experiments by Gibbs et al. [148] in Sodium where they observed both

---

transistor action and bistable behavior. Among the early theoretical and experimental works some of the following works in Refs. [149, 150, 151] are noteworthy. Since then there has been lot of activity in achieving efficient bistable devices for wide range of applications, from optical communication to optical realization of quantum computing.

5.1   What is Optical Bistability ?

On injecting a cw laser beam on an *empty* optical cavity the transmitted intensity is *proportional* to the input intensity. The proportionality constant depends on the *cavity mistuning* and the *finesse* of the cavity. When the cavity is filled with either an absorptive or dispersive material the transmitted intensity becomes a *nonlinear* function of the input intensity. The behavior of the system depends on the ratio of absorption coefficient (α) × length (L) of the active medium and the cavity mirror transmissivity (T). Above a critical value of the co-operative parameter $(\alpha L/T)$, we have the bistable behavior. In the lower branch of the hysteresis loop of bistability the atoms no longer evolve individually but act in *unison* . Hence the term *co-operative* phenomenon. Only when the atom-field interaction leads to such a co-operative (collective) effects do we get bistability. *Optical bistability is said to occur when for a range of input values of the incident field intensity, there are two stable (bistable) output states* . It involves interplay of both *feedback* from the mirrors (cavity) and *nonlinearity* of the atom-field interaction.

These systems have great potential as devices because they can work as optical transistors, all-optical memory elements, or all-optical pulse shapers as they eliminate noisy features of the input light (discriminators, clippers and limiters). Presently there is major thrust in making practical, miniaturized and fast bistable devices which would eventually lead to realization of efficient all-optical processing devices, hopefully in the near future. Our work is a step in that direction, here we propose among other features schemes of lowering the threshold for switching as high threshold for bistability is one of the bottlenecks in the direction of miniaturization. We also show that multistable operation can be got by merely changing the control field parameters, similarly transistor action and bistable operation requires a proper choice of control field parameters. This opens up a possibility of using the *same* device for multiple operations.
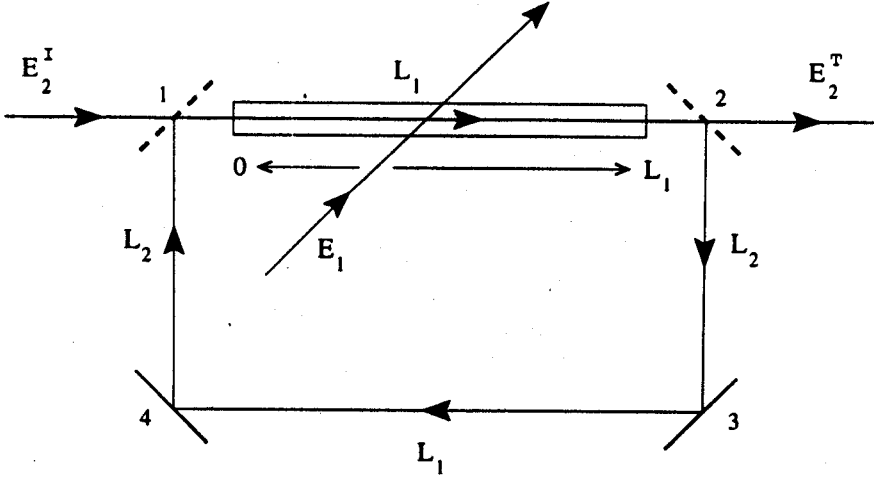
Figure 5.1: Uni-directional ring cavity with atomic sample of length L_1 with n homogeneously broadened atoms with atomic configuration as given in Fig. 5.2. E_2^I and E_2^T are the incident and transmitted fields respectively and E_1 is the control field. For the mirrors 1 and 2 $R + T = 1$, and mirrors 3 and 4 have $R = 1$.

We demonstrate the application of electromagnetic field induced transparency and quantum interference effects in the *co-operative phenomenon of optical bistability* . We use another control field to tailor the polarization of the bistable transition. The control field used along with the usual electromagnetic field of the two-level scheme results in a considerable *lowering* of the *threshold intensity* . We study the transient response of the system in the *mean field limit* and describe the regression to the steady state when perturbed away from it; in our system the regression exponent is itself dependent on the control field. We also demonstrate the possibility of control field induced *multistability* and the *fine control* one has on its various threshold characteristics.

5.2   Model Calculations

In order to keep the analysis as simple as possible we consider an uni-directional ring cavity (Fig. 5.1) with the mirrors 3 and 4 with 100% reflectivity and the mirrors 1 and 2 have the reflection and transmission coefficient (R and T, respectively) such that $R + T = 1$. This is the standard model of optical bistability given by Bonifacio and Lugiato [150, 152]. The atomic system is a collection of n homogeneously broadened
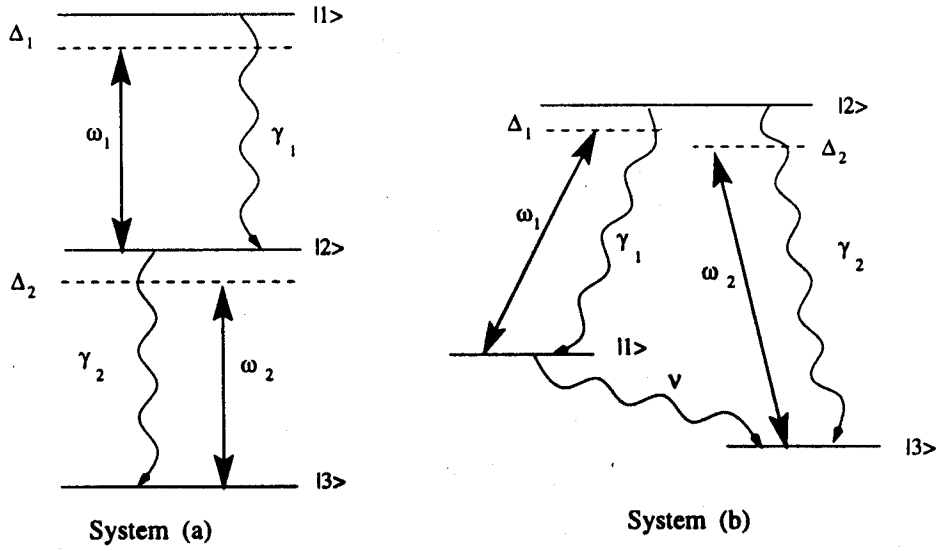
System (a)   System (b)

Figure 5.2: The transitions labeled $|2\rangle$ and $|3\rangle$ are the bistable transitions, the control field $\vec{E}_1$ couples the excited state $|2\rangle$ to another level above (for system (a)) or below (for system (b)) the excited state. Here Δ_i's are the detunings and γ_i's are the decays of the corresponding levels.

two-level atoms which have their excited states coupled to yet another level which could be energetically *above* or *below* this excited state (we consider both such cases, as shown in Fig. 5.2, the system (a) and (b), respectively). The field at the atom that couples these various transitions can be written as

$$\vec{E} = \vec{E}_1 e^{-i\omega_1 t} + \vec{E}_2 e^{-i\omega_2 t} + c.c., \tag{5.1}$$

where the subscripts 1 and 2 refer to the transitions $|1\rangle \leftrightarrow |2\rangle$ and $|2\rangle \leftrightarrow |3\rangle$, respectively. In both these systems the coherent field $\vec{E}_2$ applied to the transition $|2\rangle \leftrightarrow |3\rangle$ corresponds to the usual two-level scheme and $|1\rangle \leftrightarrow |2\rangle$ is the transition on which the *control field* $\vec{E}_1$ is applied. The *control field does not circulate in the cavity* and thus its dynamical evolution can be *ignored*. The present scheme should not be mixed up with two-photon bistability [153] which in general deals with situations where the intermediate state is *far* from resonance. In our present work we deal with the *control of single-photon bistability*. We consider the system (a) as shown in Fig. 5.2 where the level $|1\rangle$ decays through spontaneous emission to level $|2\rangle$ with Einstein A - coefficient $2\gamma_1$, and level $|2\rangle$ decays to $|3\rangle$ with Einstein A-coefficient $2\gamma_2$. Similarly in system (b) the level $|2\rangle$ decays to levels $|1\rangle$ and $|3\rangle$ with the Einstein A-coefficients $2\gamma_1$ and $2\gamma_2$, respec-

tively; and the level $|1\rangle$ decays to $|3\rangle$ with the decay rate of 2ν (Fig. 5.2). We describe the dynamics of the atom plus the radiation fields by the well known *Maxwell-Bloch* equations. The unperturbed Hamiltonian of the atom is given as

$$H_o = \hbar\omega_{13}|1\rangle\langle1| + \hbar\omega_{23}|2\rangle\langle2|, \tag{5.2}$$

where energies are measured from the ground state $|3\rangle$. In the *dipole approximation* the interaction Hamiltonian between the atom and the external fields is given by $H_{int} = -\vec{d}\cdot\vec{E}$, where $\vec{d}$ is the atomic dipole moment operator having only the off-diagonal elements

$$\vec{d} = \vec{d}_{12}|1\rangle\langle2| + \vec{d}_{23}|2\rangle\langle3| + c.c. \tag{5.3}$$

The total Hamiltonian for the system is given by $H = H_o + H_{int}$. Density matrix formalism is used to study the evolution of the system. Incoherent processes like the spontaneous emission from different levels are included phenomenologically in the standard way as described in section 2.1.

We undertake the *rotating wave approximation* for the fields and neglect the rapidly oscillating terms like $e^{\pm 2i\omega_1 t}$ and $e^{\pm 2i\omega_2 t}$ which is quite valid in the optical regime where the fields oscillate at $\sim 10^{14} Hz$. This transforms the evolution equations of the density matrix $\rho_{\alpha\beta}$ for system (a) to those for slowly varying quantities $\tilde{\rho}_{\alpha\beta}$, where

$$\begin{aligned}
\tilde{\rho}_{ii} &= \rho_{ii}, i = 1, 2, 3 \\
\tilde{\rho}_{12} &= \rho_{12}e^{i\omega_1 t}, \\
\tilde{\rho}_{23} &= \rho_{23}e^{i\omega_2 t}, \\
\tilde{\rho}_{13} &= \rho_{13}e^{i(\omega_1+\omega_2)t},
\end{aligned} \tag{5.4}$$

The equations of evolution of the density matrix are:

$$\begin{aligned}
\dot{\tilde{\rho}}_{11} &= -2\gamma_1\tilde{\rho}_{11} + iG_1\tilde{\rho}_{21} - iG_1^*\tilde{\rho}_{12}, \\
\dot{\tilde{\rho}}_{12} &= -(\gamma_1 + \gamma_2 + i\Delta_1)\tilde{\rho}_{12} + iG_1(\tilde{\rho}_{22} - \tilde{\rho}_{11}) - iG_2^*\tilde{\rho}_{13}, \\
\dot{\tilde{\rho}}_{13} &= -(\gamma_1 + i(\Delta_1 + \Delta_2))\tilde{\rho}_{13} + iG_1\tilde{\rho}_{23} - iG_2\tilde{\rho}_{12}, \\
\dot{\tilde{\rho}}_{22} &= 2\gamma_1\tilde{\rho}_{11} - 2\gamma_2\tilde{\rho}_{22} - iG_1\tilde{\rho}_{21} + iG_1^*\tilde{\rho}_{12} + iG_2\tilde{\rho}_{32} - iG_2^*\tilde{\rho}_{23}, \\
\dot{\tilde{\rho}}_{23} &= -(\gamma_2 + i\Delta_2)\tilde{\rho}_{23} + iG_1^*\tilde{\rho}_{13} + iG_2(\tilde{\rho}_{33} - \tilde{\rho}_{22}), \\
\dot{\tilde{\rho}}_{33} &= 2\gamma_2\tilde{\rho}_{22} - iG_2\tilde{\rho}_{32} + iG_2^*\tilde{\rho}_{23}.
\end{aligned} \tag{5.5}$$

For the system (b), the following transformations are undertaken to get rid of the rapidly rotating terms

$$
\begin{aligned}
\tilde{\rho}_{ii} &= \rho_{ii}, i = 1, 2, 3 \\
\tilde{\rho}_{12} &= \rho_{12} e^{i\omega_1 t}, \\
\tilde{\rho}_{23} &= \rho_{23} e^{i\omega_2 t}, \\
\tilde{\rho}_{13} &= \rho_{13} e^{i(\omega_1 - \omega_2)t},
\end{aligned}
\tag{5.6}
$$

The equations of motion for the system (b) in the rotating wave approximation are:

$$
\begin{aligned}
\dot{\tilde{\rho}}_{11} &= 2\gamma_1 \tilde{\rho}_{22} - 2\nu\tilde{\rho}_{11} - iG_1\tilde{\rho}_{12} + iG_1^*\tilde{\rho}_{21}, \\
\dot{\tilde{\rho}}_{12} &= -(\gamma_1 + \gamma_2 + \nu + i\Delta_1)\tilde{\rho}_{12} - iG_1^*(\tilde{\rho}_{11} - \tilde{\rho}_{22}) - iG_2^*\tilde{\rho}_{13}, \\
\dot{\tilde{\rho}}_{13} &= -(\nu + i(\Delta_1 - \Delta_2))\tilde{\rho}_{13} + iG_1^*\tilde{\rho}_{23} - iG_2\tilde{\rho}_{12}, \\
\dot{\tilde{\rho}}_{22} &= -2(\gamma_1 + \gamma_2)\tilde{\rho}_{22} + iG_1\tilde{\rho}_{12} - iG_1^*\tilde{\rho}_{21} + iG_2\tilde{\rho}_{32} - iG_2^*\tilde{\rho}_{23}, \\
\dot{\tilde{\rho}}_{23} &= -(\gamma_1 + \gamma_2 - i\Delta_2)\tilde{\rho}_{23} + iG_1\tilde{\rho}_{23} - iG_2(\tilde{\rho}_{22} - \tilde{\rho}_{33}), \\
\dot{\tilde{\rho}}_{33} &= 2\nu\tilde{\rho}_{11} + 2\gamma_2\tilde{\rho}_{22} - iG_2\tilde{\rho}_{32} + iG_2^*\tilde{\rho}_{23}.
\end{aligned}
\tag{5.7}
$$

The overdots in eqns. (5.5) and (5.7) denote first order time derivative of the corresponding variables. The parameters $2G_1 = 2\vec{d}_{12} \cdot \vec{E}_1/\hbar$ and $2G_2 = 2\vec{d}_{23} \cdot \vec{E}_2/\hbar$ are the Rabi frequencies associated with the laser fields $\vec{E}_1$ and $\vec{E}_2$, respectively. The detunings of the field from the atomic transitions are given by $\Delta_1 = \omega_{12} - \omega_1$ and $\Delta_2 = \omega_{23} - \omega_2$. It is the field at frequency ω_2 that *circulates* through the cavity and shows bistable behavior, hence we examine the induced polarization on the $|2\rangle \leftrightarrow |3\rangle$ transition which is given by

$$
P(\omega_2) = nd_{32}\tilde{\rho}_{23},
\tag{5.8}
$$

where n is the number of atoms per unit volume.

In the ring cavity (Fig. 5.1) the coherent field E_2^I at frequency ω_2 enters into the cavity from the semi-silvered mirror 1 and drives the atomic sample. The control field at frequency ω_1 further regulates the induced polarization $P(\omega_2)$ through Autler-Townes effect and interference effects, which alters the *absorption* and the *dispersion* profiles of the active medium at the field frequency ω_2. The boundary conditions for the ring cavity impose the following conditions between the incident field E_2^I, the transmitted field E_2^T, the fields $E_2(0,t)$ and $E_2(L_1,t)$ which are fields at positions 0 and L_1 in the

cavity,

$$E_2^T(t) = \sqrt{T} E_2(L_1, t)$$

$$E_2(0,t) = \sqrt{T} E_2^I(t) + Re^{-i\delta_o} E_2(L_1, t - \Delta t), \tag{5.9}$$

where L_1 is the length of the sample, and $\Delta t = (L_1 + 2L_2)/c$ is the time light takes to travel from mirror 2 to mirror 1. The *cavity detuning* $\delta_o = (\omega_c - \omega_o)L_T/c$, where ω_c is the frequency of the cavity nearest to resonance with the incident field frequency ω_o, and $L_T = 2(L_1 + L_2)$ is the *total length* of the cavity. In eqn. (5.9) the first condition is for the transmitted field amplitude which is merely determined by the *field* at the end of the sample at position L_1 in the cavity times the square root of the *transmission coefficient* of the semi-silvered mirror 2; while the second boundary condition in eqn. (5.9) is at the position 0, where two field amplitudes add up - one contribution is from the incoming field transmitted through the input mirror 1, and the second contribution comes from the feedback (i.e. the field at L_1 at an earlier time $t - \Delta t$) which could utmost be out of phase by a factor δ_o due to cavity mistuning.

The field equation in the *slowly varying envelope approximation* (described in eqn. (2.9)),

$$\frac{\partial E_2}{\partial t} + c\frac{\partial E_2}{\partial z} = 2\pi i\, \omega_2\, d_{32}\, P(\omega_2), \tag{5.10}$$

with the boundary conditions (5.9) is solved in the *steady state* limit, i.e. $\partial E_2/\partial t = \partial \tilde{\rho}_{ij}/\partial t = 0$. Unlike the two-level system where the induced polarization $P(\omega_2)$ reduces to a relatively simple analytical form we had to resort to numerically solving these self-consistent set of field-matter equations. To obtain the polarization we solve the set of simultaneous coupled equations (5.5) or (5.7) for the system (a) or (b), respectively. Then using the relation (5.8) we integrate equation (5.10) in the steady state limit over the length of the sample inside the cavity. The boundary conditions used in the *steady state* limit reduce eqn. (5.9) to

$$E_2^T = \sqrt{T} E_2(L_1)$$

$$E_2(0) = \sqrt{T} E_2^I + Re^{-i\delta_o} E_2(L_1). \tag{5.11}$$

We also note that in the limit of the control field $G_1 \to 0$ for system (a), and on taking the multiple limit $G_1 \to 0$, $\gamma_1 \to 0$ for system (b), *both* the systems reduce to the
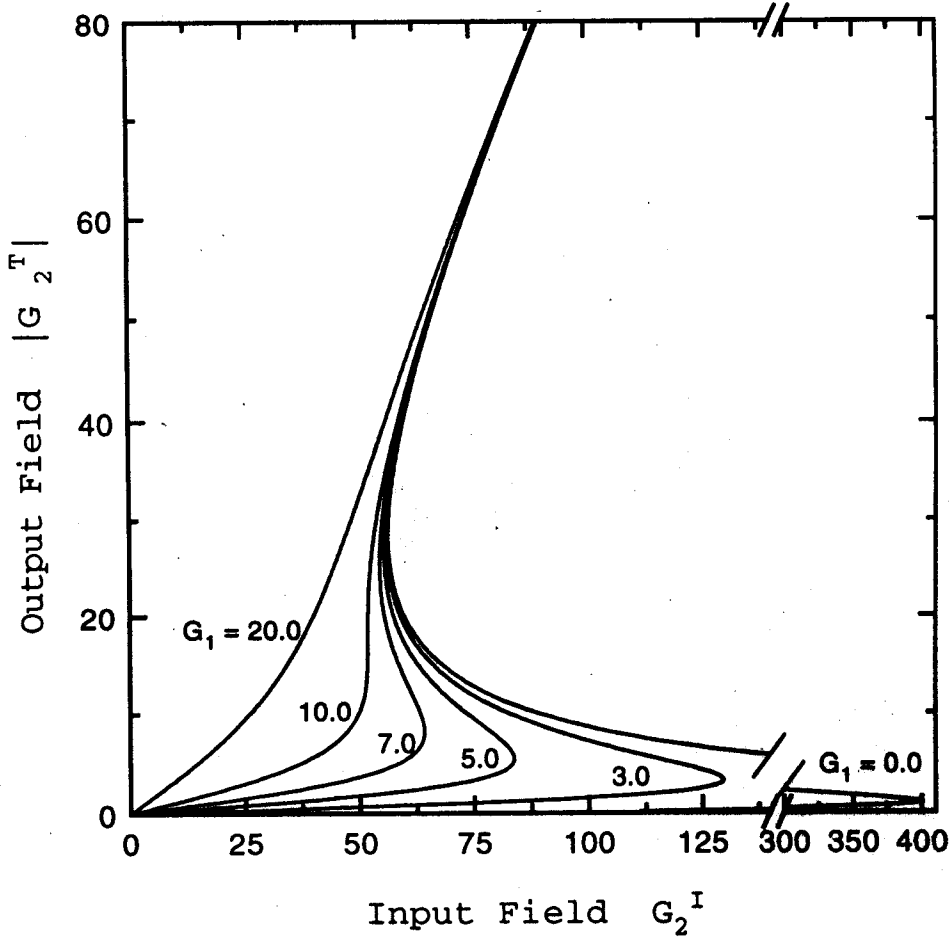
Figure 5.3: Shows the decrease in the threshold due to the control field for system (a) compared to the usual two-level bistable system. The threshold can be controlled by changing the control field $G_1/\gamma_2 = 3, 5, 7, 10, 20; C = 400$; and $\Delta_1 = \Delta_2 = 0$. Note the possibility of transistor action for $G_1/\gamma_2 = 10$.

conventional *two-level* scheme where the absorption coefficient α on the $|2\rangle \leftrightarrow |3\rangle$ transition is given by

$$\alpha = \frac{4\pi \, \omega_{32} \, d_{32}^2 \, n}{\hbar \, c \, \gamma_2}. \tag{5.12}$$

In order to compare the results with the two-level system we define the usual *co-operation parameter* C such that $C = \alpha L_1 / 2T$, same as in the two-level system [152, 154].

5.3   Electromagnetic Control of Optical Bistability

In this section we present details of our numerical results. We show that on application of the control field one can *drastically modify the threshold for switching*. Fig. 5.3 gives
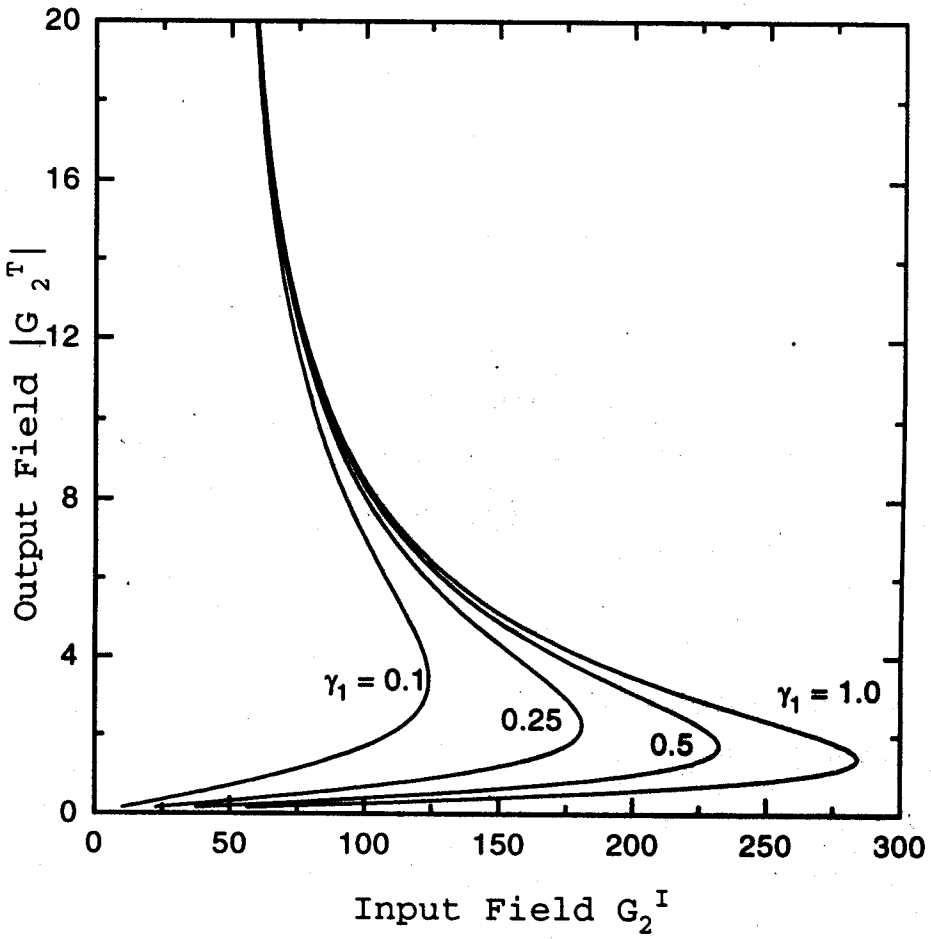
Figure 5.4: The quantum interference effect induced decrease in the threshold by having a long lived state $|1\rangle$, i.e., $\gamma_1/\gamma_2 = 0.1, 0.25, 0.5, 1.0$; $G_1/\gamma_2 = 1.0, C = 400$; and $\Delta_1 = \Delta_2 = 0$.

the bistable behavior of the two-level system subjected to a control field on the upper transition in system (a). Clearly the control field leads to the lowering of the bistability threshold owing to the *Autler-Townes splitting* . The control field creates a dressed state doublet at $\pm\sqrt{\Delta_1^2 + 4|G_1|^2}$. The absorption at the linecenter decreases with increase in the control field G_1. As the control field gets too large the bistable behavior disappears, as for large G_1 there is hardly any linear absorption and even the linear dispersion at the linecenter is zero.

We now examine the perturbative result to understand the quantum interference effect. For the ladder system Fig. 5.2 (a), the linear susceptibility on the transition $|2\rangle \leftrightarrow |3\rangle$ to all orders in the strength of the control field G_1 and to first order in the

cavity field G_2 is given by

$$\chi_{(a)}(\omega_2) \propto \left[(\Delta_2 - i\gamma_2) - \frac{G_1^2}{(\Delta_1 + \Delta_2 - i\gamma_1)} \right]^{-1} \qquad (5.13)$$

In absence of the control field the susceptibility $\chi_{(a)}(\omega_2)$ in eqn. (5.13) has only the first term, the second term comes about due to interference between the *two possible absorption channels* of the field at the frequency ω_2 to the dressed state doublet created by G_1 on the transition $|1\rangle \leftrightarrow |2\rangle$. Due to this interference term the absorption of population from $|3\rangle$ is now dependent on the decay of the coherence $\tilde{\rho}_{13}$ though the transition $|1\rangle \leftrightarrow |3\rangle$ is not dipole allowed. At resonance i.e. $\Delta_1 = \Delta_2 = 0$, eqn. (5.13) reduces to

$$\chi_{(a)}(\omega_2) \propto \frac{i\gamma_1}{G_1^2 + \gamma_1\gamma_2} \qquad (5.14)$$

The absorption at the linecenter again decreases with a decrease in γ_1. Thus if the level $|1\rangle$ is *long lived* then we can achieve further lowering of the bistability threshold. This is demonstrated in the Fig. 5.4. We see that over and above the reduction due to the Autler-Townes splitting there is a further reduction of the threshold due to the *interference effect* . The reduction in the threshold is quite significant, its more than 50% as one decreases γ_1 from 1.0 to 0.1.

We do not expect any change in the second bistability threshold (i.e., the threshold for switching from the *on* state to the *off* state), as here the field G_2 becomes too large thereby *offsetting* the advantage of a long lived state $|1\rangle$, this is also clearly seen in eqn. (5.14). We also demonstrate this by calculating the all order response of the control field on the $|2\rangle \leftrightarrow |3\rangle$ transition. The result of this calculation is shown in Fig. 5.5. We see that the atomic coherence decay γ_1 from the upper level plays little role for large G_2. The response at the bistable transition is drastically modified by this decay.

Furthermore we compare the bistability threshold for the two-level system, and the control field scheme (say for example system (a)). We arrange various parameters such that both have the same degree of absorption (i.e. same value of the Imaginary part of $\tilde{\rho}_{23}$). To this end, in the two-level system the input field is *detuned* by an amount so that the *linear absorption is same* as that at the linecenter in presence of the control field. As the Fig. 5.6 shows there is substantial advantage in using a control field as the threshold of switching is much lower with the control field than without it.
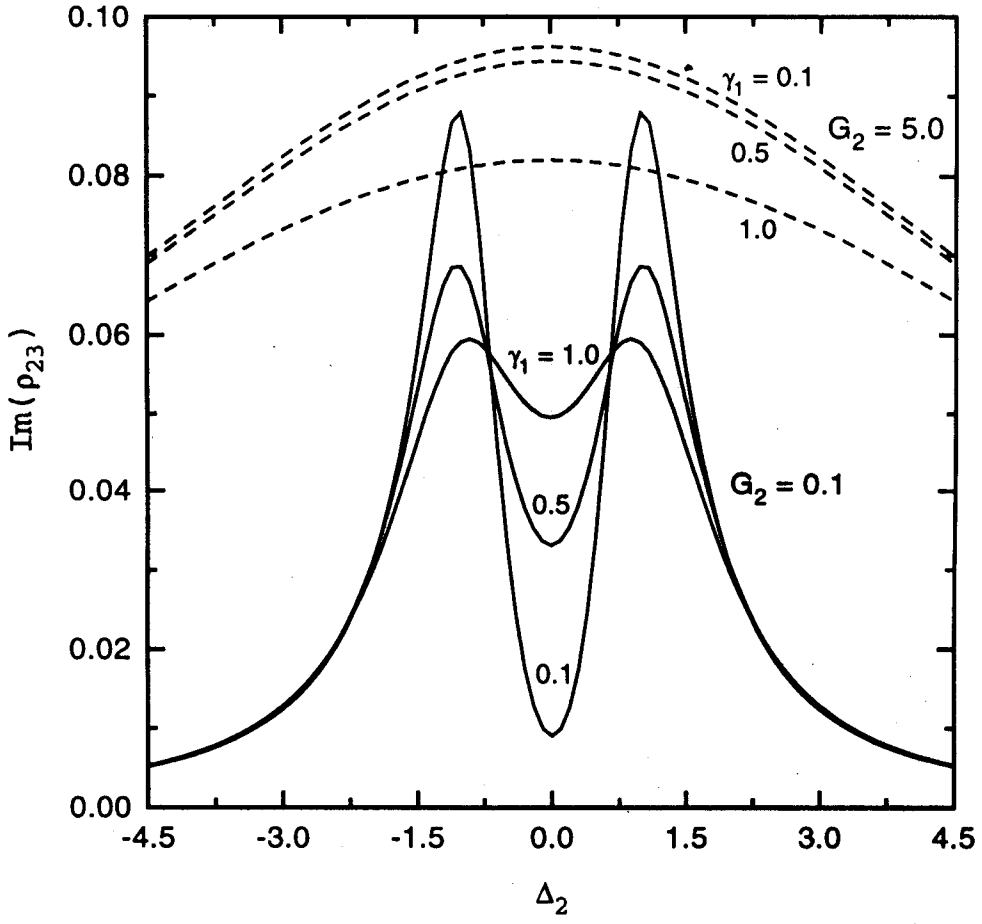
Figure 5.5: The all order nonlinear absorption for different values of the cavity field $G_2/\gamma_2 = 0.1, 5.0$ and $G_1/\gamma_2 = 1.0$.

We next present the modifications in the bistability characteristics if the control field is applied on the transition as in Fig. 5.2(b). In the absence of the parameter ν the coherent population trapping (section 2.2) occurs if the two detunings are *equal* . This leads to disappearance of the bistability hysteresis. In the presence of decay ν and operating on resonance, the absorption on the $|2\rangle \leftrightarrow |3\rangle$ transition is again proportional to the decay ν of level $|1\rangle$ which is not dipole connected to level $|3\rangle$.

Recently Shang-quing Gong et al. [155] analyzed *our model* for the case with $\nu \to 0$, where by taking into account the effect of *phase fluctuations* in the control field at the coherent population trapping condition they get back the bistable behavior which was lost due to the coherent population trapping phenomenon. With increase in the linewidth of the control laser they found that the threshold increased (bistable hysteresis loop became wider). Furthermore they also analyzed our three-level Λ-model in
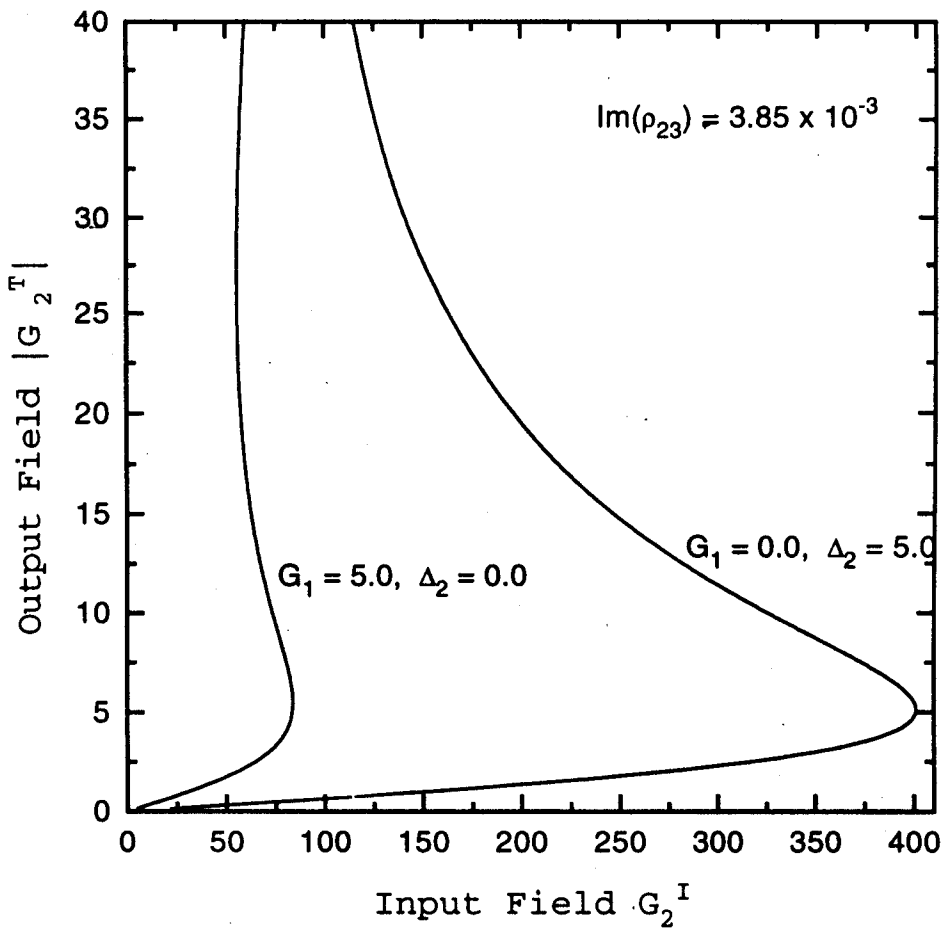
Figure 5.6: For the same level of absorption, i.e., $Im(\tilde{\rho}_{23}) = 3.85 \times 10^{-3}$, the appropriately detuned two-level system ($G_1/\gamma_2 = 0.0$, $\Delta_1 = 0.0$, $\Delta_2 = 5.0$) requires a much larger threshold than the three-level scheme (a) with the control field for $C = 400$, $G_1/\gamma_2 = 5.0$, $\Delta_1 = \Delta_2 = 0.0$.

which the atoms in the closely spaced lower levels (system (b) without ν and closely spaced levels $|1\rangle$ and $|3\rangle$) are initially prepared in a *coherent superposition state* [156]. They found that bistability characteristics can also be controlled by *varying the initial coherence* between these lower levels. This initial coherence could be obtained in many ways, say through a microwave field coupling the two lower levels. With increase in the *initial* coherence they obtained wider bistable hysteresis loop.

Coming back to our system (b) (Fig. 5.1 (b)) the analog of eqn. (5.13) for the Λ-system is,

$$\chi_{(b)}(\omega_2) \propto \left[-\Delta_2 - i(\gamma_1 + \gamma_2) - \frac{G_1^2}{(\Delta_1 - \Delta_2 - i\nu)} \right]^{-1}. \tag{5.15}$$

Fig. 5.7 gives the changes in the bistability characteristics as the strength of the control
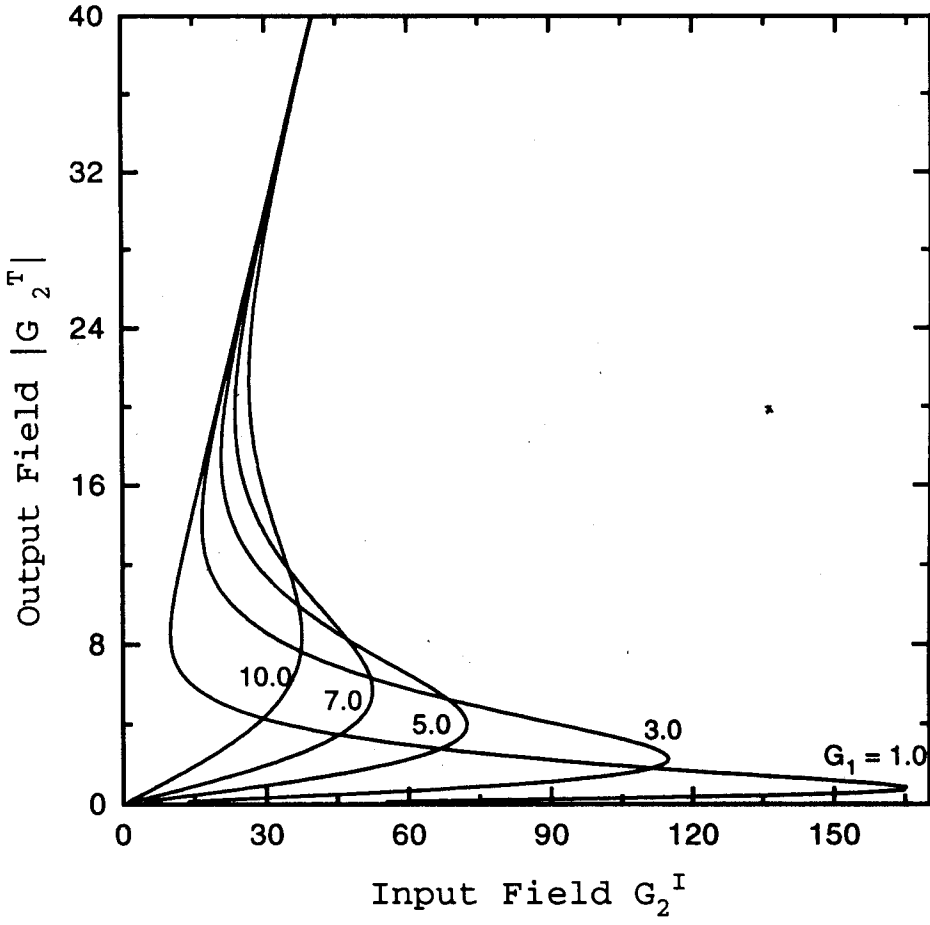
Figure 5.7: Effect of quantum interferences for system (b) for $\nu = 0.0, C = 400, \Delta_1 = 0.0, \Delta_2 = 1.0, G_1/\gamma_2 = 1., 3., 5., 7., 10.$. The behavior is similar to that for the ladder system (Fig. 5.4).

field is changed. We have chosen $\Delta_1 = 0$, $\nu = 0$, and to avoid the coherent population trapping condition we choose our field frequencies such that $\Delta_2 \neq 0$. The results are somewhat similar to those for situation of Fig. 5.3, we see substantial reduction in the bistability threshold (more than 50%) with increase in the control field strength. We discuss in the next section the transient response of our proposals.

5.4 Control Field Induced Changes in Transient Response

For simplicity we consider the *transient response* of the system in the *mean field approximation* [150], i.e. in the multiple limit $\alpha L_1 \rightarrow 0$, $T \rightarrow 0$, and $\delta_o \rightarrow 0$. It is called the *mean field limit* as the field inside the cavity does not change very much in each pass, due to the weak coupling ($\alpha L_1 \rightarrow 0$) but the mean lifetime of the photons (L_T/cT) in the
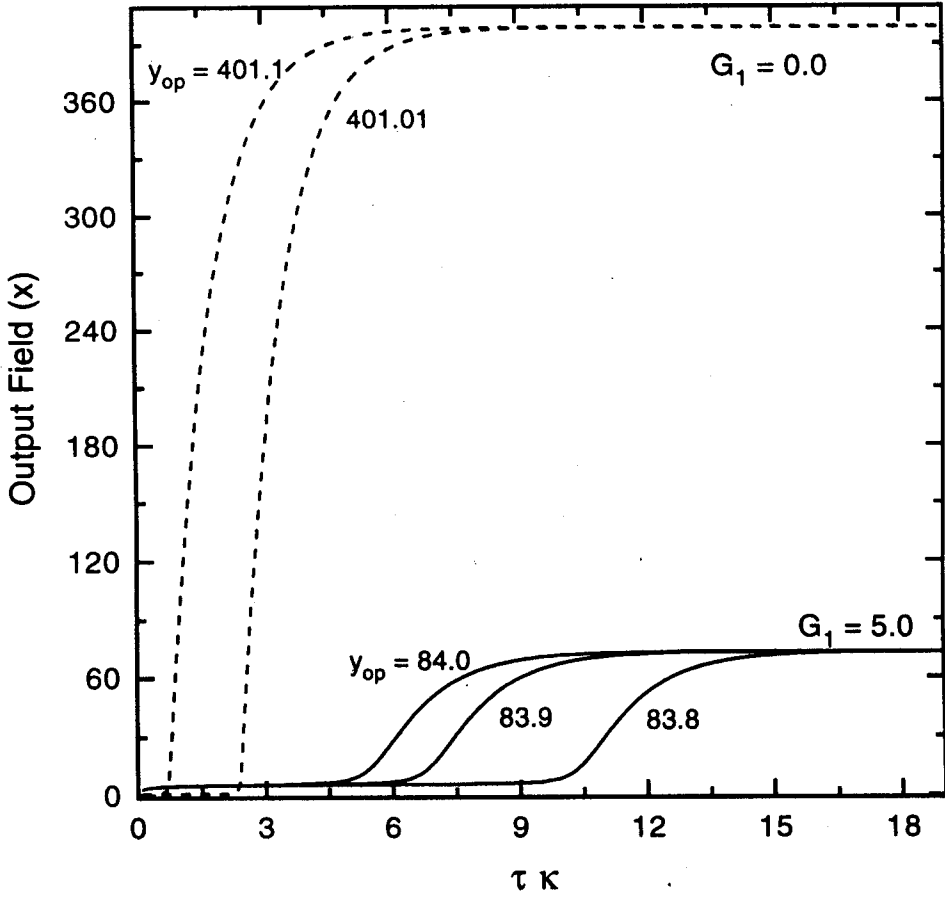
81

Figure 5.8: Comparison between the two-level scheme and the proposed schemes, the rise time is equal to ($\tau\kappa \sim 5.0$). The temporal evolution is shown for different operating points, in the two-level system $y_{op} = 401.01, 401.1$ and for system (a) $y_{op} = 83.8, 83.9, 84.0$ one observes critical slowing down phenomenon as we approach the switch up intensity. We choose $C = 400$, $\Delta_1 = \Delta_2 = 0.0$.

cavity is large because $T \to 0$. Thus the photons even in this *weak coupling limit* experience *substantial* interaction with the atoms due to the many passes they make through the sample owing to longer photon lifetimes. The limit $\delta_o \to 0$ implies that the cavity detuning is smaller than the free spectral range but of the same order of magnitude as the cavity lifetime κ^{-1}, thus ensuring that we operate in the cavity mode resonant with the incident field. It should be noted that our previous discussion on control of the switching threshold is completely general and *no* mean field approximation is made.

The time evolution of the transmitted field in a good cavity (i.e. $\kappa^{-1} \ll \gamma_2$) and with
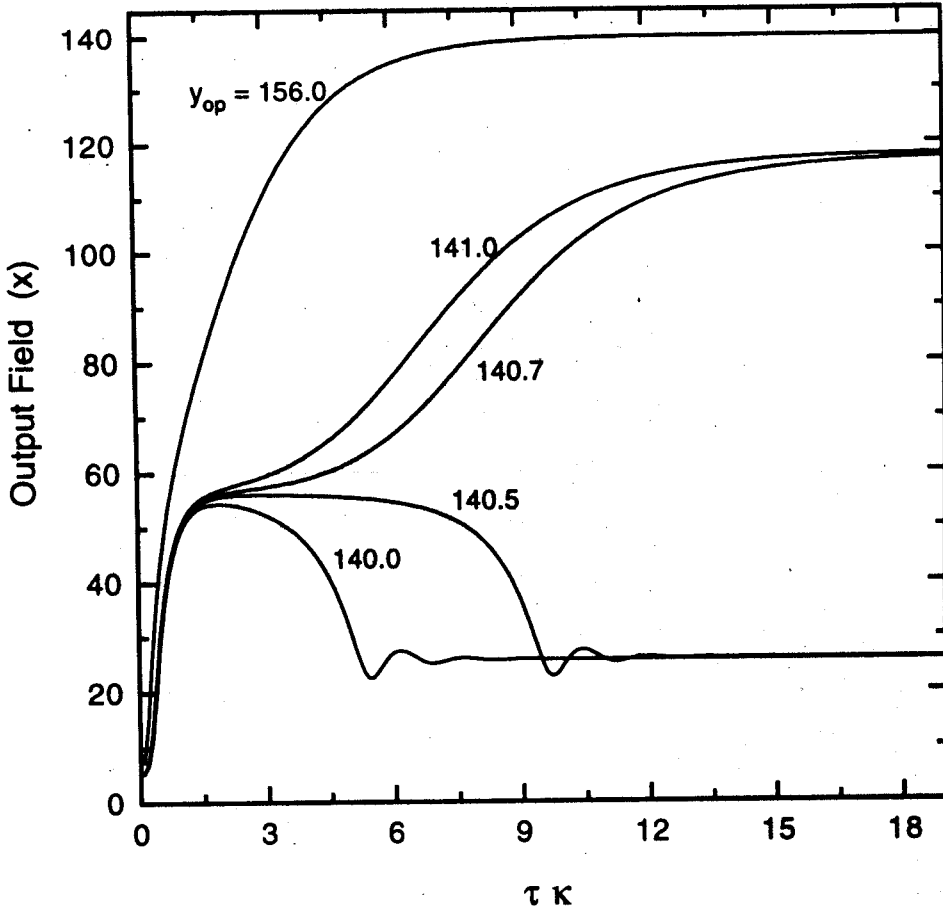
Figure 5.9: Temporal evolution in the multistable domain, the switching to the second stable state at $y_{op} = 140, 140.5$ is oscillatory with a small rise time($\leq \tau\kappa = 5.0$), switching to the third stable state at $y_{op} = 140.7, 141.0$ takes longer time ($\geq \tau\kappa = 15.0$). Also the operating point beyond the multistable region $y_{op} = 156.0$ takes similar time ($\sim \tau\kappa = 15.0$).

$\delta_o = 0$ is given by

$$\kappa^{-1}\frac{\partial x}{\partial t} = -(x - y) - 2CP_o, \tag{5.16}$$

where $\kappa^{-1} = cT/L_T$ is the cavity lifetime, x and y are the normalized amplitudes of the transmitted and the incident fields, respectively. Here the decays $\gamma_1 = \gamma_2 = \gamma$, and the dimensionless normalized fields are, $x = d_{32}\, E_2^T/(2\hbar^2\gamma^2 T)^{1/2}$ (transmitted field) and $y = d_{32}\, E_2^I/(2\hbar^2\gamma^2 T)^{1/2}$ (incident field); and P_o is the normalized nonlinear response of the medium defined as $P_o = (n/\sqrt{2})^{-1}[P(\omega_2)/i]$, on similar lines as in Ref. [152]. The transmitted amplitude x is complex, whereas the incident field y is assumed to be real. We initially begin with no input field, i.e. $y = 0$, $x = 0$ and then set the input field y to

an operating point y_{op}, and observe the dynamical evolution of the transmitted field by integrating eqn. (5.16) till the output field reaches its steady state value corresponding to the input field y_{op}. The polarization P_o in eqn. (5.16) is derived from inverting the equations (5.5) or (5.7) in the steady state for the scheme (a) or (b), respectively. The transient response with the control field (solid line) has a very similar behavior to the usual two-level case (dotted line) as is shown in Fig. 5.8. We see that the rise time ($\tau\kappa \sim 5.0$) for both the cases, with and without the control field. As is shown later in section 5.6 *multistability* is observed for an appropriate choice of the control field parameters like intensity and detunings. The transient study shows that if we choose the operating point (y_{op}) in the *multistable case* the output switches to the second stable state in an oscillatory fashion but with a fast response time, see Fig. 5.9. The switching times are relatively longer for switching from the second to the third stable state very similar to that of an operating point chosen beyond the multistable region.

5.5 Regression to steady state

In this section, we discuss how a system responds to perturbation when its initially in a stable stationary state. When the system is slightly displaced from this stable state the regression to the steady state is governed by the eigenvalues of the relaxation matrix obtained from *linearizing* eqn. (5.16) around the stationary state. In eqn. (5.16) we consider $x \rightarrow x_o + \delta x$, where x_o is the steady state value and δx is small perturbation such that $\delta x \ll x_o$. We expand $P_o(x, x^*)$ in Taylor series around the stationary state value (x_o) and take only the terms linear in δx, i.e.

$$P_o(x_o + \delta x, x_o^* + \delta x^*) \approx P_o(x_o, x_o^*) + \delta x \left(\frac{\partial P_o(x_o)}{\partial x_o}\right) + \delta x^* \left(\frac{\partial P_o(x_o)}{\partial x_o}\right)^*. \qquad (5.17)$$

On linearizing eqn. (5.16) we get the following eigenvalue equation

$$\kappa^{-1}\frac{\partial}{\partial t}\begin{bmatrix} \delta x \\ \delta x^* \end{bmatrix} = -\begin{bmatrix} 1 + 2C\left(\frac{\partial P_o}{\partial x_o}\right) & 2C\left(\frac{\partial P_o}{\partial x_o}\right)^* \\ 2C\left(\frac{\partial P_o}{\partial x_o}\right) & 1 + 2C\left(\frac{\partial P_o}{\partial x_o}\right)^* \end{bmatrix}\begin{bmatrix} \delta x \\ \delta x^* \end{bmatrix}. \qquad (5.18)$$

We are considering here the following situation. Let us assume that the system is initially in a steady state corresponding to the input field value E_2^I. If the incident field E_2^I is rapidly changed to $E_2^I + \delta E_2^I$ ($|\delta E_2^I| \ll E_2^I$) the system approaches the new, slightly
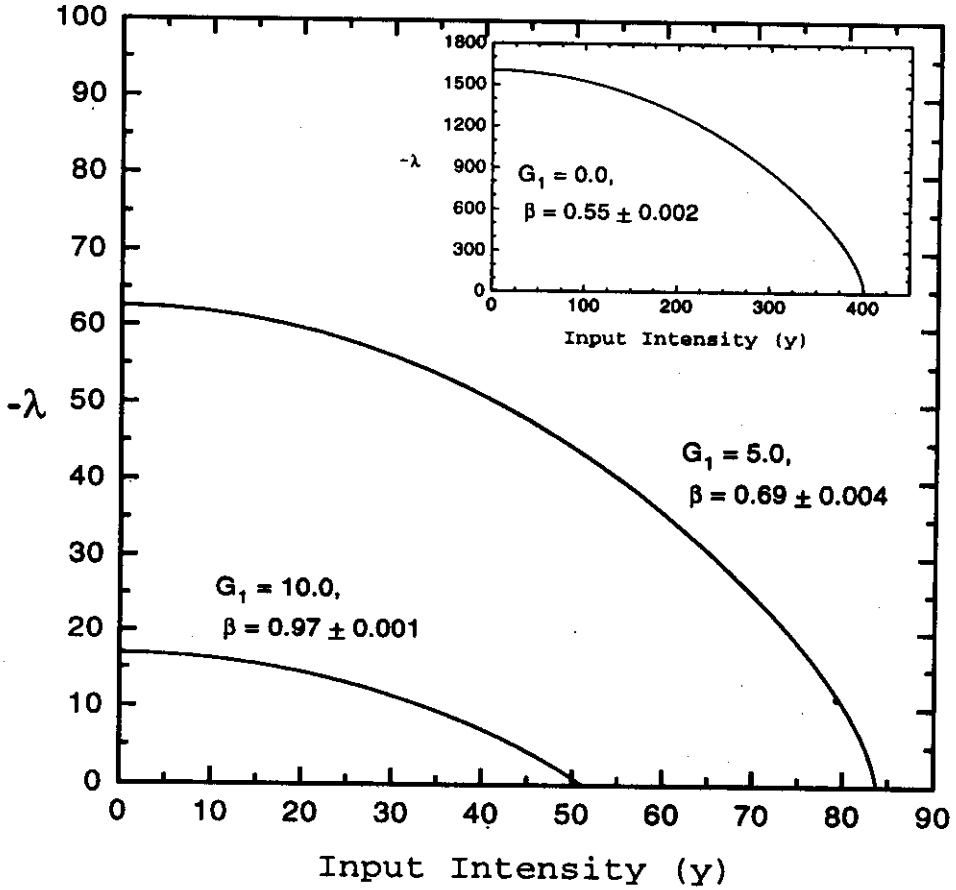
Figure 5.10: The regression to steady state is governed by the eigenvalue $\lambda \propto (y_{th} - y)^\beta$, where β depends on the control field. With increase in control field the system takes longer time to return to its steady state, the inset depicts the usual two-level system where $\beta \approx 0.5$.

different steady state corresponding to the input field value of $E_2^I + \delta E_2^I$. This can be experimentally observed by looking at the *transient* behavior of the transmitted light. The solution of the linearized equations (5.18) are linear combinations of exponentials $e^{\lambda_i t}$. The *smallest eigenvalue* of eqn. (5.18) (one with the smallest real part) governs this *rate of regression* to the steady state. If we consider the system approaching the lower threshold, i.e. as $y \to y_{th}$ then we have the eigenvalue $\lambda \to 0$, as $(y_{th} - y)^\beta$, where $\beta = 1/2$ for the *two-level* atom model (see inset of Fig. 5.10). The regression to the steady state goes as $e^{\lambda t}$ and as $\lambda \to 0$ we observe the phenomenon of *critical slowing down* as we approach the threshold point. The value of β is no longer a constant as in the two-level atom case but is now *dependent* on the the control field, see Fig. 5.10. This changes the slope of the curves in Fig. 5.10 and now the eigenvalue λ near the thresh-
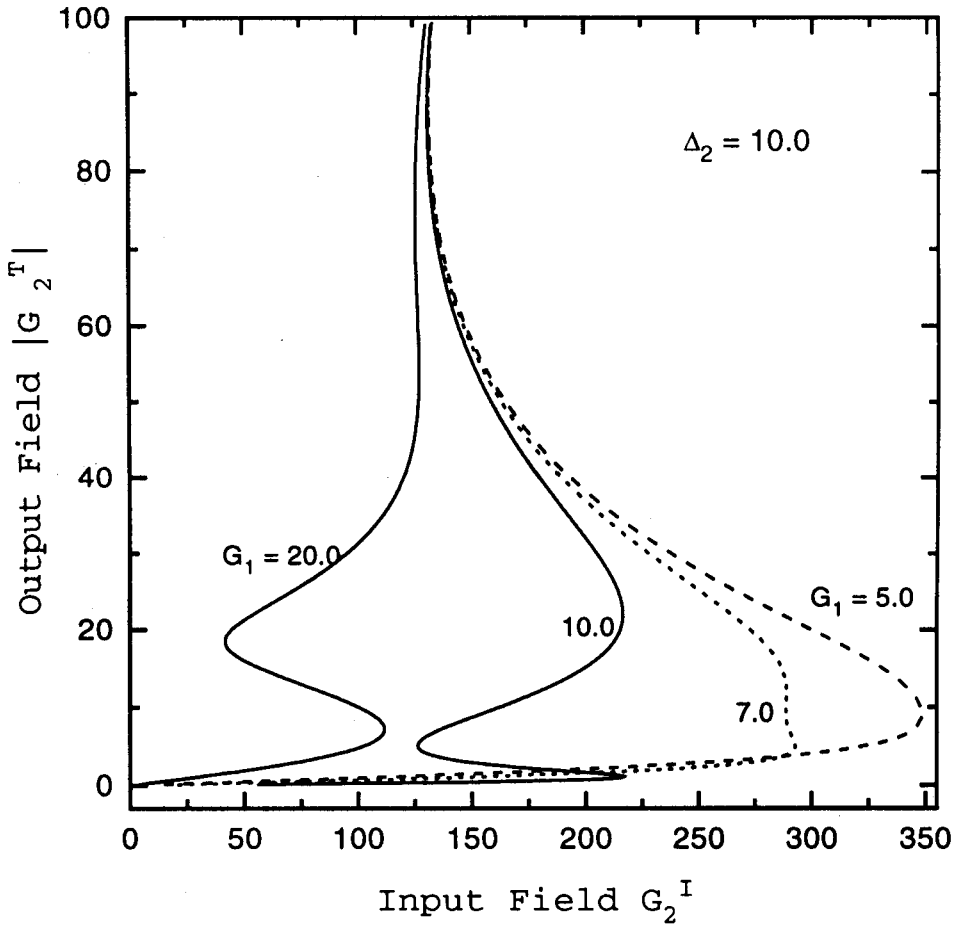
Figure 5.11: Control field induced multistability for $C = 400$, $\Delta_1 = 0$, $\Delta_2 = 10.0$ and $G_1/\gamma_2 = 5., 7., 10., 20.$

old has a different power law dependence, i.e. $\lambda \propto (y_{th} - y)^\beta$ where β *now depends on the control field* and with the increase in G_1 the system takes *longer time* to revert back to its steady state value. In the next section we describe control field induced multistability.

5.6 Control Field Induced Multistability

We describe in this section the possibility of obtaining *multistability* due to the control field. The multistability in three level systems has been reported under various conditions [157]. The aspect that we report is that, multistability in two-level systems can be induced by a control field which is not a second cavity field. In the presence of the control field the polarization of the medium is found to be the ratio of two polynomials

of order 5 and 6 in G_2,

$$P_o(G_2) = \frac{G_2(c_1 + c_2|G_2|^2 + c_3|G_2|^4)}{c_4 + c_5|G_2|^2 + c_6|G_2|^4 + c_7|G_2|^6},$$ (5.19)

where c_1 to c_7 are complex parameters that depend on the detunings, lifetimes, and

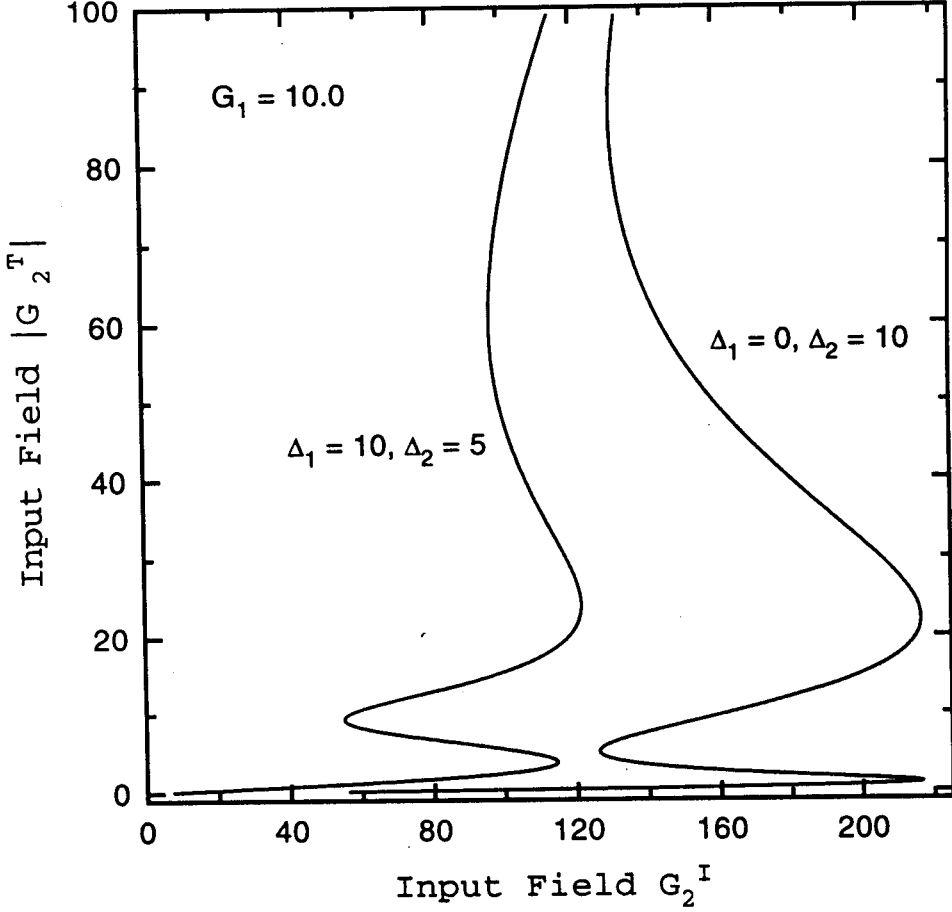Figure 5.12: The region of multistability could be relocated by varying the detunings $\Delta_1 = 10.$, $\Delta_2 = 5.$ and $\Delta_1 = 0.0, \Delta_2 = 10.0$. Here, $C = 400$ and $G_1/\gamma_2 = 10$.

the control field strength of the respective systems. For the usual two-level system we have only the first order term in the numerator and up to the second order term in G_2 in the denominator, giving rise only to *bistability* . Whereas in presence of the control field in the appropriate parameter domain (i.e. choice of c_i's) one has the possibility of *multistability* . These multistable solution would correspond to the various roots of the polarization given by the polynomial in eqn. (5.19).

In Fig. 5.11, 5.12 and 5.13 we show some representative situations of multistable behavior for different parameters like strengths and detunings of the control field. As
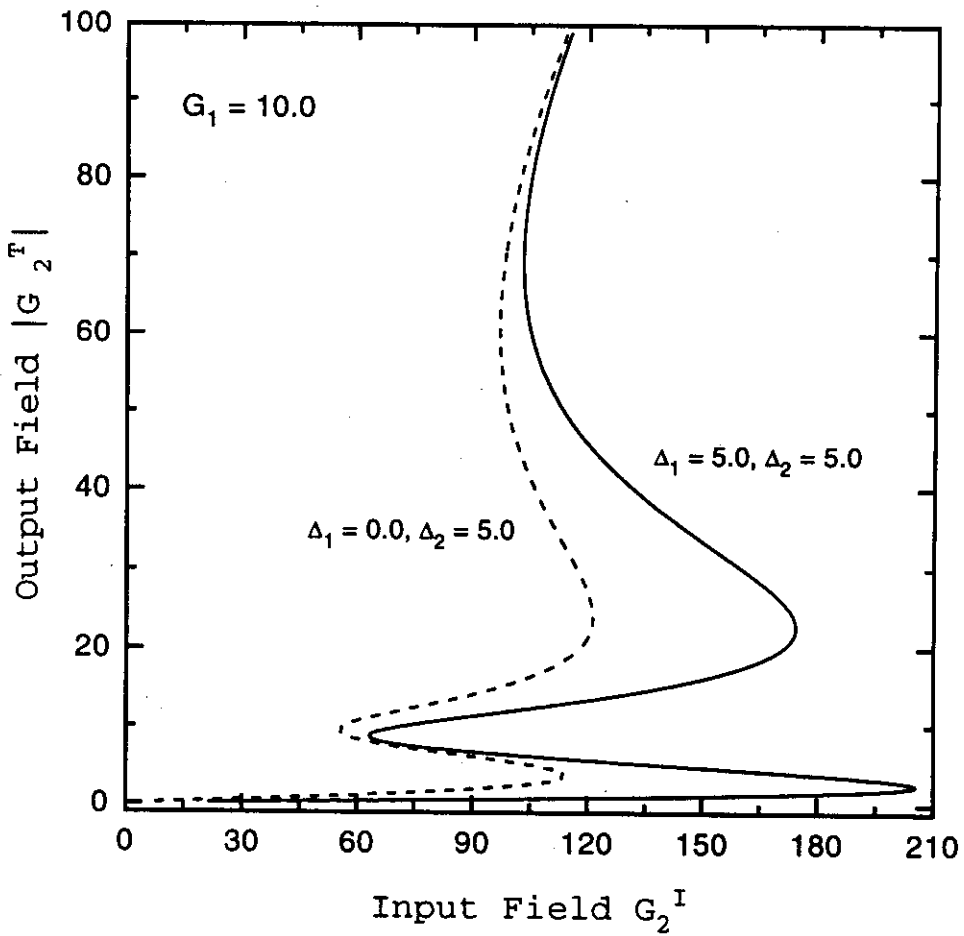
Figure 5.13: The region of input intensities over which there is multistability is broadened by increasing $\Delta_1 = 0., 5.,$ Here $C = 400$ and $G_1/\gamma_2 = 10$.

we increase the field strength of the control field (from $G_1 = 5.0$) we see the onset of the multistable hump at $G_1 = 7.0$, and it has completely manifested for $G_1 = 10.0$ and 20.0, as shown in Fig. 5.11. One does not merely get multistability but by changing the parameters of the system, one can *choose / alter the region of multistability* as shown in Fig. 5.12. In Fig. 5.13 we show that my merely changing the detuning of the control laser, one can increase the region of multistable behavior. All these show that one has greater control over the various regions of operation due to the external *control field* which can be varied independently. Hence by changing these external field parameters we can alter the region in which this multistate switch can operate.

In conclusion, we have demonstrated schemes with which one can *substantially decrease* the threshold required for a bistable device using field induced transparency

and quantum interference effects. We also studied the transient response of these control field induced bistable schemes. We have shown existence of multiple hysteresis for an appropriate choice of control field parameters. This provides for a possibility of versatile use of the *same* device configuration in more than one application, both as a bistable as well as a multistable switch.

Enhanced Nonlinear Signal Generation under Coherent Population Trapping Conditions[1]

In nonlinear optics one of the goals has been - how to improve the *efficiency* of the generation. We have reviewed in section 2.5 some of the recent experiments where enhancement of the efficiency of the nonlinear generation process has been achieved by coherent preparation of the medium. Indeed the ideas of atomic coherence have been used in very wide variety of applications such as to lasing without inversion (section 2.8), large refractive index and magnetometry (section 2.9). In many of these proposals atomic coherence plays a vital role. We know that the atomic coherence is *maximized* in a coherent population trapping state (section 2.2). Recently, an ensemble of Pb atoms prepared in this maximum coherence state was utilized for efficient conversion of blue to ultraviolet light [53]. Atomic coherence was utilized to obtain the effective *nonlinear* susceptibility to be of the same order as the *linear* susceptibility. This was accomplished by using EIT to prepare near-maximal atomic coherence on a Raman transition. They obtained efficiency of $\sim 40\%$ in the conversion of intense blue laser light at 425 nm to violet light at 293 nm. Here we study in detail the enhancement of nonlinear signal by utilizing this *maximal* coherence of the CPT state, we augment their findings in the *non-perturbative* regime.

Most of the previous studies have been carried out in the weak probe case, in this chapter we develop a *non-perturbative* approach to study the generation of nonlinear signals in a coherently prepared medium. We study the nonlinear generation process in a system prepared in the coherent population trapping state. We calculate enhancement factors of the order of $\sim 10^2$ in the generated signal under a variety of conditions.

In our scheme we have two fields acting *simultaneously* on *each transition* in a Λ-system. By choosing the detunings of the pump fields such that we operate at the

---

[1]This work has been accepted for publication as a regular article in Physical Review A, titled **Enhancement of Nonlinear Optical Signal under Coherent Population Trapping Conditions**, Ref. [158]. Also presented in an invited talk at *National Laser Symposium - 97*, Physical Research Laboratory, Ahmedabad, INDIA.
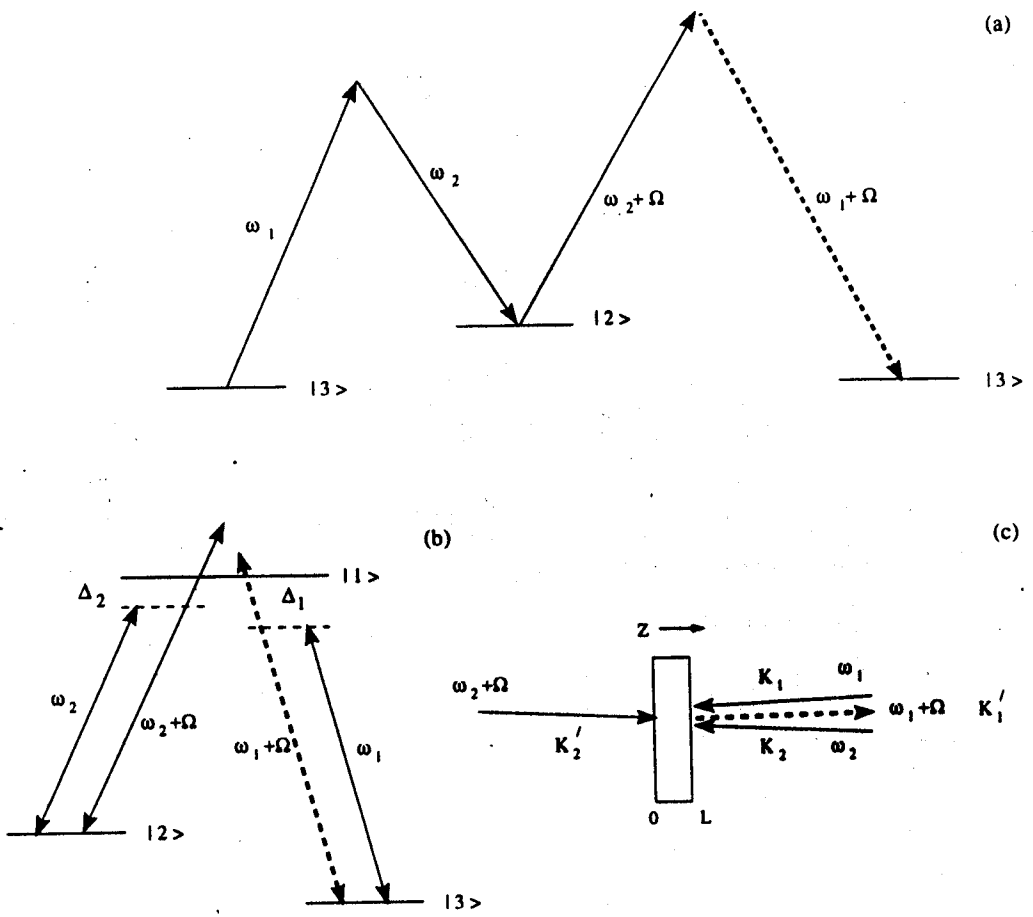
Figure 6.1: (a) The generation of nonlinear signal at $\omega_1 + \Omega$, in the nonlinear process, produced by absorption of ω_1, $\omega_2 + \Omega$ and emission of ω_2. (b) The Λ - configuration for the atom and the four fields coupled to the various transitions. (c) The possible wave mixing geometry for this process in a thin medium. The fields at ω_i and $\omega_i + \Omega$ are almost collinear and hence the relative angles between them do not matter. All the dashed lines refer to the generated field at $\omega_1 + \Omega$.

coherent population trapping condition, we create the required atomic coherence.

We study the enhancement of $\omega_1 + \Omega$ generated by the nonlinear process $(\omega_1 + \Omega) = \omega_1 - \omega_2 + (\omega_2 + \Omega)$, under CPT conditions in a three-level Λ-system. Fig. 6.1 (a) depicts this process, where ω_1 and $\omega_2 + \Omega$ are absorbed and ω_2 is emitted to generate the field at $\omega_1 + \Omega$. Our analysis is *non-perturbative*, hence all the fields at ω_1, ω_2 and $\omega_2 + \Omega$ can be *strong*. Our approach also enables us to study other related issues like *pulse matching* in the non-perturbative domain. Our non-perturbative analysis enables us to answer, if for a thick medium pulse matching will occur at high probe powers. We find the remarkable result that even at higher probe intensities pulse matching takes place.

6.1 Non-perturbative Formulation

We consider a Λ-system Fig. 6.1 (b). The excited state $|1\rangle$ is coupled to $|3\rangle$ ($|2\rangle$) by the monochromatic field $\vec{E}_1$ ($\vec{E}_2$) with frequency ω_1 (ω_2). We have another set of fields $\vec{E}'_1$ ($\vec{E}'_2$) at frequency $\omega_1 + \Omega$ ($\omega_2 + \Omega$) acting again on the same set of transitions $|1\rangle \leftrightarrow |3\rangle$ ($|1\rangle \leftrightarrow |2\rangle$). The total Hamiltonian of the system is given as

$$H_T = \hbar\omega_{13}A_{11} + \hbar\omega_{23}A_{22} - \vec{d}_{12} \cdot (\vec{E}_2 e^{-i(\omega_2 t - \vec{k}_2 \cdot \vec{r})} + \vec{E}'_2 e^{-i((\omega_2+\Omega)t - \vec{k}'_2 \cdot \vec{r})})A_{12}$$
$$-\vec{d}_{13} \cdot (\vec{E}_1 e^{-i(\omega_1 t - \vec{k}_1 \cdot \vec{r})} + \vec{E}'_1 e^{-i((\omega_1+\Omega)t - \vec{k}'_1 \cdot \vec{r})})A_{13} + h.c. \tag{6.1}$$

where A_{ij} is the atomic transition operator $|i\rangle\langle j|$. The energy is measured from the ground state $|3\rangle$, and $\hbar\omega_{13}$ ($\hbar\omega_{23}$) is the energy difference between level $|1\rangle$ ($|2\rangle$) from the ground level $|3\rangle$. Here $\vec{d}_{ij}$ is the dipole interaction term for the transition $|i\rangle \leftrightarrow |j\rangle$; $\vec{k}$'s are the wave-vectors of the corresponding fields with amplitudes $\vec{E}$'s. The equations of motion for the density matrix after applying the rotating wave approximation are

$$\frac{d\rho_{11}}{dt} = -2(\gamma_1 + \gamma_2)\rho_{11} + i(G_2 + G'_2 e^{-i\Omega t})\rho_{21} - i(G_2^* + G_2'^* e^{i\Omega t})\rho_{12}$$
$$+i(G_1 + G'_1 e^{-i\Omega t})\rho_{31} - i(G_1^* + G_1'^* e^{i\Omega t})\rho_{13},$$

$$\frac{d\rho_{12}}{dt} = -(\gamma_1 + \gamma_2 + i\Delta_2)\rho_{12} - i(G_2 + G'_2 e^{-i\Omega t})(\rho_{11} - \rho_{22}) + i(G_1 + G'_1 e^{-i\Omega t})\rho_{32},$$

$$\frac{d\rho_{13}}{dt} = -(\gamma_1 + \gamma_2 + i\Delta_1)\rho_{13} + i(G_2 + G'_2 e^{-i\Omega t})\rho_{23} - i(G_1 + G'_1 e^{-i\Omega t})(2\rho_{11} + \rho_{22} - 1),$$

$$\frac{d\rho_{22}}{dt} = 2\gamma_2\rho_{11} - i(G_2 + G'_2 e^{-i\Omega t})\rho_{21} + i(G_2^* + G_2'^* e^{i\Omega t})\rho_{12},$$

$$\frac{d\rho_{23}}{dt} = i(\Delta_2 - \Delta_1)\rho_{23} + i(G_2^* + G_2'^* e^{i\Omega t})\rho_{13} - i(G_1 + G'_1 e^{-i\Omega t})\rho_{21}, \tag{6.2}$$

where the Rabi frequencies of various fields are given by $2G_1 = 2(\vec{d}_{13} \cdot \vec{E}_1 e^{i\vec{k}_1 \cdot \vec{r}})/\hbar$, $2G_2 = 2(\vec{d}_{12} \cdot \vec{E}_2 e^{i\vec{k}_2 \cdot \vec{r}})/\hbar$, and similarly the Rabi frequencies $2G'_1$, $2G'_2$ for the primed fields $\vec{E}'_1$, $\vec{E}'_2$, respectively. The quantities $2\gamma_1$ ($2\gamma_2$) are the spontaneous emission decay rates from $|1\rangle$ to $|3\rangle$ ($|2\rangle$) and the detunings are $\Delta_1 = \omega_{13} - \omega_1$ and $\Delta_2 = (\omega_{13} - \omega_{23}) - \omega_2$. As we are dealing with a closed three level scheme we have $\rho_{11} + \rho_{22} + \rho_{33} = 1$. Note the *explicit* time dependence of $e^{\pm i\Omega t}$ in eqns. (6.2), as *two fields simultaneously couple each transition*. In order to obtain non-perturbative solution of eqns. (6.2) we expand $\rho_{\alpha\beta}$ in terms of its Fourier components as

$$\rho_{\alpha\beta} = \sum_{n=-\infty}^{\infty} e^{-in\Omega t}\rho_{\alpha\beta}^{(n)}. \tag{6.3}$$

On substituting the relation (6.3) in eqns. (6.2) and equating the various coefficients of $e^{\pm in\Omega t}$, we obtain coupled set of equations (6.4) for each Fourier component. Each Fourier term is denoted by n and is coupled to the nearest neighbour components $n+1$ and $n-1$. These coupled equations have been solved numerically using the *matrix continued fractions* [159] as is shown in some detail in the next section. The advantage of this method lies in the fact that one is *not restricted to weak fields* at $\omega_i + \Omega$ but the fields involved could be of *arbitrary* strengths.

6.2   Matrix Continued Fraction

In this section, we show the methodology of using the *matrix continued fractions* technique to solve the coupled set of equations which we obtained in the previous section. We need to solve non-perturbatively for all the Fourier components, and these equations can be cast into the matrix form as

$$\mathbf{A}_n\boldsymbol{\Phi}_n + \mathbf{A}^+\boldsymbol{\Phi}_{n+1} + \mathbf{A}^-\boldsymbol{\Phi}_{n-1} = \mathbf{r}^0\delta_{n,0} + \mathbf{r}^+\delta_{n-1,0} + \mathbf{r}^-\delta_{n+1,0} \ , \qquad (6.4)$$

where $\boldsymbol{\Phi}_i$ are 8×1 column matrices containing the *density matrix* elements $\rho_{\alpha\beta}$ for the ith Fourier component, here $\alpha, \beta = 1, 2, 3$; $\mathbf{A}_i^{\pm}$ are 8×8 square matrices containing the *coefficients* of the corresponding density matrix elements in $\boldsymbol{\Phi}$; and $\mathbf{r}$ are 8×1 column matrices which contain the inhomogeneous components, which result from elimination of the ρ_{33} term from all the equations using the relation $\rho_{33}^{(0)} = 1 - \rho_{11}^{(0)} + \rho_{22}^{(0)}$ (where the superscript $^{(0)}$ refers to the zeroth order Fourier component). All components in boldface signify that they are matrices. We observe that various Fourier components denoted by the subscript n, are coupled to its *nearest* neighbor $n \pm 1$, due to the $e^{\pm i\Omega t}$ dependence in eqn. (6.2). The *three term recursion relation* (6.4) can be cast in the form of a *matrix continued fraction* [159]. We first deal with the *homogeneous* set of equations, i.e. for $n \neq 0, \pm 1$. Hence for $n > 1$ and $n < -1$, we introduce matrices $\mathbf{Z}_n$ such that

$$\boldsymbol{\Phi}_n = \mathbf{Z}_n\mathbf{r}^0. \qquad (6.5)$$

Using eqn. (6.5) in eqn. (6.4) we obtain the following recursion relation for $n \neq 0, \pm 1$,

$$\mathbf{A}_n\mathbf{Z}_n + \mathbf{A}^+\mathbf{Z}_{n+1} + \mathbf{A}^-\mathbf{Z}_{n-1} = \mathbf{0}. \qquad (6.6)$$

93

We define the quantity X_n such that

$$X_n = Z_n Z_{n-1}^{-1}. \tag{6.7}$$

On substituting the relation (6.7) in eqn. (6.6), we obtain for $n > 1$ the following matrix continued fraction

$$X_n = -(A_n + A^+ X_{n+1})^{-1} A^-. \tag{6.8}$$

For $n < -1$ we again redefine the variables as $Y_{-n} = X_{-n}^{-1}$ and obtain another matrix continued fraction

$$Y_{-n} = -(A_{-n-1} + A^- Y_{-n-1})^{-1} A^+. \tag{6.9}$$

We now consider the equations with inhomogeneous terms, i.e. for $n = 0, \pm 1$, the following inhomogeneous set of equations are obtained from eqn. (6.4)

$$A_1 \Phi_1 + A^+ \Phi_2 + A^- \Phi_0 = r^+ \; ; \; \text{for } n = 1, \tag{6.10}$$

$$A_0 \Phi_0 + A^+ \Phi_1 + A^- \Phi_{-1} = r^0 \; ; \; \text{for } n = 0, \tag{6.11}$$

$$A_{-1} \Phi_1 + A^+ \Phi_0 + A^- \Phi_{-2} = r^- \; ; \; \text{for } n = -1. \tag{6.12}$$

On evaluating the matrix continued fraction relations (6.8) and (6.9) numerically we obtain X_2 and Y_{-2}, respectively. Then, on using relations (6.7) and (6.5) for X_2, we obtain the term Φ_2 in (6.10), and similarly we use Y_{-2} to obtain the term Φ_{-2} in eqn. (6.12). On substituting these we solve the three matrix simultaneous equations (6.10,6.11,6.12). We are interested in the response of the system at $\omega_1 + \Omega$ hence we require the solution Φ_1 of eqn. (6.4). As we have seen no assumptions are made on the *relative strengths* of various fields in the continued fraction technique. One needs to sum the series involving the Fourier expansion i.e. eqn. (6.3), to *larger* values of n as the strengths of the primed fields become comparable to the fields that create the CPT state. This essentially boils down to evaluating the matrix continued fraction equations (6.8) and (6.9), by taking larger values for n and summing more terms.

6.3 Dressed state analysis - Nonlinear signal in the perturbative limit

In the limit when the *applied field* at $\omega_2 + \Omega$ and the *generated field* at $\omega_1 + \Omega$ are *weak* we can obtain an *analytical* result for the generated field. As we are interested in the signal

generated at the CPT condition the two-photon resonance condition i.e. $\Delta_1 = \Delta_2 = \Delta$ is assumed. Moreover, the fields at frequencies ω_1 and ω_2 that create the CPT state are assumed to be strong such that the primed fields merely act as *perturbation* to these. We perform the *dressed state analysis* under these conditions.

This analysis is undertaken by solving the master equation in a representation such that the *Hamiltonian in eqn. (6.1) without the primed fields is diagonal* $(H = H_T\{\vec{E}_i' \to 0\}$, for $i = 1, 2)$. This representation is obtained through an unitary transformation S such that

$$S^\dagger H S = \Lambda, \tag{6.13}$$

where Λ is the diagonalized form of the Hamiltonian with the eigenvalues of H as its elements. The unitary transformation S at zero detuning is

$$
\begin{bmatrix}
\frac{1}{\sqrt{2}} & 0 & -\frac{1}{\sqrt{2}} \\
\frac{G_1^*}{\sqrt{2\zeta}} & -\frac{G_2}{\sqrt{\zeta}} & \frac{G_1^*}{\sqrt{2\zeta}} \\
\frac{G_2^*}{\sqrt{2\zeta}} & \frac{G_1}{\sqrt{\zeta}} & \frac{G_2^*}{\sqrt{2\zeta}}
\end{bmatrix}, \tag{6.14}
$$

where $\zeta = |G_1|^2 + |G_2|^2$. The transformation (6.13) is equivalent to going from the old basis $|1\rangle, |2\rangle, |3\rangle$ to a new basis $|\psi_\pm\rangle, |\psi_1\rangle$ which are *eigenstates* of the *diagonalized* Hamiltonian. The state $|\psi_-\rangle = (G_2|3\rangle - G_1|2\rangle)/\sqrt{\zeta}$ gets *decoupled* from the applied fields and hence from any further evolution. In this representation the equations of motion for the transformed density matrix $\bar{\rho}$ $(= S^\dagger \rho S)$ are

$$\frac{d\bar{\rho}}{dt} = -i[\Lambda, \bar{\rho}] - i[\bar{H}_\Omega, \bar{\rho}] + S^\dagger\{\mathcal{L}(S\bar{\rho}S^\dagger)\}S, \tag{6.15}$$

where the Liouville operator $\mathcal{L}$ operating on ρ contains all the decay terms of eqns. (6.2), which are transformed appropriately as decays of $\bar{\rho}$, as is shown in eqn. (6.15) (the last term on the right hand side). The second term on the right hand side in eqn. (6.15) contains the interaction of the *primed fields* at frequencies $\omega_{1,2} + \Omega$ with the atom which is treated as a *perturbation* to the Hamiltonian H of eqn. (6.13), where $\bar{H}_\Omega = S^\dagger H_\Omega S$. The radiative decay terms lead to the *coupling* of the various matrix elements of $\bar{\rho}$ to each other. Without the $\bar{H}_\Omega$ term (i.e. zeroth order in the perturbation), the steady state solution of eqn. (6.15) leads to the well known *non-coupled state*. Only one term survives that is $\bar{\rho}_{--} = 1$, all other $\bar{\rho}_{\alpha\beta} = 0$. In this perturbative limit we take just the

first Fourier component in eqn. (6.3) for the expansion of $\rho_{\alpha\beta}$ in eqns. (6.2). In the limit $\gamma_1 = \gamma_2$ and to *first order in the primed fields* $(\omega_{1,2} + \Omega)$ the relevant equations of motion for the density matrix $\bar{\rho}$ are,

$$\frac{d\bar{\rho}_{1-}^{(1)}}{dt} = -\left(\eta - i\sqrt{\zeta}\right) \bar{\rho}_{1-}^{(1)} + \eta \, \bar{\rho}_{+-}^{(1)} - i\,\mu\, \bar{\rho}_{--}^{(0)} \, e^{-i\Omega t},$$

$$\frac{d\bar{\rho}_{+-}^{(1)}}{dt} = -\left(\eta + i\sqrt{\zeta}\right) \bar{\rho}_{1-}^{(1)} + \eta \, \bar{\rho}_{1-}^{(1)} + i\,\mu\, \bar{\rho}_{--}^{(0)} \, e^{-i\Omega t}, \qquad (6.16)$$

where the constants $\eta = (\gamma_1 + \gamma_2 + i\Delta)/2$ and $\mu = (G_1' G_2 - G_2' G_1)/\sqrt{2\zeta}$. These equations are valid *approximately* even when $\gamma_1 \neq \gamma_2$, as we have ignored the terms with $(\gamma_1 - \gamma_2)/G_i$ dependence in eqns. (6.16). We also note that eqns. (6.16) are obtained without any *secular approximation* [160]. As we are examining the field generated at $\omega_1 + \Omega$ the relevant polarization is the $\rho_{13}^{(1)}(\omega_1 + \Omega) = \sum_{i,j} S_{1i}\bar{\rho}_{ij}^{(1)} S_{j3}^{\dagger}$. Hence on solving eqn. (6.16) in the steady state and using this summation relation, we get

$$\rho_{13}^{(1)}(\omega_1 + \Omega) = \frac{(G_1 G_2' - G_2 G_1')G_2^* \Omega}{\zeta\left((\frac{\gamma_1 + \gamma_2 + i\Delta}{2} + i\sqrt{\zeta} - i\Omega)(\frac{\gamma_1 + \gamma_2 + i\Delta}{2} - i\sqrt{\zeta} - i\Omega) - (\frac{\gamma_1 + \gamma_2 + i\Delta}{2})^2\right)}. \qquad (6.17)$$

Hence eqn. (6.17) gives the *lineshape* of the generated signal at CPT ($\Delta_1 = \Delta_2 = \Delta$), in the weak field limit ($G_1', G_2' \ll G_1, G_2$) and for equal decays in both arms of the Λ system ($\gamma_1 = \gamma_2$). We observe that for $\Delta = 0$ the generated signal (at $\omega_1 + \Omega$) peaks at $\pm\sqrt{|G_1|^2 + |G_2|^2}$ beside the absolute minima at $\Omega = 0$. We make a note that in deriving eqn. (6.17) we have *not* put any restriction on Ω, it could be of *arbitrary* magnitude.

We observe in eqn. (6.17) that whenever $G_1 G_2' = G_2 G_1'$ the signal goes to *zero for all* Ω. This is because the two processes $(\omega_1 + \Omega) = \omega_1 - \omega_2 + (\omega_2 + \Omega)$ and $(\omega_2 + \Omega) = \omega_2 - \omega_1 + (\omega_1 + \Omega)$ acting in opposite directions cancel each other *exactly* . At CPT the population in the states $|3\rangle$ and $|2\rangle$ is *equal,* where the fields ω_1 and ω_2 act. The first process is depicted in Fig. 6.1 (a), and the second process is similar but starting with ω_2 being absorbed from $|2\rangle$ and ω_1 being emitted, followed by absorption of $\omega_1 + \Omega$ and leading to generation of $\omega_2 + \Omega$. These processes become *equally* probable at CPT condition and act in opposite direction, leading to *exact cancellation* of these two pathways and hence there is no signal generation at $\omega_{1,2} + \Omega$.

In Ref. [53] the enhancement was observed in the regime where $\Omega \gg G_i > G_i'$, $i = 1, 2$. Here we have no such restriction on the frequency of the generated field Ω. In eqn. (6.17) we provide the *line shape* of the generated field for *all* Ω.
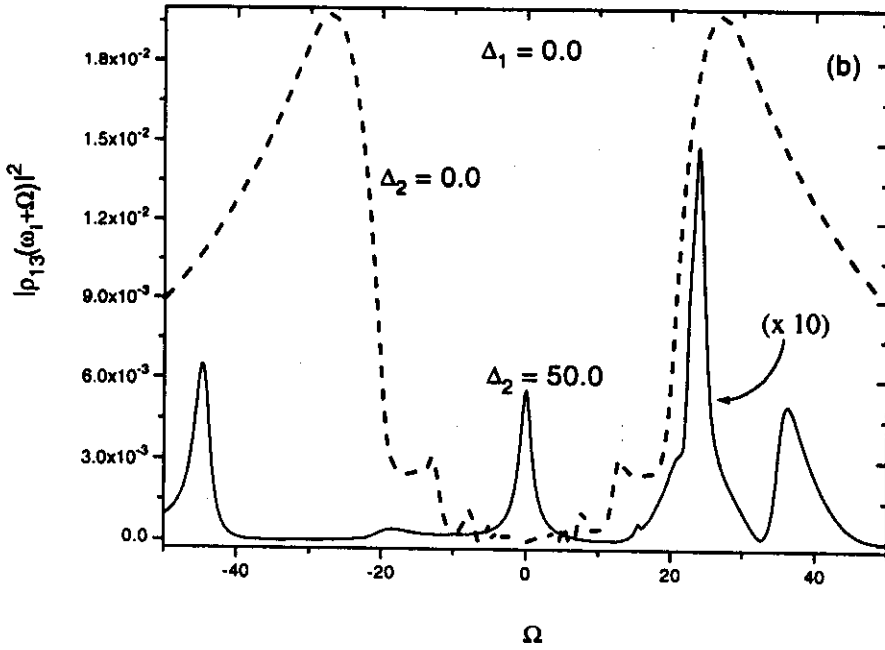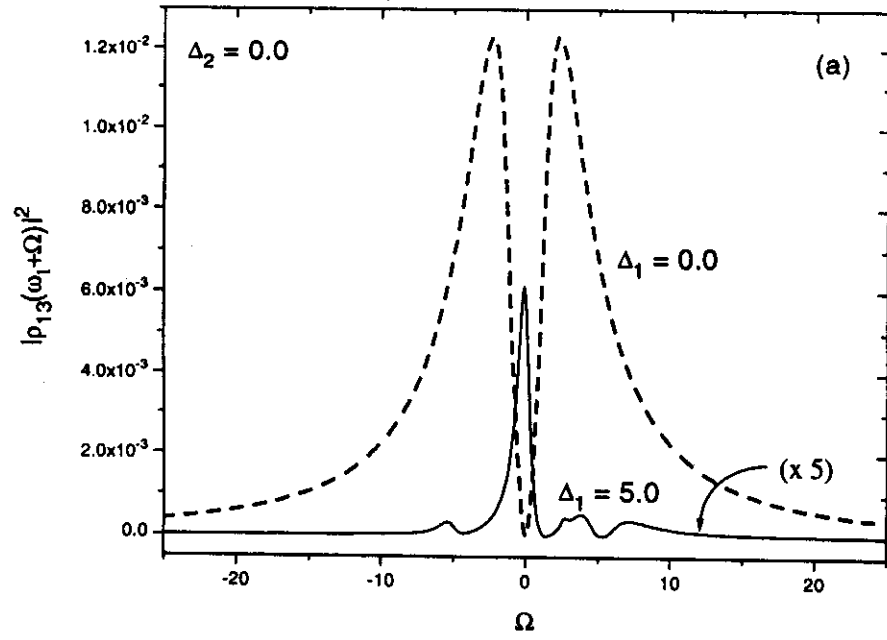
Figure 6.2: (a) The intensity of the nonlinear signal at $\omega_1 + \Omega$, for $G_1 = G_2 = G_2' = 1.0$ while operating at CPT (dotted lines) i.e. $\Delta_1 = \Delta_2 = 0$. The solid line shows the signal away from the CPT condition $(\Delta_1 = 5.0, \Delta_2 = 0.0)$, it has been enhanced by a factor of 5 for clarity. (b) The generated field intensity for higher field strengths $G_1 = G_2 = G_2' = 10.0$ while operating at CPT (dotted lines). The solid line shows the signal away from the CPT condition $(\Delta_1 = 0.0, \Delta_2 = 50.0)$, it has been enhanced by a factor of 10 for clarity. All fields and detunings are scaled in terms of γ.

6.4 Enhancement of nonlinear signals

We show in Fig. 6.2 the generated intensity when operating at CPT and away from it. The intensity of the generated signal is proportional to $|\rho_{13}(\omega_1 + \Omega)|^2$, we set $G'_1 = 0$ while calculating this polarization. To obtain the population trapped state one needs to tune the frequency of the fields ω_1 and ω_2 such that $\Delta_1 = \Delta_2$. By operating at CPT we minimize unwanted absorption, otherwise as we are dealing with intensities of the fields which are much lower than the saturation intensity of the respective transitions it would have led to pronounced absorption at resonance. We observe that at CPT in Fig. 6.2 (a), the enhancement in the generated field intensity is about 1.4×10^2 and 3×10^2, at $\Omega \approx 3$ and 30, respectively (in fact for a wide range of Ω, away from the line center the enhancement is about $\sim 10^2$). Furthermore, the minima at $\Omega \sim 5.0$ in the non-CPT case (Fig. 6.2 (a)) is because the generated field $\vec{E}'_1$ and $\vec{E}_2$ come into two-photon resonance. In contrast, the smaller peak at $\Omega \sim -5.0$ is when $\vec{E}'_2$ and $\vec{E}_1$ form a CPT state leading to slight enhancement in $\vec{E}'_1$.

We also show the *strong field* case in Fig. 6.2 (b) at CPT (dotted line), i.e. for $G_1 = G_2 = G'_2 = 10.0$ and $\Delta_1 = \Delta_2 = 0.0$. We observe an enhancement of the order of ~ 10 *and more* for all Ω away from zero. The oscillations at CPT are due to the presence of two strong fields coupling one transition. The solid line in Fig. 6.2 (b) denotes the field away from CPT with $\Delta_1 = 0.0, \Delta_2 = 50.0$. With an *increase* in the *mistuning* from the two-photon condition the enhancement *increases*. We make a note that all the profiles in Fig. 6.2 have been calculated non-perturbatively using the matrix continued fraction technique described in section 6.2.

We next discuss the source of this enhancement - why there is enhancement in performing nonlinear optical experiments at CPT? As was discussed in section 2.2 at CPT the ground state atoms evolve into a coherent superposition with approximately *equal* and *oppositely phased* probability amplitudes in states $|2\rangle$ and $|3\rangle$, i.e. $\rho_{22} = \rho_{33} = 0.5$ and $\rho_{23} = -0.5$. This atomic coherence (denoted by ρ_{23}) oscillates $180°$ out of phase with the optical coherence creating an interference minima at $\Delta_1 = \Delta_2$ [10]. This interference populates the state $|\psi_-\rangle$ and this state gets decoupled from further evolution thus making the medium transparent to these fields. The CPT state *enhances* the generation of signal at $\omega_1 + \Omega$ because, firstly it provides *enhanced coherence between* $|2\rangle$ *and* $|3\rangle$ (ρ_{23})
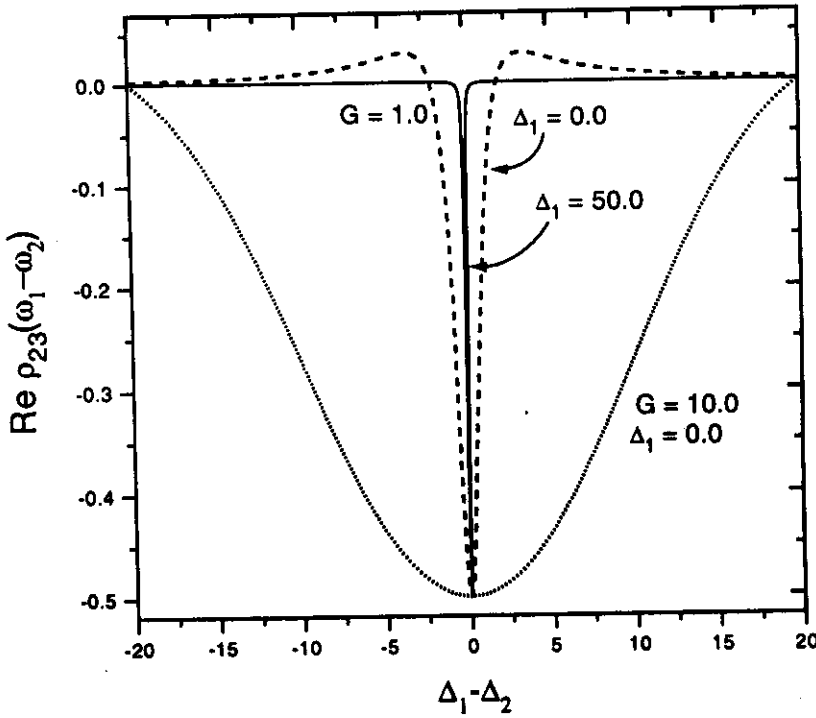
Figure 6.3: The coherence term $Re(\rho_{23})$, as a function of mistuning $\Delta_1 - \Delta_2$; For the fields tuned such that $\Delta_1 = 0$, the dashed line is for $G_1 = G_2 = 1.0$ and the dotted line for $G_1 = G_2 = 10.0$. The solid line is when the fields are away from the single photon resonant condition i.e. $\Delta_1 = 50.0$ and $G_1 = G_2 = 1.0$, note that the minima varies sharply around $\Delta_1 - \Delta_2 \approx 0.0$.

which determines the relevant optical coherence ρ_{13} (see third equation in (6.2) for $d\rho_{13}/dt$); and secondly greater population is available in $|2\rangle$ (≈ 0.5) where the field G_2' acts. In contrast, when one is away from CPT not only that ρ_{23} is small even the population is distributed in all the three levels. Thus the enhancement is not merely due to reduced absorption of G_1 and G_2 but depends crucially on the coherence term $\rho_{23}(\omega_1 - \omega_2)$ which provides the nonlinear interference in the CPT state.

In Fig. 6.3 we depict the behavior of ρ_{23} due to the fields G_1 and G_2 as a function of the mistuning (from the CPT condition). For lower amplitudes of the field G_1 and G_2 this coherence term varies sharply as a function of the mistuning from the CPT condition ($\Delta_1 - \Delta_2$). The *width* of the minimum at the two-photon resonance depends on the *field strengths* and hence in turn depends on the single photon detuning. This width decreases with increase in the detuning Δ (we discuss below the case of utilizing CPT state formed when $\Delta_1 = \Delta_2 = \Delta \neq 0$) as shown in Fig. 6.3. As is well known
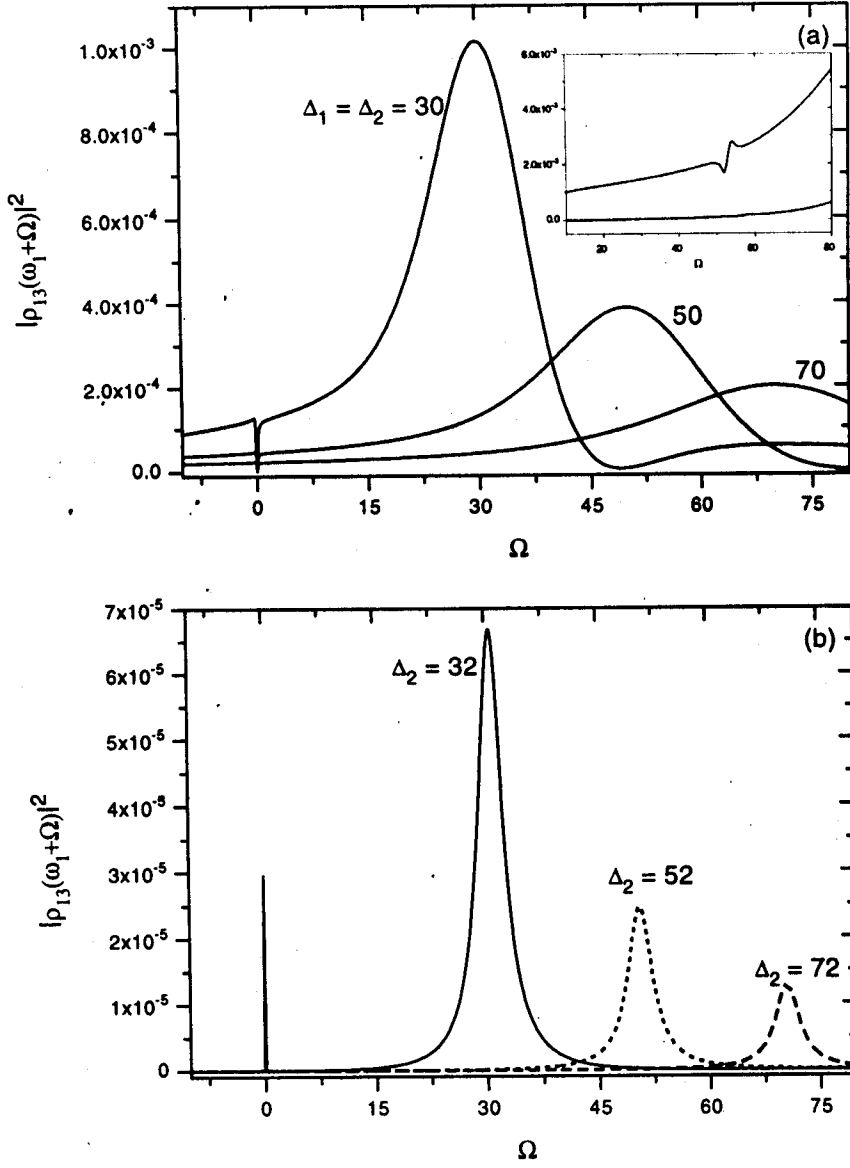
Figure 6.4: (a) The signal at CPT for $G_1 = G_2 = G'_2 = 1.0$ and for fields detuned from single photon resonant condition i.e. $\Delta_1 = \Delta_2 = 30, 50, 70$. The inset depicts the generated field for higher field strengths, $G_1 = G_2 = G'_2 = 10.0$ with $\Delta_1 = 100.0$ at CPT (upper curve $\delta = 0.0$), and away from it (lower curve $\delta = 10.0$). (b) Same as Fig. 4(a), but slightly away from the CPT condition such that $\Delta_2 - \Delta_1 = \delta = 2.0$. The solid, dotted and dashed curves are for the signal at $\Delta_1 = 30, 50$ and 70, respectively. All G's, Δ's and Ω are scaled in terms of γ.

even at low light levels the quantum interference effects at the population trapped state persists [161, 162]. Clearly *coherence term falls sharply* for certain range of trapping fields *as one moves away from the CPT condition*. This then explains the large enhancement while working at the CPT condition.

The essential condition for formation of the CPT state is the frequency of the applied fields such that $\Delta_1 = \Delta_2 = \Delta$. We now discuss the case with nonzero Δ, i.e. when we are *away from single photon resonance* of the pump fields G_1, G_2. The signal due to the CPT state formed with fields detuned from the atomic transition is shown in Fig. 6.4, for $G_1 = G_2 = G_2' = 1.0$ when $\Delta_1 = \Delta_2 = \Delta = 30.0$, 50.0, 70.0. We have also set $\gamma_1 = \gamma_2 = 1$. At CPT the response at $\omega_1 + \Omega$ is given by eqn. (6.17). For large Δ the two peaks should be at $\Delta/2 \pm \sqrt{(\Delta/2)^2 + |G_1|^2 + |G_2|^2}$. We have $\Delta \gg \gamma_i \sim G_i, i = 1, 2$, hence the peak at $\Omega \approx -(|G_1|^2 + |G_2|^2)/\Delta$ is dominated by the minima of the numerator in eqn. (6.17) and consequently we have only one maxima at $\approx \Delta$ itself (Fig. 6.4(a)). The enhancement due to the CPT state varies from 4.2×10^4, 1.5×10^2 at $\Omega \approx -25$, 75, respectively. It should also be noted that when one is away from the single photon resonance one needs to go only slightly away from CPT ($\delta = \Delta_2 - \Delta_1 = 2.0$) to see the advantage of operating at it unlike in the resonant case (with $\Delta = 0$) shown in Fig. 6.2 (a). Operating at the detuned condition (i.e. $\Delta \neq 0$) has twofold advantages, firstly one gets an increase in the generated signal (for $\Delta_i = 30, 50, 70, i = 1, 2$, the enhancement in the intensity of the signal due to CPT is $\sim 3 \times 10^2$, 2.3×10^3, 6.8×10^3 at $\Omega \approx 20$) when operated at same δ as compared to the single photon resonant case; secondly the experimental ease, as this lifts the stringent condition of operating the laser fields $\vec{E}_1$ and $\vec{E}_2$ at atomic resonance. The inset in Fig. 6.4(a) depicts the enhancement ~ 20 at CPT for larger field strengths, i.e. $G_1 = G_2 = G_2' = 10.0$ with $\Delta_1 = 100.0$. At CPT $\delta = 0.0$ which is the upper curve and the lower curve is away from CPT for $\delta = 10.0$. We have plotted only the relevant range of Ω as away from CPT at $\Omega \approx 100.0$ there is enhancement due to the *resonant* Raman process. For larger $\Delta_1 = 500.0$ and the same mistuning $\delta = 10.0$ the enhancement is 2×10^2 (not shown). At CPT for propagation to larger distances in a medium pulse matching occurs which is discussed in the next section.

6.5 Non-perturbative Regime of Pulse Matching

Pulse matching was first proposed by Harris [145] in a Λ system for *weak* probe fields. It was shown that when an ensemble of atoms *prepared in the CPT state* were probed by fields with arbitrary time-varying envelope, they establish transparency. Thus the fields propagate over lengths which are order of magnitude bigger than Beer's absorption length. The various Fourier components of the probe pulse after a characteristic distance no longer experience absorption, and hence are decoupled from the atom. Only the Fourier components that are *matched* in frequency difference, amplitude and phase, so as to preserve the CPT state *survive*. They continue to propagate through the medium without any loss due to absorption. Harris [163] derived new pair of variables which are normal modes for EIT to study matched pulses.

This matching of pulse occurs for a weak probe field, as the strength of the probe pulse is increased a coupled pulse pair propagates with a common group velocity, these pulse pairs are termed as adiabatons [164, 165]. If the time variation of the pulses is slow enough this pulse pair appears to be stable and may propagate to large distances, but because of nonadiabatic components such pulse pair is not stable [166] and after propagating a sufficient distance they evolve into a pair of matched pulses.

We now derive the equations governing this signal generation process along a medium containing N homogeneously broadened atoms per unit volume. We ignore the depletion of the fields $\vec{E}_i$ for $i = 1, 2$, and examine the evolution of the primed fields $\vec{E}_i'$ for $i = 1, 2$, along the z direction in a medium of length L and characterized by the absorption coefficient α, as shown in Fig. 6.1 (c). The wave equation after the *slowly varying envelope approximation* (section 2.9) for these primed fields is

$$\frac{d\vec{E}_i'}{dz} = i\frac{2\pi k_i'}{n_i^2}\vec{P}_i, \quad i = 1, 2. \tag{6.18}$$

where the wave vector $k_i' = (\omega_i + \Omega)n_i/c$ and n_i is the refractive index (linear) at the frequency $\omega_i + \Omega$. The polarization characterizing the medium is given as $\vec{P} = \text{Tr}(\vec{d}\rho)$ which can be separated into different components at different frequencies, thus P_1 (P_2) will be obtained from ρ_{13} (and ρ_{12}) at $\omega_1 + \Omega$ (and $\omega_2 + \Omega$), respectively.

If we calculate the polarization in the weak field limit (i.e. $\vec{E}_i' \ll \vec{E}_i$) the polarization P_i is linear in the primed fields and the wave equation (6.18) takes the following form,

which is the well known form for the evolution equations in Ref. [145]. Hence at CPT ($\Delta_i = 0$) for $\gamma_i = 1$ for $i = 1, 2$, in the limit of *non-depleting pumps* the evolution equations for the *weak probes* are

$$\frac{d}{dz}\begin{pmatrix} F_1 \\ F_2 \end{pmatrix} = \begin{pmatrix} i\kappa_1 & -i\kappa_2 e^{i\Delta\vec{k}} \\ -i\kappa_3 e^{-i\Delta\vec{k}} & i\kappa_4 \end{pmatrix}\begin{pmatrix} F_1 \\ F_2 \end{pmatrix}, \tag{6.19}$$

where we have introduced dimensionless quantities F_1, F_2 such that $F_1 = \vec{d}_{13} \cdot \vec{E}'_1/\hbar\gamma_1$ and $F_2 = \vec{d}_{12} \cdot \vec{E}'_2/\hbar\gamma_2$. The terms κ_i that qualify the medium are

$$\kappa_1 = \frac{\alpha_1\Omega|\tilde{G}_2|^2}{\zeta((1 + i\sqrt{\zeta} - i\Omega)(1 - i\sqrt{\zeta} - i\Omega) - 1)},$$

$$\kappa_2 = \frac{\alpha_1\Omega\tilde{G}_1\tilde{G}_2^*}{\zeta((1 + i\sqrt{\zeta} - i\Omega)(1 - i\sqrt{\zeta} - i\Omega) - 1)},$$

$$\kappa_3 = \frac{\alpha_2\Omega\tilde{G}_2\tilde{G}_1^*}{\zeta((1 + i\sqrt{\zeta} - i\Omega)(1 - i\sqrt{\zeta} - i\Omega) - 1)},$$

$$\kappa_4 = \frac{\alpha_2\Omega|\tilde{G}_1|^2}{\zeta((1 + i\sqrt{\zeta} - i\Omega)(1 - i\sqrt{\zeta} - i\Omega) - 1)}, \tag{6.20}$$

with $\zeta = |G_1|^2 + |G_2|^2$ and $\tilde{G}_1 = \vec{d}_{13} \cdot \vec{E}_1/\hbar$ and $\tilde{G}_2 = \vec{d}_{12} \cdot \vec{E}_2/\hbar$. The absorption coefficients α_i are given as

$$\alpha_i = \frac{4\pi(\omega_i + \Omega)\, d_{\alpha\beta}^2\, N}{\hbar c n_i \gamma_i}, \quad i = 1, 2. \tag{6.21}$$

In eqn. (6.19) the phase matching condition is $\Delta\vec{k} = (\vec{k}_1 - \vec{k}'_1) - (\vec{k}_2 - \vec{k}'_2) = 0$, which can be achieved for the geometry given in Fig. 6.1 (c). Hakuta et al. [167] observed self-induced phase matching in parametric anti-Stokes Raman scattering in solid hydrogen. In the experiment of Jain et al. [53], they have observed enhanced conversion in the regime where $\Omega \gg G_i \gg \gamma$. To obtain the correspondence with their result we redefine the fields $F_1 \to F_1\tilde{G}_2 \exp i\kappa_1 z$ and $F_2 \to F_2\tilde{G}_1 \exp i\kappa_4 z$, and take the large Ω limit. In this limit κ_i takes only real values and results in *redefining* the phase matching condition as $\Delta\vec{k} + (\alpha_1|G_2|^2 - \alpha_2|G_1|^2)/\zeta\Omega \approx 0$, which then leads to equations (1) and (2) of Ref. [53]. In our approach we do not restrict the values of Ω and hence the generated field frequency can be arbitrary.

The solution of eqn. (6.19) after phase matching and with the initial conditions that the field G'_1 is zero at the $z = 0$ and is generated along the medium given a finite input field G'_2 (i.e., $F_1(0) = 0$ and $F_2(0)$ at $z = 0$) is

$$F_1(z) = \frac{F_2(0)}{2}(1 - e^{i\kappa z}), \quad F_2(z) = \frac{F_2(0)}{2}(1 + e^{i\kappa z}). \tag{6.22}$$
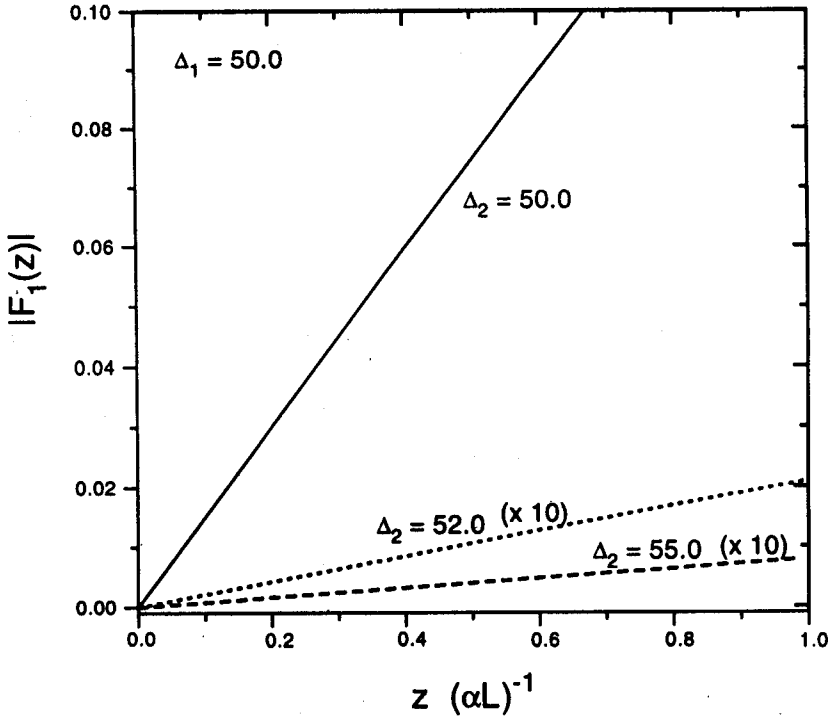
Figure 6.5: The generation of the nonlinear signal at $\omega_1 + \Omega$ along the length of the medium, as shown in wave mixing geometry (Fig. 6.1 (c)), for $\alpha L = 40$, $\Omega = 10.0$, $G_1 = G_2 = 1.0$ and the initial conditions $F_1(0) = 0.0$, $F_2(0) = 1.0$. For the detuning $\Delta_1 = 50.0$, the signal at CPT i.e. $\delta = 0$ (solid). For clarity the signal for the non-CPT case i.e. $\delta = 2$ (dotted) and 5 (dashed) have been scaled by a factor of 10. Note the enhancement due to CPT.

We observe pulse matching of Harris [145] for large z, i.e. $F_1(\infty) = F_2(\infty) = F_2(0)/2$. In Ref. [145] the medium was *initially prepared* in a CPT state and the propagation of *weak* probe fields through the medium was calculated. They used the wavefunction approach where the decay channel was such that the excited state decays *out of the Λ scheme* to either a state or a continuum. In contrast we use here the *density matrix* picture in which *all* possible decay channels can be handled. Furthermore, in our treatment the propagating probe fields could be of *comparable magnitude* with those forming the CPT state, so that the polarization in eqn. (6.19) is no longer linear but contains *all* the *higher* powers of the fields F_1 and F_2.

To calculate the polarization *non-perturbatively*, we use the expansion (6.3) in eqns. (6.2) and obtain a coupled set of equations for various Fourier components (for each n), which are solved simultaneously using *matrix continued fractions* as shown in section 6.2. The evolution of the fields inside the medium is obtained by integrating the

propagation equations (6.18) using the Runge-Kutta method. The *polarization* is calculated non-perturbatively using the fields *at each z* which in turn *modifies the fields* inside the medium along the direction of propagation; this process is *iterated* along the whole length of the medium.

In Fig. 6.5 we depict the generation of the field at $\omega_1 + \Omega$ along the length of the medium z in the units of αL ($= 40$) at $\Omega = 10.0$. We expect a *linear* dependence of the amplitude of the generated field in the thin medium. The solid line depicts the generation of signal at CPT and the dotted lines away from CPT. We see a dramatic increase in the *amplitude* of the generated signal at CPT. The enhancement of the amplitude of the generated field due to CPT is by a factor of ~ 230 and 608, in contrast to the non-CPT case for the mistuning $\delta = 2$ and 5, respectively. The generation of $\omega_1 + \Omega$ takes place at the cost of $\omega_2 + \Omega$ (not shown in the figure) as they propagate through the medium.

To observe the pulse matching at *higher probe powers* the equations (6.18) were integrated for various initial conditions; namely the generated field $F_1 = 0$ at $z = 0$ and various input levels of the field F_2. The polarization was calculated *non-perturbatively* and used to update the field at each z along the medium. In Fig. 6.6 we see the generation and build up of the field $F_1(\omega_1 + \Omega)$. This build up initially occurs at the cost of $F_2(\omega_2 + \Omega)$ (dotted lines), then there are oscillations and exchange of energy between these fields until they are *matched*, such that

$$\frac{F_1}{F_2} = \frac{\tilde{G}_1}{\tilde{G}_2}, \tag{6.23}$$

after which they propagate in the medium without any loss. The condition (6.23) is got by requiring that the CPT state is a non-interacting state in presence of all the four fields (similar to the condition in eqn. (2.29) where the Hamiltonian given in eqn. (6.1) is used instead). Moreover this steady state condition is *independent* of the relative strengths of the various fields. We now compare the weak probe case (Fig. 6.6 (a)) and the strong probe case (Fig. 6.6 (b)). We observe that for higher probe power (i.e. F_1, $F_2 \approx G_1$, G_2) the characteristic length for pulse matching is substantially *reduced* compared to the weak probe case. This is due to *reenforcement* of the CPT state in presence of stronger frequency matched components ($F_i(\omega_i + \Omega)$, $i = 1, 2$) in the propagating fields. Even for the thick medium ($\alpha L = 8 \times 10^3$) its advantageous to operate at the CPT condition. This is seen in the inset of Fig. 6.6 where we plot the generated field at $z = 0.05 \ (\alpha L)^{-1}$
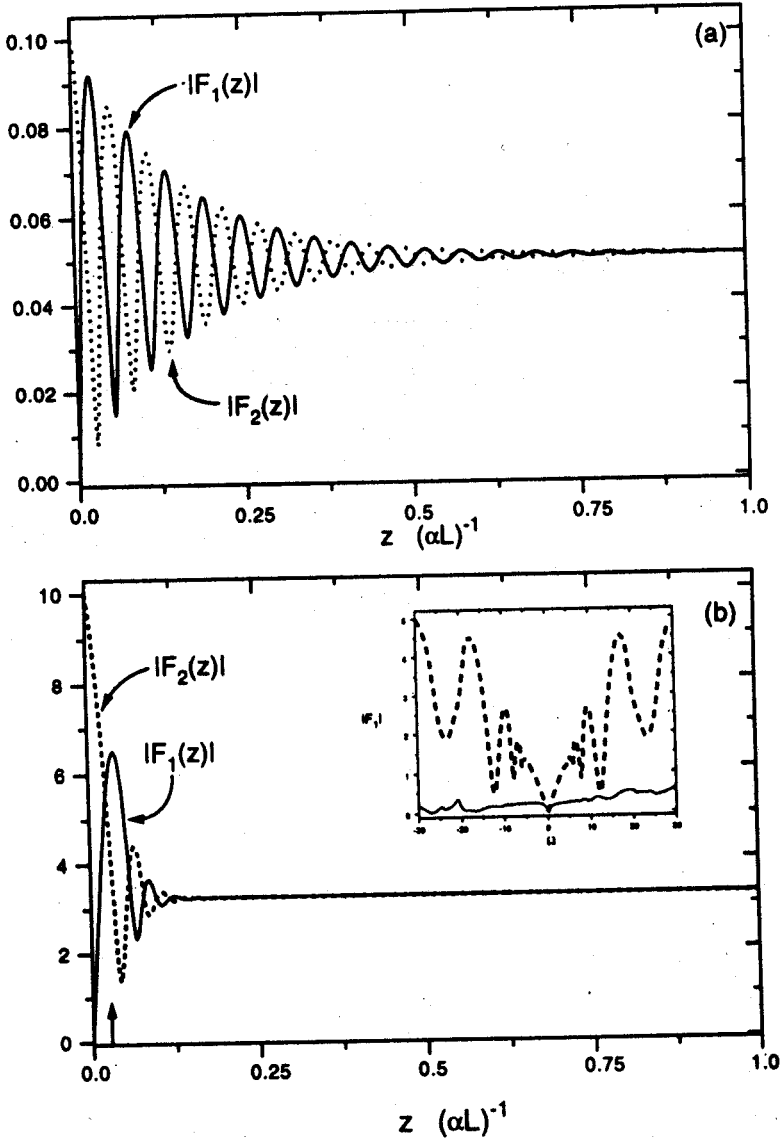
Figure 6.6: Pulse matching at higher probe powers at CPT with $\alpha L = 8 \times 10^3$, $\Omega = 10.0$, for $G_1 = G_2 = 15.0$, $F_1(0) = 0.0$ and $F_2(0) = 0.1$ (a), 10.0 (b). The solid and dashed curves give respectively the fields $|F_1(z)|$ and $|F_2(z)|$. At higher probe powers the pulse matching occurs at shorter distances. The inset depicts the field generated at $z = 0.05(\alpha L)^{-1}$ (shown by the arrow), for the strong probe case at CPT (dotted line), and away from CPT (solid line), i.e. $\delta = 50.0$, as a function of Ω.

as a function of Ω.

In conclusion, we have studied the various aspects of how the atomic coherence plays a very fundamental role in generation of nonlinear signal. By operating at the CPT condition we obtain maximum coherence which in turn leads to enhancement of the signal. We have also seen that it is useful to operate at CPT with finite detuning from the atomic resonance. Furthermore we have demonstrated pulse matching even at higher probe powers. In fact we have shown that pulse matching takes place at much shorter distances inside the medium at higher probe powers. From our analysis its clear that by choosing various other atomic schemes one could enhance other nonlinear mixing processes using the coherence of the population trapped state.

Conclusions .

We have demonstrated new population trapping states in two-level systems using classical frequency modulated field. We derived explicit conditions under which these trapping phenomenon can be observed. We found that these trapping states are accompanied by crossing of energy levels, which lead to jumps in the population of the system. We found that this trapping phenomenon is limited by the excited state lifetime.

We generalized these states to a three-level cascade system. We found that trapping of population persists, even if there is an initial phase mismatch between the two applied fields, or unequal choice of the modulation index and modulation frequency. We observed the effects of coherent evolution in between crossing of energy levels leading to quantum interference. We have also proposed a new method of creating inversion across multiple states without affecting the population of the intermediate state, this was achieved by utilizing these trapping states with appropriate choice of parameters such that all the energy levels cross simultaneously. We furthermore described a possible optical atom realization of the three-level ladder system.

We have also studied various manifestations of the quantum interference effect in optical bistability and nonlinear generation of signals.

We demonstrated the effects of field induced transparency and quantum interference in the cooperative phenomenon of optical bistability, by coupling the excited states to another level using a control field. We have demonstrated control field induced decrease in the switching threshold. We obtained decrease in the threshold by more than 50 %, using reduced absorption through Autler - Townes effect and also the quantum interference effect. We also studied the temporal evolution of switching, in our proposal, we found that the coefficient of critical slowing down is dependent on the control field parameters. We have also obtained multistable behavior for an appropriate control field, where the region of multistability could be fine tuned by a judicious choice of the control field parameters.

In nonlinear generation, we studied various aspects of how atomic coherence plays a vital role in this phenomenon, we demonstrated enhancement of the signal by operating the pump fields at the coherent population trapping condition. We found that its useful to operate at CPT with finite detuning from the atomic resonances. We obtained enhancements of more than 10^2 in the generated signal intensity. We also developed a non-perturbative approach to deal with problems involving two strong fields coupling the same transition. We have also studied the pulse matching phenomenon for higher probe powers and demonstrated that pulse matching does occur at higher probe powers. In fact we have shown that pulse matching takes place at much shorter distances inside the medium at higher probe powers.

Bibliography

[1] M. Planck, Verh. dt. phys. Ges. **2**, 202 (1900).

[2] A. Einstein, Annln Phys. **17**, 132 (1905).

[3] G.N. Lewis, Nature **118**, 874 (1926).

[4] A. Einstein, Phys. Z. **18**, 121 (1917).

[5] P.A.M. Dirac, Proc. Roy. Soc. A **114**, 243 (1927).

[6] P.L. Kelley, P.J. Harshman, O. Blum and T.K. Gustafson, J. Opt. Soc. Am. B **11**, 2298 (1994).

[7] G.S. Agarwal, *Quantum Statistical Theories of Spontaneous Emission* (Springer-Verlag, Berlin), **70** (1974).

[8] L. Allen and J.H. Eberly, *Optical Resonance and Two-Level Atoms* (Dover, New York), (1987).

[9] E.T. Jaynes and F.W. Cummings, Proc. IEEE, **1**, 89 (1963).

[10] For a recent review on coherent population trapping see E. Arimondo in *Progress in Optics*, Vol. XXXV, ed. E. Wolf (North-Holland, Amsterdam) p. 257 (1996).

[11] For a review on early studies in coherent population trapping, see, P.L. Knight, M.A. Lauder, and B.J. Dalton, Phys. Rep. **190**, 1 (1990).

[12] G. Alzetta, A. Gozzini, L. Moi and G. Orriols, Nuovo Cimento Soc. **36 B**, 5 (1976).

[13] H. Gray, R. Witley and C. Stroud, Jr., Opt. Lett. **3**, 218 (1978).

[14] E. Arimondo and G. Orriols, Lett. Nuovo Cimento, **17**, 333 (1976).

[15] B.J. Dalton and P.L. Knight, J. Phys. B **15**, 3997 (1982).

[16] G.S. Agarwal, Phys. Rev. Lett. **71**, 1351 (1993).

[17] M. Fleischhauer, Phys. Rev. Lett. **72**, 989 (1994).

[18] J.R. Kuklinski, U. Gaubatz, F.T. Hioe, and K. Bergmann, Phys. Rev. A **40**, 6741 (1989).

[19] For an recent review of EIT see S.E. Harris, Phys. Today **52**, 36 (1997).

[20] M. Jain, A.J. Merriam, A. Kasapi, G.Y. Lin and S.E. Harris, Phys. Rev. Lett. **75**, 4385 (1995).

[21] K.J. Boller, A. Imamoglu and S.E. Harris, Phys. Rev. Lett. **66**, 2593 (1991).

[22] J.E. Field, K.H. Hahn and S.E. Harris, Phys. Rev. Lett. **67**, 3062 (1991).

[23] Y. Li and M. Xiao, Phys. Rev. A **51**, 4959 (1995).

[24] S.E. Harris, J.E. Field and A. Kasapi, Phys. Rev. A **46**, R29 (1992).

[25] M. Xiao, Y.-Q. Li, S.-Z. Jin, and J. Gea-Banacloche, Phys. Rev. Lett. **74**, 666 (1995); J. Gea-Banacloche, Y.-Q. Li, S.-Z. Jin, and M. Xiao, Phys. Rev. A **51**, 576 (1995).

[26] A. Kasapi, M. Jain, G.Y. Yin and S.E. Harris, Phys. Rev. Lett. **74**, 2447 (1995).

[27] A. Kasapi, G.Y. Yin, M. Jain and S.E. Harris, Phys. Rev. A **53**, 4547 (1996).

[28] S.A. Hopkins, E. Usadi, H.X. Chen and A.V. Durrant, Opt. Commun. **138**, 185 (1997).

[29] D.J. Fulton, S. Shepherd, R.R. Mosley, B.D. Sinclair and M.H. Dunn, Phys. Rev. A **52** , 2302 (1995).

[30] G. Vemuri, G.S. Agarwal and B.D.N. Rao, Phys. Rev. A **53**, 2842 (1996).

[31] S. Shepherd, D.J. Fulton, M.H. Dunn, Phys. Rev. A **54**, 5394 (1996).

[32] B. Lü, W.H. Burkett and M. Xiao, Opt. Commun. **141**, 269 (1997).

[33] Y. Li and M. Xiao, Phys. Rev. A **51**, R2703 (1995).

[34] S.J. van Enk, J. Zhang and P. Lambropoulos, Phys. Rev. A **50**, 2777 (1994).

[35] S.E. Harris, Opt. Lett. **19**, 2018 (1994).

[36] A. Kasapi, Phys. Rev. Lett. **77**, 1035 (1996).

[37] S.E. Harris and Z.F-. Luo, Phys. Rev. A **52**, R928 (1995).

[38] S.E. Harris, Phys. Rev. Lett. **77**, 5357 (1996).

[39] Y. Zhao, C. Wu, B-S Ham, M.K. Kim and E. Awad, Phys. Rev. Lett. **79**, 641 (1997).

[40] B.S. Ham, P.R. Hemmer and M.S. Shahriar, Opt. Commun. **144**, 227 (1997).

[41] S.P. Tewari and G.S. Agarwal, Phys. Rev. Lett. **56**, 1811 (1986).

[42] G.S. Agarwal and S.P. Tewari, Phys. Rev. Lett. **70**, 1417 (1993).

[43] S.E. Harris, J.E. Field and A. Imamoglu, Phys. Rev. Lett. **64**, 1107 (1990).

[44] S.P. Tewari and G.S. Agarwal, Phys. Rev. Lett. **66**, 1797 (1991).

[45] M. Jain, G.Y. Lin, J.E. Field and S.E. Harris, Opt. Lett. **18**, 998 (1993).

[46] S.E. Harris and M. Jain, Opt. Lett. **22**, 636 (1997).

[47] K. Hakuta, L. Marmet and B.P. Stoicheff, Phys. Rev. A **45**, 5152 (1992).

[48] G.Z. Zhang, K. Hakuta, and B.P. Stoicheff, Phys. Rev. Lett. **71**, 3099 (1993).

[49] G.Z. Zhang, M. Katsuragawa, K. Hakuta, R.I. Thompson, and B.P. Stoicheff, Phys. Rev. A **52**, 1584 (1995).

[50] G.Z. Zhang, D.W. Tokaryk, B.P. Stoicheff and K. Hakuta, Phys. Rev. A **56**, 813 (1997).

[51] P.R. Hemmer, D.P. Katz, J. Donoghue, M. Cronin-Goloumb, M.S. Shahriar and P. Kumar, Opt. Lett. **20**, 982 (1995); a theoretical calculation of the signals has been done by P.R. Hemmer, L. Hollberg, M. Loeffler, M.D. Lukin and M.O. Scully, to be published.

[52] T.T. Grove, M.S. Shahriar, P.R. Hemmer, P. Kumar, V.S. Sudarshanam and M. Cronin-Goloumb, Opt. Lett. **22**, 769 (1997).

[53] M. Jain, H. Xia, G.Y. Yin, A.J. Merriam and S.E. Harris, Phys. Rev. Lett. **77**, 4326 (1996).

[54] S.E. Harris, Phys. Rev. Lett. **62**, 1033 (1989).

[55] G.S. Agarwal, Phys. Rev. A **55**, 2467 (1997).

[56] G.S. Agarwal and W. Harshawardhan, Phys. Rev. Lett. **77**, 1039 (1996).

[57] R.H. Dicke, Phys. Rev. A **93**, 99 (1954). For a review on *superfluorescence* see, M.F.H. Schuurmans, Q.H.F. Vrehen, D. Polder and H.M. Gibbs, Adv. At. Mol. Phys. **17**, 167 (1981).

[58] M.O. Scully, S.Y. Zhu, and A. Gavrielides, Phys. Rev. Lett. **62**, 2813 (1989).

[59] S.Y. Zhu and M.O. Scully, Phys. Rev. Lett. **76**, 388 (1996).

[60] H.R. Xia, C.Y. Ye and S.Y. Zhu, Phys. Rev. Lett. **77**, 1032 (1996).

[61] G.S. Agarwal, Phys. Rev. Lett. **67**, 980 (1991).

[62] L.M. Narducci, M.O. Scully, G.L. Oppo, P. Ru and J.R. Tredice, Phys. Rev. A **42**, 1630 (1990).

[63] Y.F. Zhu, D.J. Gauthier and T.W. Mossberg, Phys. Rev. Lett. **66**, 2460 (1991).

[64] S.Y. Zhu, L.M. Narducci and M.O. Scully, Phys. Rev. A **52**, 4791 (1995).

[65] G.S. Agarwal, Phys. Rev. A **54**, R3734 (1996).

[66] M. Winters, J. Hall and P. Toschek, Phys. Rev. Lett. **65**, 3116 (1990).

[67] U. Fano, Phys. Rev. **124**, 1866 (1961).

[68] A. Imamoglu, Phys. Rev. A **40**, 2835 (1989).

[69] O. Kocharovskya and Ya.I. Khanin, Pis'ma Zh. Eksp. Teor. Fiz. **48**, 581 (1988) [JETP Lett. **48**, 630 (1988)].

[70] G.S. Agarwal, Phys. Rev. A **44**, R28 (1991).

[71] A. Imamoglu, J.E. Field and S.E. Harris, Phys. Rev. Lett. **66**, 1154 (1991).

[72] Y. Zhu, Phys.Rev. A **45**, R6149 (1992).

[73] G.A. Wilson, K.K. Meduri, P. Sellin and T.W. Mossberg, Phys. Rev. A **50**, 3394 (1994).

[74] G.B. Prasad and G.S. Agarwal, Opt. Commun. **86**, 409 (1991).

[75] Y. Zhu and J. Lin, Phys. Rev. A **53**, 1767 (1996).

[76] A.S. Zibrov, M.D. Lukin, D.E. Nikonov, L. Hollberg, M.O. Scully, V.L. Velichansky and H.G. Robinson, Phys. Rev. Lett. **75**, 1499 (1995).

[77] O. Kocharovskaya and P. Mandel, Opt. Commun. **84**, 179 (1991).

[78] M. Fleischhauer, C.H. Keitel, M.O. Scully, C. Su, B.T. Ulrich and S.Y. Zhu, Phys. Rev. A **46**, 1468 (1992).

[79] G.G. Padmabandu, G.R. Welch, I.N. Shubin, E.S. Fry, D.E. Nikonov, M.D. Lukin and M.O. Scully, Phys. Rev. Lett. **76**, 2053 (1996)

[80] O. Kocharovskya, Phys. Rep. **219**, 175 (1992).

[81] P. Mandel, Contemporary Physics, **34**, 235 (1993).

[82] M.O. Scully, Quantum Opt. **6**, 203 (1994).

[83] E.S. Fry, X. Li, D. Nikonov, G.G. Padmabandu, M.O. Scully, A.V. Smith, F.K. Tittle, C. Wang, S.R. Wilkinson and S.Y. Zhu, Phys. Rev. Lett. **70**, 3235 (1993).

[84] J.Y. Gao, C. Guo, X. Guo, G. Jin, P. Wang, J. Zhao, H. Zhang, Y. Jiang, D. Wang and D. Jiang, Opt. Commun. **93**, 323 (1992).

[85] A. Nottelman, C. Peters and W. Lange, Phys. Rev. Lett. **70**, 1783 (1993).

[86] W. van der Veer, R.J.J. van Diest, A. Dönszelmann and H.B. van Linden van den Heuvell, Phys. Rev. Lett. **70**, 3243 (1993).

[87] M.O. Scully, Phys. Rev. Lett. **67**, 1855 (1991).

[88] M.O. Scully and S.Y. Zhu, Opt. Commun. **87**, 134 (1992).

[89] M. Fleischhauer, C.H. Keitel, M.O. Scully, and C. Su, Opt. Commun. **87**, 109 (1992).

[90] A. Shnitman, I. Sofer, I. Golub, A. Yogev, M. Shapiro, Z. Chen and P. Brumer, Phys. Rev. Lett. **76**, 2886 (1996).

[91] A.S. Zibrov, M.D. Lukin, L. Hollberg, D.E. Nikonov, M.O. Scully, H.G. Robinson and V.L. Velichansky, Phys. Rev. Lett. **76**, 3935 (1996).

[92] R. Moseley, Phys. Rev. Lett. **74**, 670 (1995).

[93] M.O. Scully and M. Fleischhauer, Phys. Rev. Lett. **69**, 1360 (1992).

[94] O. Kocharovskaya, P. Mandel and M.O. Scully, Phys. Rev. Lett. **74**, 2451 (1995).

[95] G.S. Agarwal and W. Harshawardhan, Phys. Rev. **A 50**, R4465 (1994).

[96] P. Meystre, G. Rempe and H. Walther, Opt. Lett. **13**, 1078 (1988).

[97] P.K. Lam and C.M. Savage, Phys. Rev. A **50**, 3500 (1994).

[98] N. Nayak and G.S. Agarwal, Phys. Rev. A **31**, 3175 (1985); J. Opt. Soc. Am. B **1**, 164 (1984).

[99] S. Chakmakjian, K. Koch and C.R. Stroud, Jr., J. Opt. Soc. Am. B **5**, 2015 (1988); S. Papademetrious, S. Chakmakjian, C.R. Stroud, Jr., *ibid.* **9**, 1182 (1992).

[100] M. Sanjay Kumar, M.L. Pons and J.H. Eberly, Phys. Rev. A **44**, 1995 (1993); H. Freedhoff and Z. Chen, Phys. Rev. A **41**, 6013 (1990); S.P. Tewari and M. Krishna Kumari, Phys. Rev. A **41**, 5273 (1990).

[101] W.M. Ruyten, Phys. Rev. A **46**, 4077 (1992); Opt. Lett. **14**, 506 (1989).

[102] J.H. Eberly and V.D. Popov, Phys. Rev A **37**, 2012 (1988); T.W. Mossberg and M. Lewenstein, Phys. Rev. A **39**, 163 (1989); Q. Wu, D.J. Gauthier and T.W. Mossberg, Phys. Rev. A **49**, 1519 (1994).

[103] J.E. Golub and T.W. Mossberg, Phys. Rev. Lett. **59**, 2149 (1987).

[104] The advantages of the spin analogy of the two-level atomic transition was first fully displayed in, R.P. Feynman, F.L. Vernon, Jr., and R.W. Hellwarth, J. Appl. Phys. **28**, 49 (1957).

[105] *Handbook of Mathematical Functions, ed.* M. Abramowitz and I. A. Stegun (Dover Publications, New York. 1965).

[106] P.M. Radmore, S. Tarzi and K.L. Tang, J. Mod. Opt. **42**, 2213 (1995).

[107] L.D. Landau, Phys. Z. Sowjetunion **2**, 46 (1932).

[108] C. Zener, Proc. R. Soc. London A, **137**, 696 (1932).

[109] E.E. Nikitin, *Theory of elementary atomic and Molecular processes in gases*, Oxford University press, pg. 107 (1974).

[110] D.R. Bates, Proc. R. Soc. London A, **257**, 22 (1960).

[111] F.T. Arecchi, E. Courtens, R. Gilmore and H. Thomas, Phys. Rev. A **6**, 2211 (1972).

[112] N. Rosen and C. Zener, Phys. Rev. **40**, 502 (1932).

[113] I.I. Rabi, Phys. Rev. **51**, 652 (1937).

[114] F. Hund, Z. Phys. **43**, 805 (1927).

[115] W.A. Lin and L.E. Ballentine, Phys. Rev. Lett. **65**, 2927 (1990).

[116] F. Grossmann, T. Dittrich, P. Jung and P. Hanggi, Phys Rev. Lett., **67**, 516 (1991); Z. Phys. B **84**, 315 (1991).

[117] J.M. Gomez Llorente and J. Plata, Phys. Rev. A **45**, R6958 (1992).

[118] R. Bavli and H. Metiu, Phys. Rev. Lett. **69**, 1986 (1992); Phys. Rev. A **47**, 3299 (1993).

[119] M. Holthaus, Phys. Rev. Lett. **69**, 351 (1992).

[120] Y. Dakhnovskii and H. Metiu, Phys. Rev. A **48**, 2342 (1993).

[121] S.Ya. Kilin, P.R. Berman and T.M. Maevskaya, Phys. Rev. Lett. **76**, 3297 (1996).

[122] W.J. Orvitle-Thomas in *Internal Rotations in Molecules*, (John Wiley & Sons, London), (1974).

[123] W.E. Moerner and T. Basche, Angew. Chem. Int. Ed. Engl. **32**, 457 (1993).

[124] P.W. Anderson, B.I. Halperin and C.M. Varma, Philos. Mag. **25**, 1 (1972).

[125] L. Peliti in *Biologically Inspired Physics*, (Plenum, NewYork), (1992); D.L. Stein in *Spin Glasses and Biology* (World Scientific, Singapore), (1992).

[126] W. Harshawardhan and G.S. Agarwal, Physical Review **A 55**, 2165 (1997).

[127] Y.N. Demkov and V.I. Osherov, Zh. Éksp. Teor. Fiz. **53**, 1589 (1967) [Sov. Phys. JETP. **26**, 916 (1968)].

[128] H. Nakamura, J. Chem. Phys., **87**, 4031 (1987).

[129] J. Oreg, F.T. Hioe and J.H. Eberly, Phys. Rev. A **29**, 690 (1984); C. Liedenbaum, S. Stolte and J. Reuss, Phys. Rep. **178**, 1 (1989).

[130] D.H. Dunlap and V.M. Kenkre, Phys. Rev. **B 34**, 3625 (1986); Phys. Rev. **B 37**, 6622 (1988).

[131] S. Raghavan, V.M. Kenkre, D.H. Dunlap, A.R. Bishop and M.I. Salkola, Phys. Rev. **A 54**, R1781 (1996).

[132] M.V. Berry, Proc. Roy. Soc. Lon. **A 392**, 45 (1984).

[133] M.V. Berry, Proc. Roy. Soc. Lon. **A 430**, 405 (1990).

[134] D. Bouwmeester, G.P. Karman, C.A. Schrama and J.P. Woerdman, Phys. Rev. A **53**, 985 (1996).

[135] M. Gatzke, R.B. Watkins and T.F. Gallagher, Phys. Rev. **A 51**, 4835 (1995).

[136] N.V. Vitanov and P.L. Knight, Phys. Rev. **A 52**, 2245 (1995).

[137] C.E. Carroll and F.T. Hioe, Phys. Rev. Lett. **68**, 3523 (1992).

[138] B. Broers, H.B. van Linden van den Heuvell and L.D. Noordam, Phys. Rev. Lett. **69**, 2062 (1992).

[139] For a review of optical atoms see R.J.C. Spreeuw and J.P. Woerdman in *Progress in Optics, ed.* E. Wolf (North Holland, Amsterdam. 1993) Vol. XXXI, pg. 263; R.J.C. Spreeuw, M.W. Beijersbergen and J.P. Woerdman, Phys. Rev. A **45**, 1213 (1992).

[140] H.A. Haus, H. Statz and I.W. Smith, IEEE J. Quant. Electron. **QE 21**, 78 (1985); R.J.C. Spreeuw, R. Centeno Neelen, N.J. van Druten, E.R. Eliel and J.P. Woerdman, Phys. Rev. A **42**, 4315 (1990).

[141] A.E. Siegman in *Lasers*, (University Science Books, California) p. 1165 (1986).

[142] D. Lenstra, L.P.J. Kamp and W. van Haeringen, Opt. Commun. **60**, 339 (1986); R.J.C. Spreeuw, J.P. Woerdman and D. Lenstra, Phys. Rev. Lett. **61**, 318 (1988).

[143] H.A. Haus and C.G. Fonstad, Jr., IEEE J. Quant. Electron., **QE 17**, 2321 (1981).

[144] W. Harshawardhan and G.S. Agarwal, Physical Review A **53**, 1812 (1995).

[145] S.E. Harris, Phys. Rev. Lett. **70**, 552 (1993).

[146] A. Szöke, V. Daneu, J. Goldharand N.A. Kurnit, Appl. Phys. Lett. **15**, 376 (1969).

[147] S.L. McCall, Phys. Rev. A **9**, 1515 (1974).

[148] H.M. Gibbs, S.L. McCall, T.N.C. Venkatesan, Phys. Rev. Lett. **36**, 113 (1976).

[149] F.S. Felber and J.H. Marburger, Appl. Phys. Lett. **28**, 731 (1976).

[150] R. Bonifacio and L.A. Lugiato, Opt. Commun. **19**, 172 (1976); Phys. Rev. A **18**, 1129 (1978).

[151] P.W. Smith and E.H. Turner, Appl. Phys. Lett. **30**, 280 (1977).

[152] L.A. Lugiato, in *Progress in Optics*, edited by E. Wolf (North- Holland, Amsterdam), Vol. **XXI**, p. 69 (1984).

[153] F.T. Arecchi and A. Politi, Lett. Nuovo. Cim. **23**, 65 (1978); G.P. Agarwal and C. Flytzanis, Phys. Rev. Lett. **44**, 1053 (1980); J.A. Hermann and B.V. Thompson, Phys. Lett. A **83**, 376 (1981); G.S. Agarwal, Opt. Commun. **35**, 149 (1980); P. Grangier, J.F. Roch, J. Roger, L.A. Lugiato, E.M. Pessina, G. Scandroglio and P. Galatola, Phys. Rev. A **46**, 2735 (1992).

[154] The literature on optical bistability is very exhaustive and we refer to excellent review article by Lugiato (Ref. [152]) and *Optical Bistability: Controlling Light with Light*, H.M. Gibbs (Academic Press, Inc.) (1985).

[155] Shang-quing Gong, Si-de Du, Zhi-zhan Xu and Shao-hua Pan, Phys. Lett. A, **222**, 237 (1996).

[156] Shang-quing Gong, Si-de Du and Zhi-zhan Xu, Phys. Lett. A, **226**, 293 (1997).

[157] F.T. Arecchi, J. Kurmann and A. Politi, Opt. Commun. **44**, 421 (1983).

[158] W. Harshawardhan and G.S. Agarwal, accepted for publication in Phys. Rev. A, tentatively scheduled to be published in the issue of 01-May-1998.

[159] H. Risken *The Fokker - Planck Equation*, (Springer-Verlag, Berlin) p. 196 (1984).

[160] In the hierarchy of approximations made on the response of a medium to the incident field, the *secular approximation* is higher than the *rate equation* approximation. In the rate equations only the dynamics of the populations of various levels are interconnected, whereas the effects of coherence i.e. the off-diagonal terms is neglected (in the limit that the Electric field varies slowly in the atomic lifetime). In the strong field limit, the secular approximation amounts to consideration of the off-diagonal terms which are related to themselves, along with the rate equations for the populations of various levels. This approximation is valid in the limit when the Rabi frequency (G) of the fields involved is much greater than the decays (Γ). The coupling of the off-diagonal terms to each other is neglected, as these terms would vary as Γ/G.

[161] Y. Li and M. Xiao, Phys. Rev. A **51**, 4959 (1995)

[162] I.V. Jyotsna and G.S. Agarwal, Phys. Rev. A **52**, 3147 (1995).

[163] S.E. Harris, Phys. Rev. Lett. **72**, 52 (1994)

[164] J.H. Eberly, M.L. Pons, and H.R. Haq, Phys. Rev. Lett. **72**, 56 (1994).

[165] R. Grobe, F.T. Hioe and J.H. Eberly, Phys. Rev. Lett. **73**, 3183 (1994).

[166] M. Fleischhauer, and A.S. Manka, Phys. Rev. A **54**, 794 (1996).

[167] K. Hakuta, M. Suzuki, M. Katsuragawa and J.Z. Li, Phys. Rev. Lett. **79**, 209 (1997).